4-18-2018

Computational Validation of Aerodynamic Paramenters on a Multi-Sided Cylinder

Christopher Ong

THE UNIVERSITY OF NEW HAVEN

COMPUTATIONAL VALIDATION OF AERODYNAMIC PARAMENTERS ON A MULTI-SIDED CYLINDER

A THESIS

Submitted in partial fulfillment

of the requirements for the degree of

MASTER OF SCIENCE IN MECHANICAL ENGINEERING

BY

Christopher Ong

University of New Haven
West Haven, Connecticut
April 4th, 2018

COMPUTATIONAL VALIDATION OF AERODYNAMIC PARAMENTERS ON A MULTI-SIDED CYLINDER

APPROVED BY

Byungik, Chang, Ph.D., PE, MBA
Thesis Advisor

Maria-Isabel, Carnasciali, Ph.D.
Thesis Co-Advisor

Ravi Gorthala, Ph.D.
Program Coordinator and Committee Member

Ronald, S, Harichandran, Ph.D., PE
Dean of the College

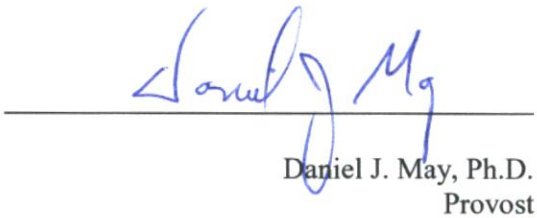

Daniel J. May, Ph.D.
Provost

ACKNOWLEDGMENTS

I would like to thank my thesis advisor, Dr. Byungik Chang of the University of New Haven, for guiding the thesis work. Dr. Chang has been a helpful, guiding hand throughout the duration of my Master's studies. He has given me guidance and provided many opportunities for me to grow as a student. I would like to thank Dr. Carnasciali and Dr. Gorthala for serving on the thesis committee. Dr. Carnasciali has aided and advised me during my thesis work regarding CFD and fluid dynamics. Dr. Gorthala has mentored me through my undergraduate and graduate course work, as well as other endeavors. I would like to thank my parents for being supportive and supporting me as I pursued my education at the University of New Haven. I would also like to thank my brother for his assistance during my time completing my Master's degree.

ABSTRACT

There are fundamental problems in fluid dynamics. One common problem is fluid flow around cylinder-shaped bodies which range from circular to multi-sided polygons. These basic geometric shapes are found in various applications. With the increased availability of computational power, the use of Computational Fluid Dynamics (CFD) becomes an avenue for studying fluid flow around theses shapes. The fluid flow over cylindrical bodies is a widely studied problem used to validate the accuracy and reliability of CFD codes before working on more complex engineering problems. This validation is done by comparing selected flow parameters to experimental results to determine the accuracy of the CFD codes.

Fluid-Structural Interaction (FSI) problems are of interest in mechanical and civil engineering fields due to how fatigue and oscillatory loading from fluid motions can cause failure of complex machinery or structures. The current study involves the use of CFD to simulate the fluid flow around a dodecagonal cylinder. Dodecagonal cylinders are typically used for High Mast Light Poles (HMLP). Such poles are often subjected to wind induced loading from various types of flow. Work has been done to study the effects on HMLP structures with accompanying wind tunnel experiments used to investigate the dynamic behavior of the system.

The objectives for the study are to simulate the fluid flow around a dodecagonal cylinder in CFD for different conditions and validate the computational results with experimental wind tunnel results. Both static and dynamic modeling of a dodecagonal cylinder using CFD produced values similar to wind tunnel test results.

TABLE OF CONTENTS

Contents

LIST OF TABLES

LIST OF FIGURES

CHAPTER 1. INTRODUCTION

1.1 PROBLEM STATEMENT

High mast light poles (HMLP) are used nationwide on major interstates and at local intersections for luminary purposes. A HMLP structure collapsed in an open area parallel to the interstate, near Sioux City in Iowa in 2003. Oscillatory fatigue that led to crack progradation proved to be the primary cause for the failure. Following the collapse, similar HMLP structures in Iowa were taken out of service and inspected. Some of examined poles showed significant cracking, which provided information to determine the type of failure loads. These inspections identified oscillatory wind loading as the cause of the cracks.

Vortex-induced vibrations (VIV) are caused by oscillating wind loads moving pass HMLP structures. The oscillating motion causes alternating pressures which lead to the fatigue failure mode. The greatest damage occurs when the oscillatory frequency becomes similar to the structure's natural frequency (Caracoglia 2007).

To understand the response of HMLP structures by vortex loading, long-term monitoring of a single HMLP together with wind tunnel experiments were conducted. The experiments sought to study identify important aerodynamic parameters. The results of the wind tunnel and field results discussed in the report conducted by Chang (2010) were about the stresses caused by the wind, and the expected life. HMLP structure fatigue occurs at low wind speeds, 5-8 mph. At such wind speeds large crack propagation is caused by vortex-induced vibrations (Chang 2010). Field and experimental measurements offer insight into this behavior but can be prohibitively expensive. Computational Fluid Dynamics (CFD) offers another avenue of investigation. CFD code can be validated using physical wind tunnel experimental data.

The proposed research is a computational replication study of wind tunnel experiments on a dodecagonal (12-sided) rigid cylinder subjected to a range of velocities for both static and oscillatory cases. Wind tunnel experiments were performed to obtain aerodynamic parameters for a static cylinder case and to investigate the dynamic properties of a mass-spring cylinder case.

1.2 OBJECTIVES

The primary objective of the research project was to validate the computational fluid dynamic tools with comparison against wind tunnel experiments. Use of CFD permits simulation of complex, multi-physical problems in a finite domain. The only costs using CFD are computational resources and time for the CFD simulation to run when compared to the labor and material costs of conducting wind tunnel tests. The results of the wind tunnel experiments can used to validate CFD modeling. CFD offers an opportunity for exploratory investigation of how different wind conditions affect structural behavior.

The objective of the first validation was to compare static case wind tunnel data with CFD data for the drag forces of front and corner orientations of a dodecagonal cylinder at varying Reynolds numbers. The lift force on the static cylinder were studied at varying angles of attack for the front flat and corner orientations for the cylinder. This initial validation set the expectation for the accuracy of further simulations. The final validation was for the structural response of the cylinder at different Reynolds numbers corresponding to different vortex shedding frequencies associated with lock-in and in the reduced velocity range.

The dynamic response wind tunnel experiment was conducted with a weighted cylinder setup with various springs which limited the cylinder's movement to only the tangential direction in regard to the

freestream of the flow. Both the mass and spring contribute to the natural frequency of the system. The lock-in range is the range of fluid velocity, where the shedding frequency of the fluid flow matches the natural frequency of the structure. Vortex shedding occurs where the flow velocity becomes high enough that the flow separates from a body and creates an oscillatory region in the wake of the cylinder. Within the lock-in range, the greatest tangential displacement and movement of the pole is observed. During the CFD numerical simulation, the oscillatory motion was monitored for each validation case and the temporal effects were decomposed using a Fast Fourier Transform (FFT) to the component frequencies with the largest being for the vortex shedding frequency. This type of analysis permitted observations of the unsteadiness of the flow in terms of frequency. With the oscillatory behavior of the cylinder, the natural frequency can be seen super imposed on the frequency of the vortex shedding.

The CFD data compared to the wind tunnel experimental results permitted calculation of the expected accuracy and error of the CFD method. This validation demonstrates the usefulness of CFD fluid behavior simulation in a three-dimensional domain for a dodecagonal cylinder. This research sets the foundation for further studies of CFD applications to real world fluid flow situations. The validation of the CFD computational tool was performed using wind tunnel data on a small scale model of the dodecagonal cylinder. Once the CFD results are validated, various other conditions, including extreme winds or weather, can be simulated to see how the structure respond to different situations.

1.3 THESIS OUTLINE

This thesis is composed of seven chapters. Chapter 1 provides a general description of the goals of the research. Literature review and background are covered in Chapter 2 specifically with respect to fluid-structure interaction and fluid dynamics of civil structures. Chapter 3 and Chapter 4 provides the general background regarding the physics of vortex-induced vibrations (VIV) of cylinders, fluid physics, and the numerical models. Chapter 5 discusses applied procedures for using CFD models and the

considerations that need to be taken for the CFD simulations. The results and validation of the CFD approach with wind tunnel experimental data are discussed in Chapter 6. Chapter 7 provides conclusions and plans for future research.

CHAPTER 2. LITERATURE REVIEW

2.1 SECTION INTRODUCTION

The field of wind engineering can be described as the study of aerodynamics effects of man-made structures and the surrounding environment. This encompasses atmospheric development of its boundary layer and conditions of extreme winds like what is found in cyclones, the effects of wind and weather on urban and pedestrian centers, and structural aerodynamics. The current work focuses on computer-aided structural analysis and particularly focus on Computational Fluid Dynamics (CFD) with a cursory glance at other approaches. As used here the term "bluff-body" is defined as a body whose primary drag force arising from the pressure caused by a moving fluid.

Because computational modeling is significantly less expensive than physical modeling of structural performance, numerical techniques, such as CFD, are used by academics, industrial engineers, and scientists to predict the response of engineered features to natural forces. CFD allows for the creation of complex modeling at relatively low costs. This is an attractive alternative to costly wind tunnel experiments. CFD models can, for some physical cases, provide greater insight of structural response mechanisms. However, there are concerns about the accuracy and reliability of the results generated by CFD. Physical wind tunnel experimentation are often employed to validate the accuracy of the CFD results. Nevertheless, CFD can complement and support experimental fluid research.

The least computationally intensive approach is the Reynolds-Averaged Navier-Stokes (RANS) method, which models all scales of turbulence with the use of statistical averaging of terms. With all modeling, there can be inherent issues which limit applicability of the models to resolve certain physical parameters. For bluff-bodies, the main issues is the prediction for boundary layer transition and wake development from laminar to turbulent flow regimes. The modeling for turbulence becomes more

difficult for the wake at high Reynolds numbers, with increased influence of span-wise variance on the accuracy of predicted models. Some of the aforementioned issues can extend to Large Eddy Simulation (LES) models, especially in the boundary layer. The LES method models the smaller scale eddies. The most computationally expensive method is the Direct Numerical Simulation (DNS), which resolves all temporal and spatial scales. This leads to long computation times, which limit the applicability of DNS to simple flow cases.

Man-made structures can experience oscillating behavior from laminar to fully turbulent flows, but more commonly at high Reynolds number (Re). The oscillatory behavior is commonly quantified as vortex-induced vibration (VIV) frequencies, lift and drag forces, and other observable behaviors such as frequencies phases caused by other physical behaviors. Computational studies on bluff-bodies, such as triangular (Ng, Z. et al 2016) and square (Cheng, M. et al. 2007; Saeedi, M., et al. 2014) cross sections are less common. These studies have focused on lower Reynolds numbers, where the flows are laminar or transitional turbulent boundary layer regimes. The more common studies, such as with circular cylinders (Dong, S., and Karniadakis, G. 2009; Franke, J. and Frank, W. 2002; Elmiligui, A., et al. 2004) and bridge-rectangular (Lee, N. et al. 2016; Zhang, H. et al. 2016) sections, have a greater range of Reynolds numbers in the computational studies.

The bluff-body problems are normally treated as two-dimensional problems or extruded three-dimensional cases as non-deflecting, statically supported bodies. There has been an increased in studies on how simple bluff-body cylinders behave due to fluid motion caused by aerodynamic galloping (Tang, Y. et al. 2015) and VIV effects (Shimada, K. and Ishihara, T. 2012, and Alawadhi, E. 2013). Interest in Fluid-Structural Interaction (FSI) problems have furthered the development of approaches which couple CFD methods with other techniques to determine structural movement and response. Szabó, G., and

Györgyi, J. (2009) studied three-dimensional bridge aeroelasticity. Another three-dimensional bridge section studied was performed by Frandsen (2004).

Because of the nature of the conducted research this review focuses on simple bluff-body studies in two-dimensional and three-dimensional dealing with VIV, and other similar flow parameters such as fluttering and wind-induced structural deformation. An in-depth analysis was performed on the methods used and the relative accuracy of the methods. The review specifically scrutinizes complex problems with a focus on FSI and building dynamics influences on urban spaces.

2.2 STATIONARY CIRCULAR CYLINDER

Man-made, bluff-body structures typically experience low-to-moderate Reynolds numbers and extreme Reynolds numbers only in special cases. For Low Reynolds numbers where the flow is considered laminar, the fluids structures are treated as two-dimensional. When the fluid flow becomes turbulent, the eddy structures become three-dimensional in the wake of the bluff-body. Turbulent structures are difficult to simulate without vast computational resources, which is why different modeling approaches are considered. The three-dimensional structures need sufficient mesh resolution to be able to capture the fluid wake structures. This need for increased mesh resolution can be further exacerbated when considering the span-wise boundary conditions and the span-wise length, which would affect the full resolution of the wake eddy structures. All these considerations must be addressed by the model, especially for conditions affected by Vortex-Induced Vibrations (VIV).

2.2.1 LOW TO MODERATE REYNOLDS NUMBER

Circular cylinders are a common geometry for fundamental research in fluid dynamics. Great efforts have been made to study it experimentally (Roshko, A. (1961) & Williamson (1996)). These experimental studies can be used for the validation of computational results. Stationary cylinders

observed under a wide range of Reynolds flow conditions have well-established drag coefficients and Strouhal numbers (Roshko, A. 1961). These results for computational validation have led to studies for determining the sensitivity of results to specific parameters and determination of which parameters are needed and what parameters can be neglected. These cases are often subject for benchmarking new methods or currently established models.

Table 2.1 is a comparison of different computational results at varying Reynolds (Re) numbers. The Table includes a comparison to a few referenced experimental results. When the Re is low, the flow is laminar. As the Re increases, the flow becomes transient. Then, the separation of the flow becomes turbulent while the boundary layer is still laminar. There is a transition where the boundary layer becomes turbulent. Finally the flow becomes fully turbulent. For Section 2.2.1, most of the cases will have turbulent wakes with the flow growing to turbulent boundary layers around the object at high Re values. From the compared studies, little to no discussion of transition in the near wall boundary layer were found.

Table 2.1 Circular Cylinder Results

Re	Method	C_D	St	$-C_P$	Reference
200	DNS (30 Diameters)	1.3	0.19	-	Cao, S. et al. (2010)
300	FCM/FEM (2D)	-	0.17	-	Oñate, E., et al. (2007)
500	SGS-LES	1.25	0.21	-	Cao, S. and Tamura, Y. (2008)
800	FCM/FEM (2D)	-	0.21	-	Oñate, E., et al. (2007)
1000	Laminar	1.53	0.24	-	Rohde. A. (2011)
1000	Exp.	1	0.2	-	Williamson (1996)
1000	SGS-LES	1	0.22	-	Cao, S. and Tamura, Y. (2008)
1000	SL-LES (30 Diameters)	1.02	0.22	-	Cao, S. et al. (2010)
1000	SF-LES (2π*Diameters)	1.16	0.22	-	Labbé, D.F.L. and Wilson, P.A. (2007)
1000	SF-LES (π*Diameters)	1.2	0.22	-	Labbé, D.F.L. and Wilson, P.A. (2007)
1000	SF-LES (2π*Diameters)	1.2	0.22	-	Labbé, D.F.L. and Wilson, P.A. (2007)
2580	SL-LES (3D)	1.55	0.22	-	Liang, C. and Papadakis, G. (2007)
2580	Dynamic-LES (3D)	1.57	0.22	-	Liang, C. and Papadakis, G. (2007)
3900	Exp.	0.98	0.215	0.9	Ong and Wallace (1996)
3900	SL-LES	0.99	0.21	0.88	Franke, J. and Frank, W. (2002)
4×10^4	Exp.	1.19	0.19	-	Gopalkrishnan (1993)
4×10^4	DNS (40 Diameters)	1.12	0.21	-	Dong, S., and Karniadakis, G. (2005)
4×10^4	k-Omega SST (2D)	1.11	0.25	1.8	Rosetti, G., Vaz, G., and Fujarra, A. (2012)

5×10^4	Exp.	0.98-1.25	0.18-0.21	0.9-1.2	Elmiligui, A., et al. (2004)
5×10^4	SST-LES (2D)	1.69	0.21	2.05	Elmiligui, A., et al. (2004)
5×10^4	PANS (2D)	1.67	0.22	2.1	Elmiligui, A., et al. (2004)
5×10^4	SST-LES (3D)	1	0.22	0.9	Elmiligui, A., et al. (2004)
5×10^4	PANS (3D)	1.1	0.21	1.03	Elmiligui, A., et al. (2004)
5×10^4	SST (2D/3D)	1.08	0.23	1.03	Elmiligui, A., et al. (2004)
1×10^5	k-Omega SST (2D)	1.23	0.25	0.8	Rosetti, G., et al. (2012)
1.4×10^5	Exp.	0.62-0.74	0.28	0.85	Lakshmipathy, S., et al. (2010)
1.4×10^5	PANS k-ε (3D)	0.67	0.27	0.64	Lakshmipathy, S., et al. (2010)
5×10^5	k-Omega SST (2D)	0.28	0.3	0.75	Rosetti, G., et al. (2012)
10^6	Exp.	0.24	0.22	0.33	Shih et al. (1993)
10^6	k-ε RANS	0.4	0.31	-	Catalano, P., et al. (2003)
10^6	LES	0.31	0.35	-	Catalano, P., et al. (2003)

The flow around circular cylinders have patterns of behavior from laminar to fully turbulent flows based on the Reynolds number. This flow behavior holds true for other geometries. The flows below 150 Re are fully laminar with transitions occurring between 150 and 300 Re, where the flow becomes turbulent (Zdravkovich, M. 1997). For flows considered laminar, the flow equations are fully discretized with no modeling needed. The DNS method can be applied for higher Reynolds numbers, but the computational requirements limit widespread application. For higher Reynolds number, there are methods for modeling the turbulence scales that cut the computational time and allow for solving complex problems.

The flows at Reynolds numbers at 300 or lower can be simulated without modeling using a direct discretized form of the Navier-Stokes equations. This is referred to as Direct Numerical Simulation (DNS), when dealing with turbulent flows. This discussed in the report by Cao, S. et al. (2010). The study was conducted with three-dimensional DNS for low unsteady Reynolds flow to investigate the shear effects on the cylinder flow. The conclusion of the Cao report, regarding this flow, is that wake instability was suppressed. This leads to a two-dimensional type of problem for cases with non-shearing

flow, Figure 2.1a. Cao believes three-dimensional effects do not need considered for laminar flow cases. The rest of the Figure 2.1 shows transition occurs around a Re of 200 from laminar to turbulence with addition of fluid flow braiding caused by the von Karmen shedding. In Figure 2.1d the fully turbulent wake can be seen in the case of Re of 1000.

Another study regarding laminar flow problems was performed by Choi, H. (2004) which focused on the behavior of the flow affected by suction/blowing forces acting on the cylinder. These forces reduced the intensity of oscillations in the wake but were found to have no effect on the laminar cases. Oñate, E. et al. (2007) applied a modified finite element method (FEM) discretization scheme termed the finite-calculus method (FIC). FIC is derived using the balancing laws in mechanics with the use of a space-time domain of finite size and with new terms that detail the space-time characteristics. This was used for Re number ranging from 100 to 1000. The cases of Re numbers of 300 and 800 are shown in Table 2.1.

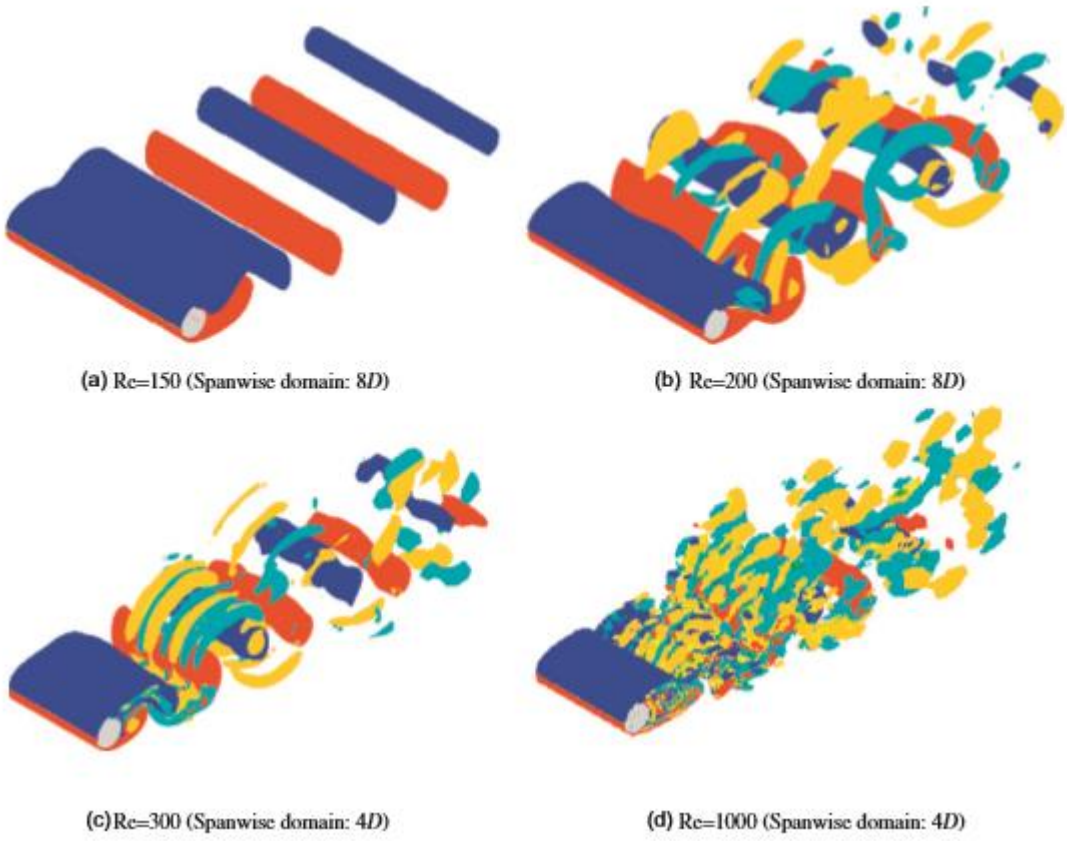

Figure 2.1 Isovorticity Surfaces of Instantaneous Wake (Cao, S. et al. 2010)

Rohde, A. (2011) applied the total diminishing principle to develop an inviscid form of the Navier-Stokes equations. These were applied to solve two-dimensional compressible flow around a cylinder. The flow at sub 100 Re produced two-dimensional laminar flow. Flows at a Re of 1000 showed turbulent vortex shedding. Cao, S. and Tamura, Y. (2008) use an SGS-LES approach and a Re of 1000 to study the two-dimensional flow case with shearing flow behavior at the inlet. Lift and drags forces became dependent on the asymmetric behavior of the inlet, while the vortex frequency was independent of the shear flow.

Results and experimental comparisons from the studies addressed prior in Table 2.1, and in Section 2.2.1 showed reasonable accuracy because they addressed problems dealing with flow over a cylinder. These studies were done with little concern to the span-wise effects of the turbulence structures. Labbé,

D.F.L. and Wilson, P.A. (2007) included the span-wise length effects that develop the turbulence structures at Re of 1000, Table 2.1. The span-wise variations were considered shorter than the cases for laminar VIV, suggesting less than four diameters of the span-wise direction were sufficient for accuracy. From their study, it is suggested that the assumptions can be considered for higher Reynolds number, but they failed to describe under what range. The minimum span-wise length was concluded to be satisfactory for flows below the subcritical range, for a circular geometry.

Regarding computation resources, the studies discussed here show direct discretization or LES modeling were sufficient for unsteadiness, transitional, or the fully turbulent regime. Labbé, D.F.L. and Wilson, P.A. (2007) applied a high order, Structured Function LES which provided the necessary accuracies for modeling smaller eddies, where structure function over predicted the local fluid forces. Cao, S. and Tamura, Y. (2008) and Choi, H. (2004) applied a standard SGS-LES formulation to study the flow around a cylinder. When compared to experimental results their coefficients are accurate, Table 2.1.

Liang, C. and Papadakis, G. (2007) performed a study to see how pulsating affects the flow and wake of the cylinder, using two different LES approaches at a Re of 2580. Their two models were the dynamic model approach and the standard Smagorinsky model. It was found that the non-pulsating flows had comparable results with experiments. When pulsating was included, the drag increased as expected and shedding frequencies remained unchanged.

2.2.2 HIGH REYNOLDS NUMBER

At higher Reynolds numbers, it is predictable for the flow to become more turbulent with a wider range of eddy length scales. What proved to be accurate numerical approaches for low Reynolds flows such as LES or different direct discretization methods are not good predictor at higher Reynolds number

flows. This is a result of greater need for mesh and temporal resolutions to capture all the necessary flow detail. Such a requirement lead to increased computational times. Different turbulent approaches have a greater diversity with the use RANS modeling, hybrid RANS-LES approaches, and LES modeling, because of this. Hybrid methods, generally, are RANS equations which are used for smaller scale modeling in the near wall region. The LES, after the transition from RANS modeling, will simulate the larger eddy structures in the wake and flow field.

DNS was applied for fully turbulent flows by Dong, S., and Karniadakis, G. (2009) for a stationary and oscillating cylinder. The results for a Re of 10000 showed reasonable accuracy when comparing the drag coefficient and Strouhal number to expected experimental results in the report of Dong, S., and Karniadakis, G. (2009). This comparison represented the stationary case only. The study was performed using a cylinder length of 40 diameters, with comparison of the spectral elements and span-wise mesh dependencies. Another study used the k-ω SST in a two-dimensional domain at a Re range of 100 to 10^4. The lower Reynolds numbers shared comparable drag force compared to experimental results. However, at greater Re values, the k-ω SST over predicts the force coefficients.

A comprehensive study performed by Elmiligui, A., et al. (2004) using different turbulence modeling approaches at a greater Re numbers used two-dimensional and three-dimensional cases. The two turbulence cases compared were the Partially-Averaged Navier-Stokes (PANS) and a hybrid Spalart-Almaraz (SA) RANS-LES approach, Table 2.1. The two-dimensional cases showed higher lift and drag coefficients when compared to experimental numbers. The shedding frequency, in these cases, is close to experimental values. When extending the domain to three-dimensional the results for coefficients, such as pressure and drag, were within the expected range, Table 2.1. This indicates three-dimensional factors needed to be considered, especially with methods that reduce the modeling for several of the eddy

scales. Two-dimensional and three-dimensional RANS cases were compared with no variation in lift coefficients, drag coefficients or Strouhal number.

Another high Reynolds numbers study was the PANS k-ε work by Lakshmipathy, S., and Girimaji, S. (2010). Three-dimensional factors were considered and proved to give reasonable results when compared to experiments. For higher Reynolds number, Rosetti, G. et al. (2012) and Catalano, P. et al. (2003) at Re 5×10^6 and 10^7, performed RANS k-ω formulations, with what was discussed as accurate results for what was done in the study.

2.3 OSCILLATING CYLINDERS

A stationary bluff-body experiences vortex shedding at Re numbers ranging between 40 and 150 for laminar flow and becomes fully turbulent beyond a Re number of 300 (Zdravkovich, M. 1997). Cylinders are rarely stationary and have some movement associated with them. Additional movement caused by vortices is called Vortex-Induced Vibration (VIV). In extreme cases for large deflections, the velocity range is referred to as the lock-in region, where the natural frequency of the structure matches the frequency of the vortex shedding. This complex problem has led to many experimentally and computational studies. Stationary cylinders at moderate to high Re numbers require vast computational resources to solve Fluid-Structure Interaction (FSI) problems. FSI require moving mesh methods, therefore increase computational time (Lee, A.H., et al. 2014).

2.3.1 MODELING APPROACH

The laminar flow cases (Re < 150) of Abdullah, M., et al. (2005); Zheng, Z., and Zhang, N. (2008); Chern, M. et al. (2014); Chern, M. et al. (2017) used a Direct Numerical Simulation (DNS) approach with different techniques that handled the additional forces and deflection terms. A common agreement was found amongst the mentioned studies was that applied methods were sufficient to predict the

movement, frequencies and force coefficient of an oscillating cylinder. This was not the case for Abdullah, M., et al. (2005), where the coupling approach did not offer accurate capturing of the selected lock-in velocities.

Availability of computing power limits the applicability of DNS and LES approaches for complex fluid problems such as FSI cases. DNS was applied in the studies of Xie et al. (2012) and Bourguet, R, et al. (2011). In the Bourguet, R, et al. (2011), mentioned the requirement to have 512 cores to have sufficient calculating the time steps for mesh displacement. Jus, Y., et al. (2014) applied a standard LES approach which over predicted force coefficients. High Performance Computing (HPC) resources are needed to model the moving mesh. DNS and LES approaches offer accurate results for moderate Re numbers (Re < 5000), but available computer resources prohibit the widespread application of both approaches.

Researchers lacking access to HPC resources have also tried other approaches. Lee, A.H., et al. (2014), computational time limited the range of their study with only a few span-wise cases and a two-dimensional case for the oscillatory movement. The modeling approaches often considered are RANS or hybrid RANS-LES approach. In the study performed by Chen, W. and Li (2009), a SST RANS model was used. The general behavior was examineded with regards to the wake. A Delayed-Detached Eddy Simulation (DDES) hybrid approach was used in the study by Lee, A.H., et al. (2014). DDES was able to model the turbulence behavior in the study and was within the acceptable range of %-difference when compared to expected results.

2.3.2 MOVING MESH TREATMENT

Chern, M. et al. (2014), and Chern, M. et al. (2017) used the Direct-Forcing Boundary method (DFB) for VIV effects on the structure. DFB adds a virtual displacement term in the Navier-Stokes. It acts

based on the expected behavior of the cylinder movement, without the need of mesh updating at each time step for any discretization method. The accuracy of the methods are show in Figure 2.2, which compared the experimental results of the St (Roshko 1953). A similar study by Zheng, Z., and Zhang, N. (2008) showed another non-moving mesh approach, called the Immersed Boundary Method (IBM). The IBM approach modifies the Navier-Stokes equations using a velocity correction term for the near wall mesh to calculate the forced displacement. The IBM method used by Zheng, Z., and Zhang, N. (2008) predicted full scope of the lock-in behavior.

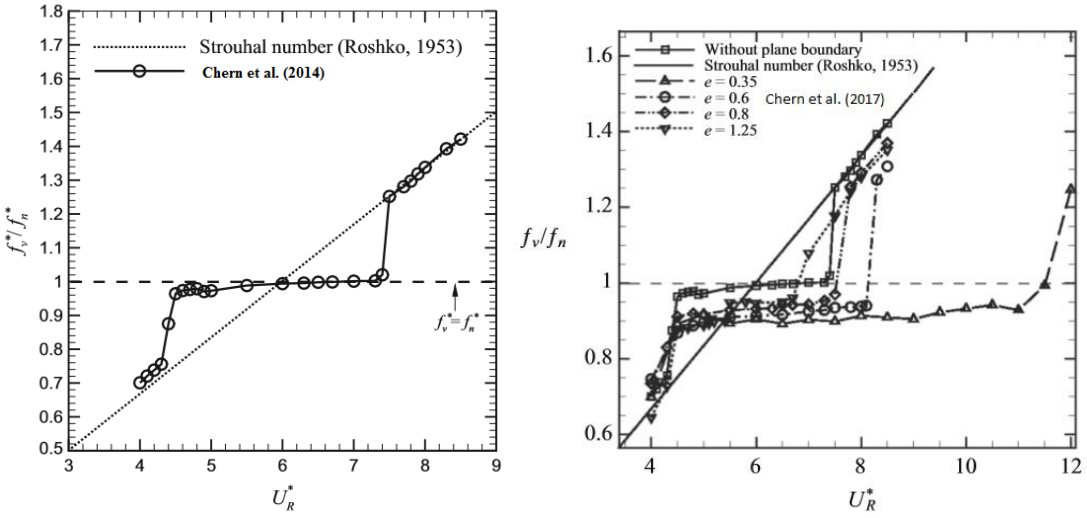

Figure 2.2 Lock-in Results (Left) (Chern, M. et al. (2014)); (Right) (Chern, M. et al. (2017))

The traditional approach for dealing with FSI cases uses moving mesh techniques with solid and fluid solvers. An early study by Abdullah, M., et al. (2005), for low Re of 108.5 and 115 corresponding to lock-in, created a coupling method of segregated solvers, which calculated the displacement caused by the force and then updated the mesh with the new coordinates of the cylinder. The coupled solvers showed unexpected displacement behavior where lock-in occurred and was considered inaccurate.

Jus, Y., et al. (2014) used an Arbitrary Lagrangian Eularian (ALE) approach to handle the moving mesh, which impacts on the convective term of the Momentum equation. Lee, A.H., et al. (2014), applied a fixed-point iteration Finite Element Analysis (FEA) to deal with the moving boundary. This iteration

completes calculations using the forces for the expected displacement of the solid boundary. ALE and the FEA solvers were able to replicate the expected displacement amplitudes occurring in the lock-in range. The moving mesh behavior can be seen in Figure 2.3.

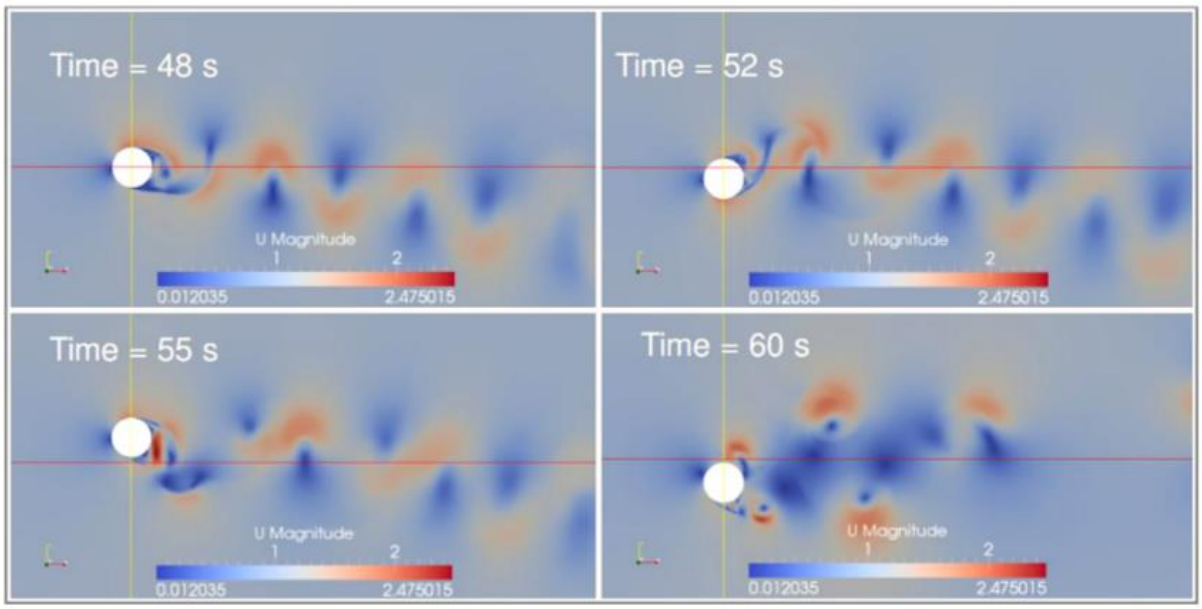

Figure 2.3 Cylinder Displacement Oscillation Behavior (Lee, A.H., et al. 2014)

For a flexible cylinder, Xie, Deng, Xiao and Yao (2012) used the Euler-Bernoulli beam theory that was discretized with Finite-Difference schemes to handle the expect behavior. This showed the extreme amplitude cases for oscillation and that structural deformation affects the wake structures. Bourguet, R, et al. (2011) used a spectral method approach which applies a hybrid scheme which employed a Fourier expansion for the span-wise direction and directs the Jacobi-Galarkin formulations. The approach provided insights and original observable behavior on the cylinder dynamics. Chen, W., and Li (2009) also studied the wake behavior to observe the frequency modes in the wake.

2.3.3 SPAN-WISE EFFECTS

Laminar flow cases are inherently two-dimensional, as previously shown in Figure 2.1a and the two-dimensional assumptions of Abdullah, M., et al. (2005), Chern, M. et al. (2014), and Chern, M. et al.

(2017). For these cases, the lock-in behavior can be observed within the lock-in velocities below turbulent wake transition.

For turbulent cases, the span-wise length becomes more important because the turbulence scales are inherently three-dimensional. For the deforming cylinder cases the span-wise lengths were selected by Xie et al. (2012), Chen, W. and Li (2009), and Bourguet, R, et al. (2011) to provide sufficient length for cylinder wakes to develop. It was observed that the deflections in the cylinder contributed to the wake structures in scales and amplitudes. To see what impact the span-wise length might have Jus, Y., et al. (2014) selected span-wise lengths within the range of four diameters and with a minimum span-wise length of least twenty diameters (Chen, W. and Li 2009). The lengths were selected on per bluff-body problem basis with no uniform agreement on a minimum or maximum span-wise length requirement.

Lee, A.H., et al. (2014) provided in depth study of the span-wise length using a variant of different lengths at a fully turbulent regime of 5000 Re. The results for a two-dimensional domain were sufficient for collecting information regarding the vortex shedding frequency and force coefficients. The issue with this approach was the amplitudes for displacement were over predicted. This led to another observation made by Lee, A.H., et al. (2014) that the span-wise length has a fundamental importance effect. The minimum length was not determined for accurate displacement.

2.4 TRIANGULAR CYLINDERS

Symmetrical Cylinders produce symmetrical characteristic wakes, like a circular cylinder. This is the case for other geometric bodies such as triangles or squares as a common reference, but changes with the inclination angle. Asymmetrical wakes form with different wake phases and separation points. Studies by De and Dalal (2006), Wang et al. (2015), and Tu et al. (2014) used low Re values ($Re < 200$) to study the standard force coefficients and flow frequencies at different angles of attack with little

deviation in terms of coefficients. A study by Ng, Z. et al. (2016) used a high-order spectral element technique, which yielded similar results (Table 2.2) with the techniques used in previous studies. Previous studies used common discretization techniques such as Finite Volume Method (FVM) and Finite Element Methods (FEM).

Table 2.2 Results for Triangular Cylinder at Re = 100

Angle	St	C_D	C_L	References
0°	0.197	1.761	0.297	De and Delal (2006)
	0.196	1.71	0.285	Wang et al. (2015)
	0.195	1.704	0.284	Ng et al. (2016)
60°	0.154	2.122	0.742	Tu et al. (2014)
	0.154	2.097	0.733	Wang et al. (2015)
	0.153	2.055	0.731	Ng, Z. et al. (2016)

The flows were at Re numbers of less than 200, where the flows can be considered fully laminar without any consideration for turbulent effects. This allowed for the assumption of two-dimensionality. The common findings amongst all the referenced studies is the symmetry caused two similar size recirculation bubbles to form behind the cylinder. However, flow separate occurred with increasing angles of attack. The use of the Stuart-Landau relation (Ng, Z. et al. 2016) determined critical Re occurs at 35, at angles between 18° to 30°.

At a sufficiently high Re value, vortex shedding occurs. It is a repeating pattern of swirling vortices, known as von Karman vortex sheets. The oscillating fluid over the object causes forces on the object to oscillate, leading to object vibration. Alawadhi, E. (2013) performed a comparison study to the work done by De and Dalal (2006) at a Re number of 100 for a stationary symmetrical triangular cylinder with reasonable accuracy between the two cases. Alawadhi, E. (2013) proceeded to investigate the force coefficients and flow frequencies at different oscillatory amplitudes. His work found that the lift

coefficients matched the experimental lift coefficient of the stationary, triangular cylinder, but with higher RMS values of lift with higher oscillations. For higher oscillations, the average drag value was found to decrease.

2.5 STATIONARY RECTANGULAR CYLINDERS

There a subset of fluid dynamic cases dealing with rectangular bluff-bodies, including square cross sections. The more common wind engineering studies involve structures with circular bluff bodies. These are typically supporting columns or heat exchangers. Rectangular bluff-bodies are used in buildings and other structures (Cimarelli, A. et al. 2018). Square geometries are common for skyscrapers and large structures (Tayyaba Bano et al. 2012). The difference between circular and rectangular bluff bodies is the large-scale flow separation caused at the leading edge for the rectangular bluff bodies. There is also flow reattachment before separation at the trailing edge (Cimarelli, A. et al. 2018). Extended cases found the appropriate modeling to accurately model the mean flow parameters are important for validation for more complex cases (Patruno, L. et al. (2016); Mannini, C. et al. (2011)). Other studies look to the physical characteristics of the shear flows and separation (Cheng, M. et al. 2007).

2.5.1 MODELING APPROACH

For low laminar Re number values, problems can be solved with using Finite Element Methods (FEM) or Finite Volume Method (FVM) DNS approaches. There are different approaches for the discretization of the Navier-Stokes equations. A common discretization technique is the Lattice-Boltzmann Method (LBM), which is based on the microscopic models and a mesoscopic kinetic equation for particle distribution (Cheng, M. et al. 2007). A benefit of using the LBM is the computational advantages. The main goal of Cheng, M. et al. (2007) was to study shear rates of the flow over a square cyldrical cross-section at low Re number values in the laminar regime and low transitional range. Cheng

found that increasing shear rates and increasing Reynolds number (Re) lead to decreased force statistics acting on the body.

For fully developed turbulent flows, there are more options on how to deal with turbulence prediction. A rectangular case, at a Re number of 3000, with DNS was completed in Cimarelli, A. et al. (2018). The goal of the study was to shed light onto the physical mechanisms for fully turbulent flow over rectangular body. The study involved a symetrical rectangular body uniform along the flow field, which provided statistics that allowed for quantification of inaccuraries. The two statistics developed from the study are a the span-wise correlation function and an energy spectrum used to find the pressure and velocity functions. Tayyaba Bano et al. (2012) study was at high Re number, between 3000 and 8000, with no turbulence modeling. The flow cases showed an agreement for the Strouhal number and force coefficients with Manzoor et al (2010). The main goal of the study was to simulate physical parameters that would cause a cylinder to begin to oscillate. The numerical results are for a stationary cylinder where the force results could then be used to calculate the displacement as if it was moving mesh approach.

In cases dealing with higher Re values, where the flow is fully turbulent, a mixture of modeling approaches are considered instead of the DNS approach. The work of Patruno, L. et al. (2016) had similar parameters compared to the works of Mannini, C. et al. (2011), Bruno et al. (2010), and Grozescu et al. (2011). Both the work by Bruno et al. (2010) and Grozescu et al. (2011) use the standard LES approach for flow over a 5:1 ratio rectangle at 0° angle of attack. At Re numbers above 2.7×10^4 (Table 2.3), the common dimensionless flow parameters were compared using LES modeling in the study by Patruno, L. et al. (2016). Patruno's work used additional k-ω RANS approach for the comparison. The compared works had similar results with little deviation from the expected experimental results. When compared to the work of Mannini, C. et al. (2011) that applied a hybrid RANS-LES approach there was lower coefficients than the other comparative studies shown in Table 2.3.

Table 2.3 Aerodynamic Coefficient for Rectangles

Angle	Re	C_D	C_L	St	Reference
0°	2.70×10^4	1.02	-0.05	0.132	Patruno, L., et al. (2016) (LES)
	2.70×10^4	1.12	-0.02	0.121	Patruno, L., et al. (2016) (URANS)
	5.50×10^4	1.13	-0.04	0.118	CRIACIV (2015) (Exp.)
	2.00×10^4	1.03	0	0.111	Schwee (2013) (Exp.)
	4.00×10^4	0.96-1.03	-0.315 to -0.0024	0.112-0.122	Bruno et al. (2011) (LES)
	$2.0\text{-}4.0\times10^4$	0.97-0.98	0.97-0.98	0.107-0.111	Grozescdu et al. (2011) (LES)
	2.64×10^4	0.97-1.07	0.0032-0.047	0.094-0.102	Mannini (2011) (DES)
1°	2.70×10^4	1.05	0.74	0.119	Patruno, L., et al. (2016) (LES)
	2.70×10^4	1.16	0.75	0.116	Patruno, L., et al. (2016) (URANS)
	5.50×10^4	1.28	0.96	0.12	CRIACIV (2015) (Exp.)
4°	2.70×10^4	1.26	1.44	0.116	Patruno, L., et al. (2016) (LES)
	2.70×10^4	1.57	2.8	0.117	Patruno, L., et al. (2016) (URANS)
	5.50×10^4	1.63	2.02	0.126	CRIACIV (2015) (Exp.)
	2.00×10^4	1.4	2.55	0.115	Schewe (2013) (Exp.)

It is generally agreed that for high Re values turbulence modeling is more economical with computational resources than purely resolved approaches such as DNS. For high Re values in the Finite Element Method (FEM) framework, there are instabilities in the RNG k-ε caused by the convective terms (Jeong, U.Y. et al. 2002). For the work conducted by Jeong, U.Y. et al. (2002), at an Re of 22,000, the FEM was replaced with the streamline-upwind/Petrov-Galarkin (SUPG). For incompressible conditions within the flow, the velocity term is replaced with a penalty term that enforces treatment with artificial diffusivity functions. This method seemed to offer a stable solution for complex geometroc flows at high Re numbers, while providing comparable results for square geometries for LES and other URANS cases.

2.5.2 SPAN-WISE EFFECTS

Often the applicability of new method for different cases are tested with laminar flow because of the simplicity of the flow and because laminar flows can be considered two-dimensional. Laminar flow was

used in the study conducted by Cheng, M. et al. (2007). The primary consideration for span-wise two-dimensionality is to reduce computational time as grid sizing is proportional to computational time. This can be further compounded for more complex flowswhich become more computationally intensive.

Jeong, U.Y. et al. (2002) applied a new discretization formulation to handle high Re number instability. For moderate (Re < 5000) Re numbers the initial two-dimensionality studies benefit from the work by Tayyaba Bano et al. (2012) studing general fluid behavior.

Turbulent flows have three-dimensional eddy scales that need to be considered, especially for accuracy of results. Three-dimensionality was considered in the studies by Mannini, C. et al. (2011), Bruno et al. (2010), Grozescu et al. (2011), Patruno, L. et al. (2016), and Cimarelli, A. et al. (2018). There was, however, a failure to consider the span-wise length in the discussion for the inherent three-dimensional behaviors of turbulence. The study of Mannini, C. et al. (2011) mentioned the length of 1:1 or 2:1, in terms of span-wise length to reference length, was not long enough in the span-wise direction to show the full three-dimensional effects. Future studies need to consider span-wise dependency.

2.6 OSCILLATING RECTANGULAR CYLINDERS

Oscillating rectangular cylinders can experience similar Vortex-Induced Vibrations (VIV) effects similar to a circular cylinder body. When both rectangular and cylinders have symmetrical cross sections, the von-Karmen vortex shedding occurs. Unlike circular cylinders, rectangular cylinders can rotate that lead to asymmetric cross-sections to the corners of the rectangle cylinders leading to different flow development. Lock-in behavior is one phenomena of interest, but rectangular cylinders can rotate do the flow effects as well.

2.6.1 MODELING APPROACH

A study by Zhao, M. et al. (2013) used a FEM discretization approach to model laminar flow at a Re of 100. The study presented three cases at different angles of attack for the position of the cylinder corner. The stationary at an angle of 0° was compared to several two-dimensional cases of A. Sharma and V. Eswaran (2005), with little variation from C_D of 1.494 and St of 0.148. One of the cases compared was R. M. Darekar and S. J. Sherwin (2001) with the notable difference being three-dimensional but with similar results for C_D of 1.486 and St of 0.1460. The study of Zhao, M. et al. (2013) went on to present the square cylinder at different angles of attack of 45° and 22.5°, with high C_D of 1.877 at 45°. Shown in Figure 2.4 are the wake contours of different angle of attacks for a square cylinder. The widest wake field was at 45° while the narrowest was at 0°.

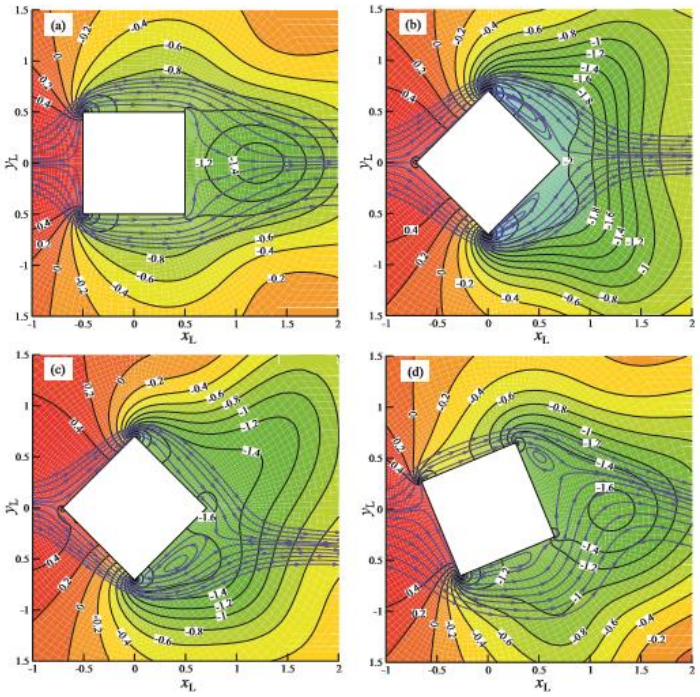

Figure 2.4 Streamlines based on the mean relative velocity and contours of the mean pressure coefficient for different flow approaching angles. (a) α = 0◦ and Vr = 5; (b) α = 45◦ and Vr = 8 att = 48.8; (c) α = 45◦ and Vr = 8 att = 62.5; (d) α =0◦ and Vr =22.5. (Zhao, M. et al. 2013)

A FEM approach was used by Singh, S., and Biswas, G. (2013) for lower end of the subcritical Re values where the flow is still laminar. Their results were considered accurate when comparing force coefficients. St. Leontini, J.S., Thompson, M.C. (2013) studied a rectangular cylinder at angle of 45°

with a Re number of 200. For a circular cylinder, this Re is within the transition region for the wake from laminar to turbulent. The DNS approach demonstrated that the transition can appropriately be modeled in this case. From a sharp upper corner on the squares, the St and C_D values become dependent on the increase corner radius reduction and the Re number for the stationary case. For the elastically mounted case, sharp corners vary the wake characteristics while reduction in the corner sharpness reduces the variation.

The early work of Murakami, S. et al. (1997) applied a three-dimensional LES approach for a square cylinder at a 0° angle of attack. The standard LES was able to reproduce the expected heavy displacement when the vortex shedding frequency matched the natural frequency of the structure. The benefit at the time for the study was to determine the useful statistics from the fluctuating pressure fields on the square. However, the researchers suggested that the more developed SGS method should be used for complex building dynamics. While there was no discussion in span-wise dependencies they found the flow field to be three-dimensional and the span-wise length only two diameters deep.

The works of Bunge, U. et al. (2003) offered a study of the rectangular characteristic length effects on the flow. Their DES hybrid approach used the SA RANS model for near wall treatment and a standard scale filtering method for the LES regimes. The problem was described as three-dimensional, with no consideration of the span-wise dependencies, even with a fully turbulent flow of around 4×10^6. They did discuss limitations in the computational resources with LES or DNS approaches. Specifically, the DES they used and the coupled method were inadequate for the frequency capturing at the time.

In a similar flow regime Bunge, U. et al. (2003) and then Shimada, K. and Ishihara, T. (2012) used the k-ε turbulence model at a Re number of 22,000 for studying rectangular instability or torsional rotation. The behavior matched the expected single degree-of-freedom torsional motion. The best cases

were for low mass ratios where the torsional rotation was seen at a reduced velocity (Ur) of 12. Further research would be needed for more complex geometries, instead of only two-dimensional behaviors.

2.6.2 MOVING MESH TREATMENT

Zhao, M., et al. (2013) considered the forces of a fluid acting on a square body to calculate the displacement of the cylinder. Then they used an ALE approach for the moving meshes. The angle of 0° showed the narrowest lock-in regime. The larger angle of attack (up to 45°) presented a wider range of lock-in behavior. Overall, the method was found to be accurate. The early work of Murakami, S. et al. (1997) added an inertia term that handled the added forces in the fluid. This approach was described as offering results similar to the ALE approach.

Bunge, U. et al. (2003) considered a coupled approach relying on the Space Conservation Law to deal with the moving boundaries. The approach calculated the forces allowing the displacement amplitude to be calculated from the expected forced displacement. The method was described as an implicit, loosely coupled approach which captured behavior of lock-in. The approach was not accurate in terms of calculating forces on the body. Leontini, J.S. and Thompson, M.C. (2013) used a similar higher-order discretization coupled solver approach for displacement.

2.7 LARGE SCALE STRUCTURES

All structures should be designed to withstand the effects of the wind. Design and analysis of large structures with wind tunnel testing can be costly, time consuming, or even impractical. Consequently, research has focused on creating numerical models to replace or supplement wind tunnel testing. The main categories of this research are large-scale bridges and buildings.

2.7.1 BRIDGE SECTIONS

The Mack Blackwell Transportation Center at the University of Arkansas simulated the flow forces acting on a bridge with the use of different turbulence models. From this work, a LES model in a Finite Element Method (FEM) framework provided the agreeable results. The grid influence was scrutinized to understand its effect on critical velocity impacting conditions of flutter and non-flutter interactions. The flow behavior was studied with experimental and numerical methods at a Re number of 1×10^5 (Selvam and Govindaswamy 2001).

A URANS model was used to study the feasibility of implementing less computationally expensive models for the study of bridge fluttering. The results were compared to experimental wind tunnels tests. For a rigid bridge model, the pressure distribution showed positive agreement with measured results. The URANS models did not accurately predict the separation bubbles around sharp corners (Sarkic, et al. 2012). A similar study was completed to consider the capabilities and limitations of CFD to evaluate the dynamic loading of aeroelastic bodies with bridge instabilities due to wind turbulence. Considering structural fluttering, the flutter derivatives were in positive agreement with experimental results. The compared turbulence models k-ε, k-ω and k-ω SST turbulence models offered similar results for the common aerodynamic parameters (i.e. C_D, C_L, St, etc.). On the other hand, it was shown that the k-ω SST has less sensitivity to inlet parameters making it the preferred model for future studies (Brusiani et al. 2013). The study simulated a two-dimensional bridge deck section with a two-dimensional dimensional bending and torsional FSI model. The work focused on the feasibility of incorporating CFD in the design stage of long span bridges. The study provided that current commercial CFD codes were sufficient for early work where the critical velocity of fluttering was needed to be determined. The compared CFD results were in positive agreement with the results from the experimental process (Attia and Ahmed 2016).

2.7.2 BRIDGES

Long-span bridges are particularly susceptible to the effects of wind. This type of wind-structure interaction (Carassale and Solari 2006) was simulated using Monte Carlo procedure to simulate complex wind-excited structures of the Messina Strait Bridge. The method can be applied to perform time-domain dynamic analysis of multi-degree-of-freedom nonlinear structures and situations involving complex topography. Schemes for representing three-dimensional turbulence over discretized spatial domains along with parallel computing techniques have been considered in order to reduce computing time. Figure 2.5 shows the bridge turbulence model with low frequency turbulence statistics used to calculate the eigenvalues for a long span-wise bridge. At higher frequencies, the behavior then became more localized.

The nonlinear effects of wind-structure interaction becomes non-negligible in the case of long-span suspension bridges. Zhang et al. (2002) considered large deformation under static wind loading, using three-dimensional nonlinear aerostatic and aerodynamic analysis. Chen and Kareem (2001) obtained similar results to Zhang et al. (2002). The study of Chen and Kareem (2001) predicted the nonlinear response of long-span bridges under turbulent winds using a time domain analysis framework. The model was a nonlinear, unsteady aerodynamic force using static force coefficients, flutter derivatives, admittance functions, and their span-wise correlations at varying angles of incidence. The approach was compared to the conventional linear method for analyzing the forces on a long-span bridge. The nonlinear method produced a slightly higher response than the conventional linear method.

A semi-infinite two-dimensional bridge sections in the span-wise direction was simulated to understand the full effect of turbulence on structures. CSD-CFD was performed with the inlet flow being increased until the critical flutter speed was found, Szabó, G. and Györgyi, J. (2009), where the motion amplitude started growing.. Besides these linear and nonlinear approaches, stability threshold and pre-critical behavior of cross-sections of long span bridges can be predicted with a time-domain indicial

approach (Costa and Borri 2006). Another method for simulating wind-induced bridge motion is finite element fluid-structure interaction. Frandsen (2004) applied this method with the incompressible Navier-Stokes equations in both Lagrangian and Eulerian reference frames. The fluid flow was fully coupled with an idealized, lumped mass, spring-dashpot system to simulate the bridge. Frandsen aimed to predict the flutter limit of the bridge and reduce the number of physical models needed to evaluate such a structure.

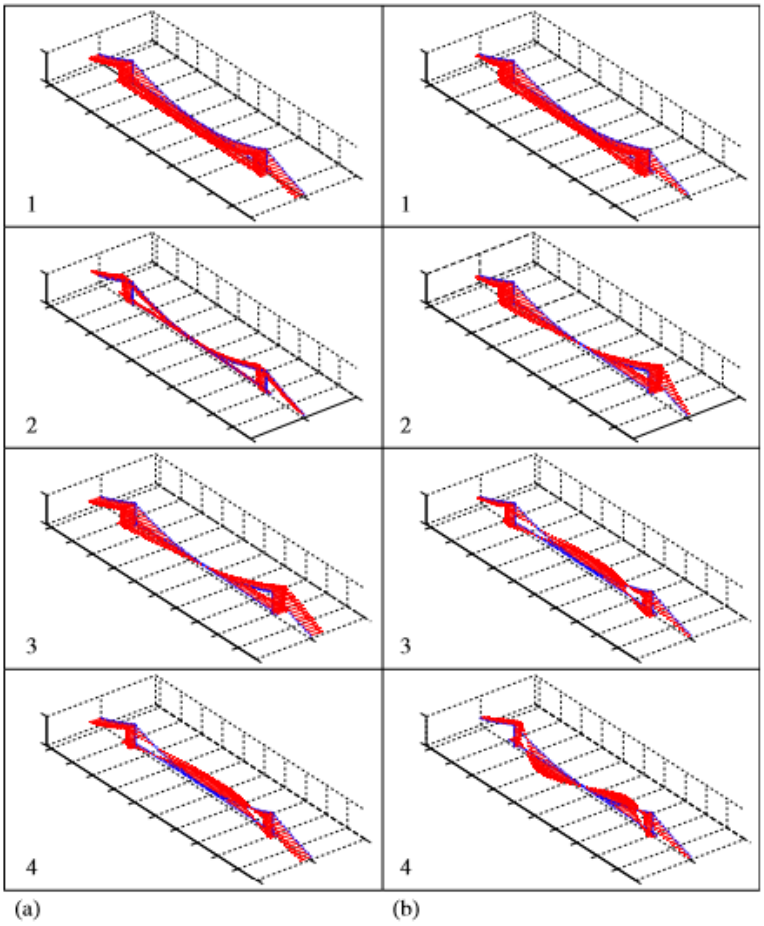

Figure 2.5 Turbulence eigenvectors for the frequency nk = 910-4 Hz (a), nk = 10-2 Hz (b) (Carassale and Solari 2006)

While bridges are susceptible to wind. Partially constructed bridges in the cantilever state can be even more susceptible to wind loading. Ying Zhou, Q.-L.Z. and Zhen-Hua Liu (2009) used ADINA software to create a fluid-structure simulation of a partial bridge situation. The wind-induced dynamic

coefficients and the wind pressure distribution coefficients were calculated to aid design and construction planning.

2.7.3 BUILDINGS

Wind loading, and wind effects become a significant consideration when designing high-rise buildings. Simulating wind effects on full-scale tall buildings using Large Eddy Simulation (LES) had been computationally impractical until recently because of the large meshes required. Huang, Lau et al. (2011) proposed a hybrid approach that combines Reynolds-Averaged Navier–Stokes (RANS) Consideration of wind loading and wind effects is a significant consideration when designing high-rise buildings. Simulating wind effects on full-scale tall buildings using Large Eddy Simulation (LES) had been computationally impractical until recently because of the large meshes required. Huang, Lau et al. (2011) proposed a hybrid approach that combines Reynolds-Averaged Navier–Stokes (RANS) simulation, which requires coarse meshes, and mesh-free Kinematic Simulation (KS). An LES approach was compared to wind tunnel experiments for a static structure. A DES approach was then applied to study VIV influences on the CAARC model (Zhang, Y. et al. 2015). The understanding from this phenomenon is important for general structural stability and occupant comfort.

The work of Saeedi, M. et al. (2013) and Tominaga (2014) studied the flow field around large rectangular structures, similar to skyscrapers, at different ranges of Re values. Saeedi, M. et al (2013) used DNS at a Re number of 12,000 to determine the general behavior of a fluid moving around a structure, and how the forces and pressures develop. Shown in Figure 2.6 is the development of the wake where the tip vortices develop from top of the structure and von-Karmen vortex sheets separate behind the building. It was noted by the researchers Saeedi, M. et al (2013), the challenge for DNS applied to bluff-bodies had issues for predicting accurate body pressures along with the interaction of vortex shedding and tip vortices. Tominaga (2014) noted the importance of accurate force predictions on a

bluff-body and how accurate methods for modeling were needed. When comparing the more common turbulence modeling to the SST model, the SST provided the most accurate predictions.

Recent research has not been restricted to just buildings with large vertical dimensions. But there has also been studies of long-span roofs. Zhang Enuo et al. (2005) analyzed wind-induced vibrations of large span roof structures using as a test from a developed program along with the use of finite-element software. The accuracy and effectiveness of their method was verified through analysis of existing projects. Lu, C.L. et al. (2012) used CFD to model wind effects on a more complex long-span roof. Inflow boundary conditions were modeled using the discretizing and synthesizing random flow generation (DSRFG) approach along with a new one-equation dynamic sub-grid scale (SGS) model for Large Eddy Simulation (LES). The numerical results aligned with wind tunnel tests. Structural engineers can use the proposed technique to assess wind effects on long-span complex roofs and irregularly shaped buildings in the design phase.

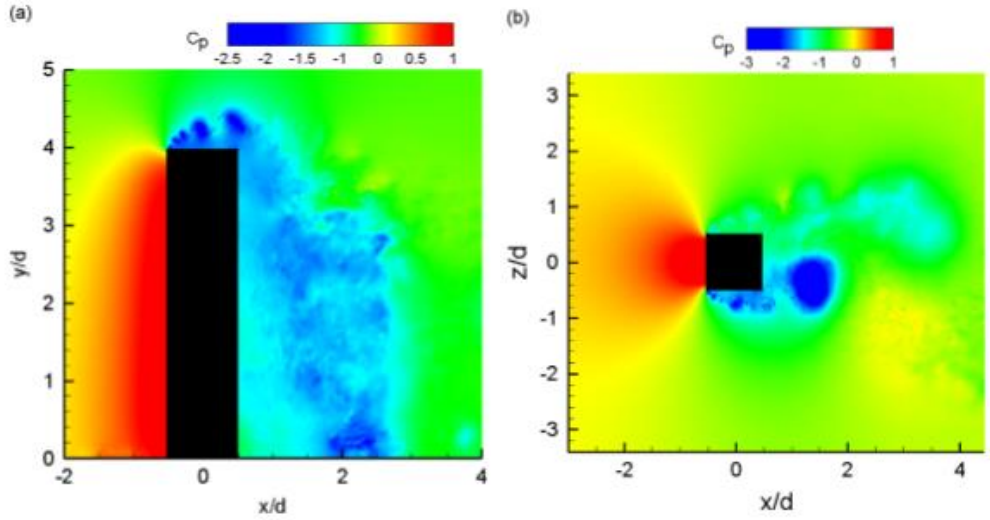

Figure 2.6 Tip vortices development from top of the structure; (b) von-Karmen vortex sheets (Saeedi, M., et al 2013)

Zhang, W. and Sarkar, P. (2010) simulated interference effects of other buildings surrounding existing low-rise buildings. Zhang used PIV methods to understand the flow around the building, then

compared the flow with numerical simulations. Blocken, B. et al (2007) simulated the flow passed two parallel similar sized buildings using a wall function roughness for the wall boundary conditions. They also studied the fully developed atmospheric boundary layer. The study was to understand the physical aspect of the flow. The flow between the buildings showed a weak Venturi effect. Also known as a reduction in fluid pressure. Shown in Figure 2.7 are the influences of wall function roughness (K) and the separation of the buildings. The closer the buildings are the more resistance to free stream flow can be seen.

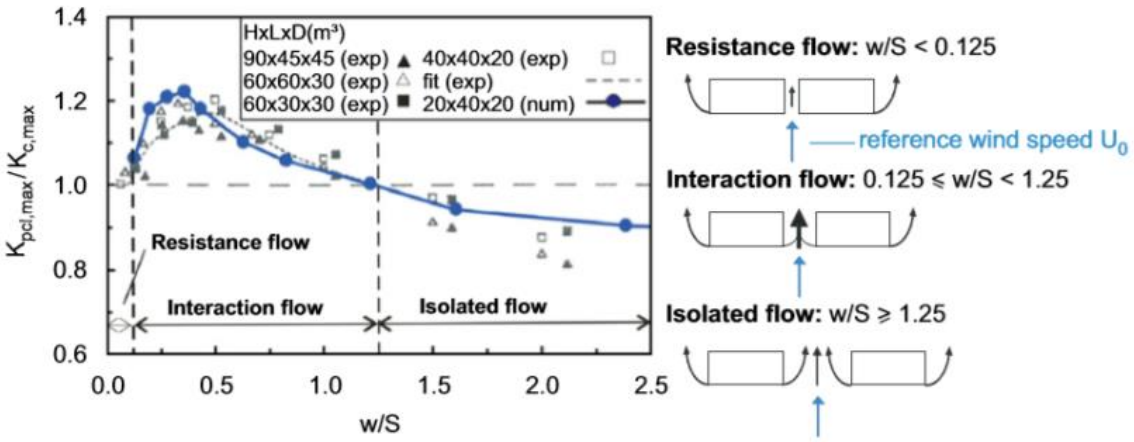

Figure 2.7 Definition and schematic representation (right, top views) of the three flow regimes for pedestrian-level wind speed in passages. (Blocken, B. et al 2007)

Table 2.4 Numerical Studies Flow around Structures

Structure	Method	Focus	Study
Bridge	Monte Carlo simulation	Numerical design	Carassale and Solari (2006)
Long-span bridge	Aero-static & -dynamic analysis	Linear & non-linear discrepancies	Zhang, Xiang et al. (2002)
Long-span bridge	Non-linear bridge response	Linear & non-linear discrepancies	Chen and Kareem (2001)
Long-span bridge	Time-domain indicial	Stability threshold &pre-critical behavior	Costa and Borri (2006)
Long-span bridge	FSI with incompressible Navier-Stokes	Reducing the number of physical models	Frandsen (2004)
Partially constructed bridge	ADINA with FSI	Dynamic coefficients	Ying Zhou (2009)

Tall building	RANS & KS	Wind loading & effects	Huang, Lau et al.(2011)
Large span roof	Developed program & FEA	Wind-induced vibrations	Zhang Enuo (2005)
Large span roof	ANSYS FLUENT with DSRFG & SGS LES	Roof and structure design analysis	Lu, Li et al. (2012)

These numerical studies show the trend toward the use of more complex and complete models in numerical simulation due to advances in computing hardware. An example of this is the progression from the simple models of (Zhang et al. 2002) and (Chen and Kareem 2001) to the use of FSI with vibration analysis (Frandsen 2004), time-domain approaches (Costa and Borri 2006), and commercial software (Ying Zhou et al. 2009). Similarly, Simulation work was done for modeling flow induced deformation for tension structures using different models to handle different aspects of the simulation. The coupling-code allows for a time-dependent process which is controlled by an iteration process, which allows for convergence to be reached within each time step. Table 2.4 compares several tools and methods discussed in this section based upon the type of structure analyzed, the methods, and the focus.

2.7.4 SECTION CONCLUSION

There has been a significant amount of numerical research in the field of wind engineering with application of CFD to study bluff-body fluid dynamics. The focus of these efforts was to supplement or replace wind tunnel testing. The need is correspondingly caused by the many situations where wind tunnel testing is too costly or even impractical. Most of the research has been conducted in the last two decades. Research in the last four to five years, confirm the advances in computing hardware. It has progressed to a point permitting development of accurate solutions to existing numerical models. The advancements in computing technology has allowed researchers to utilize more inclusive and complicated models. An example of this is the progression from simple linear or non-linear bridge analysis models to the use of FSI with vibration analysis, time-domain approaches, and commercial software.

The major focus of the research presented here and of primary interest for the present work is simulating flow around bluff body shapes. The focus of the bluff body shape efforts has been the simulation of drag coefficients, lift coefficients, pressure coefficients, Strouhal numbers, and wake phenomena. Most of this research has considered flow around circular cylinders because of their unique flow characteristics and the difficult of modeling such flow. A considerable amount of the research has focused on single circular cylinders. The studies confirmed the satisfactory performance of RANS equations when used with low Re values. As the flow regime changes to critical and transitional, LES, RANS, and DNS techniques are required to obtain satisfactory results. Further cases were studied, primarily in the low Re range for VIV oscillations where lock-in phenomena were observed. The current techniques are applied to model multi-physics problems.

Square, triangular cylinders, and bluff body cross sections have been considered. These geometries are common shapes seen in engineering applications. For rectangular and square bodies, performance studies act as primary cases for more complex problems.

Simulation of flow around structures was the second focus of recent research. A focus in this area is simulating aeroelastic response, flutter, wind-structure interaction, and force coefficients for long-span bridges. Non-linear models only deviate from linear model at extremely high wind speeds.

Some he researchers have explored improvements to existing models, with LES being the predominant tool for this type of analysis. Based on the presented research, numerical modeling may be able to take the place of more expensive wind tunnel models. Modeling tools are becoming more accurate and easier to implement. Modeling may become a common and important tool in the design phase of structures. Numerical modeling can yield insights into wind engineering problems which were not possible previously because modeling is much less constrained and restricted than physical modeling.

CHAPTER 3. FLUID BEHAVIOR AROUND A CYLINDER

3.1 FLOW PARAMETERS

Fluid statics deals with the case of a fluid at rest described in terms of hydrostatic pressure. Fluid dynamics is when the fluid is moving with applications concerning problems ranging from structural design to aerospace. Researchers have developed dimensionless parameters, typically, described ratio of flow properties.

Dimensionless numbers are parameters used by researchers to compare different quantities in fluid dynamics where similarity principles can be applied. This makes it easier to compare similar fluid cases, where the dimensionless numbers can relate forces, fluid properties, and problem scales that use different fluid or material properties. Dimensionless numbers reduce volumes of data to simple charts that can be used to better present experimental results. For the study of an oscillating cylinder there are several important parameters where numerical results can be related to experimental testing. These include Reynolds number, Strouhal number, and similar quantifiable comparisons.

3.1.1 REYNOLDS NUMBER

The most commonly used and known of the dimensionless numbers in fluid dynamics is the Reynolds number. The Reynolds number was first proposed by the British engineer Osbourne Reynolds (1842-1921), who has contributed much to the field of fluid dynamics. The Reynolds number is the dimensionless ratio of the fluid viscosity to its inertia in respect to force, Equation 3.1. The Reynolds number is used to describe the fluid flow regime and is synonymous with the fluid speeds. For a low Reynolds number, the viscosity is the dominate force compared to inertia. Due to this, the fluid flow is described as laminar where the fluid behavior is predictable. When the Reynolds number is high the inverse occurs and the inertia forces are dominate compared to the viscous. This is also when the flow can be described as turbulent.

$$\mathrm{Re} = \frac{\rho u D}{\mu} = \frac{u D}{\nu} \qquad \text{(Equation 3.1)}$$

Where:

ρ = fluid density,
u = free stream velocity,
D = diameter length of the cylinder,
μ = dynamics viscosity,
ν = kinematic viscosity, relation between fluid density and dynamics viscosity.

One of the most common studied cases in fluid dynamics is flow passing round cylindrical bodies. Such studies have applications from supporting structures to heat exchangers. The flow problem can occur in many engineering and scientific problems. Cylindrical bodies are used as initial validation cases due to being fundamental problems in fluid dynamics with a long history of associate experimental studies. These studies are used for the basis for further experimental cases like oscillating cylinders or computational studies using Computational Fluid Dynamics (CFD).

There is an abundance of cylindrical body fluid flow behavior information, Figure 3.1. Below a Reynolds number of 40, fluid flow is steady and laminar. The flow moves to the unsteady realm when it passes 40. Between 150 and 300 the flow separation begins to transition from laminar to turbulent vortex shedding. In cases passed 300 Re, the fluid flow becomes unsteady and turbulent. The regime between 300 and 3.5×10^5 is of major to engineers.

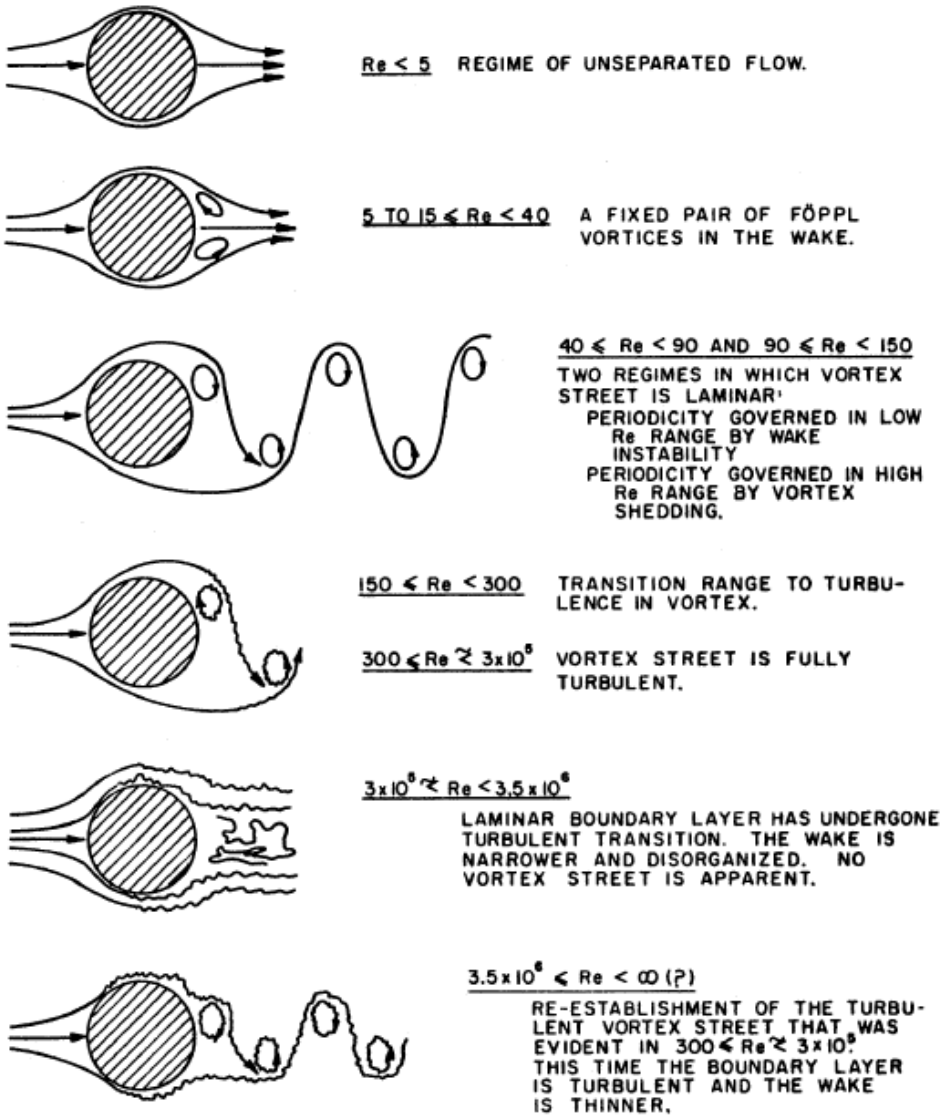

Figure 3.1 Reynolds number of Flow Passed a Circular Cylinder (Blevins, R. D. 2001)

3.1.2 FORCE COEFFICIENTS

The lift and drag coefficients are the most common wind parameters because they relate an object's motion to the fluid forces acting on the object. As the fluid moves around an object with the stream velocity acting parallel to the object, the parallel and tangential forces acting on the object by the fluid are drag and lift, respectfully. The drag coefficient is often described as the object's resistance to motion caused by the fluid. The two major contributors of the drag are pressure and viscous forces. The lift coefficient is used to describe the lift acting on the body, where lift is caused by the pressure difference

between the upper and lower bounds of the object. Depending on the reference direction, the lift and drag can be described as either negative or positive. For cylindrical, or symmetrical bodies the mean lift can be described as zero.

The general equation for describing force coefficients, with *i* corresponding to the type of force being used,

$$C_i = \frac{2F_i}{\rho u^2 A} \qquad \text{(Equation 3.2)}$$

Where:

F_i = fluid force acting either in parallel or tangentially to the geometry body,
ρ = fluid density,
u = free stream velocity
A = projected flat frontal area of the geometric bluff body.

By using Equation 3.2 (White 2009), the drag coefficient can describe the drag force acting in x-direction in its non-dimensionalized formed. Shown in Figure 3.2, the drag coefficient (C_d) can be shown as a function of the Reynolds number. At a low Reynolds number, the drag coefficient is high due to the dominate effect of body forces. The general interest for common engineering problems are found in the fluid flow range between $10^3 < Re < 10^5$. The drag coefficient is approximately between the values of 1 and 1.2.

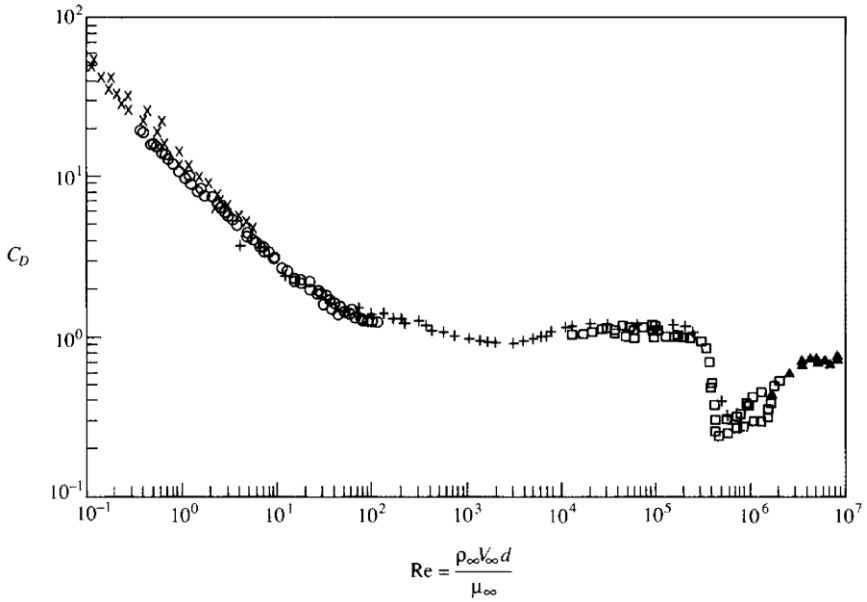

Figure 3.2 Cd vs. Reynolds number (Experimental Data compiled by Panton 2013)

3.1.3 STROUHAL NUMBER

The Strouhal number is the dimensionless ratio between the steady-state conditions of a flow to the unsteady conditions. This can be described further as the steady condition of a uniform flow with no separation. The unsteady condition is when the fluid flow starts to separate from the geometric body. Separation will disrupt the fluid flow and develop overlapping, alternating flow patterns. This condition is known as the vortex shedding. The unsteadiness of the fluid flow can be observed in the oscillatory behavior of either drag or lift forces acting on the geometric body. The vortex shedding can be visually observed by the distance a vortex sheet translates from one position to another in a certain amount of time. This behavior can be quantified as the shedding frequency and described more in Equation 3.3 (White 2009).

$$S_t = \frac{uf_s}{D} \qquad \text{(Equation 3.3)}$$

Where:

f_s = shredding frequency of the fluid,
u = free stream velocity,
D = diameter length of the cylinder.

For the range of $300 < Re < 10^{5,}$ the Strouhal number, in Figure 3.3, is approximately 0.2. This is the range where the drag coefficient is between 1 and 1.2. As the flow approaches a Reynolds number of 10^6 for a smooth stationary, circular cylinder the drag coefficient experiences a drop-in value, while the Strouhal number experiences a large increase in value close to 0.47. The phenomena are known as the drag crisis. The flow results in irregular formation of separation bubbles that generate chaotic, high frequency wake.

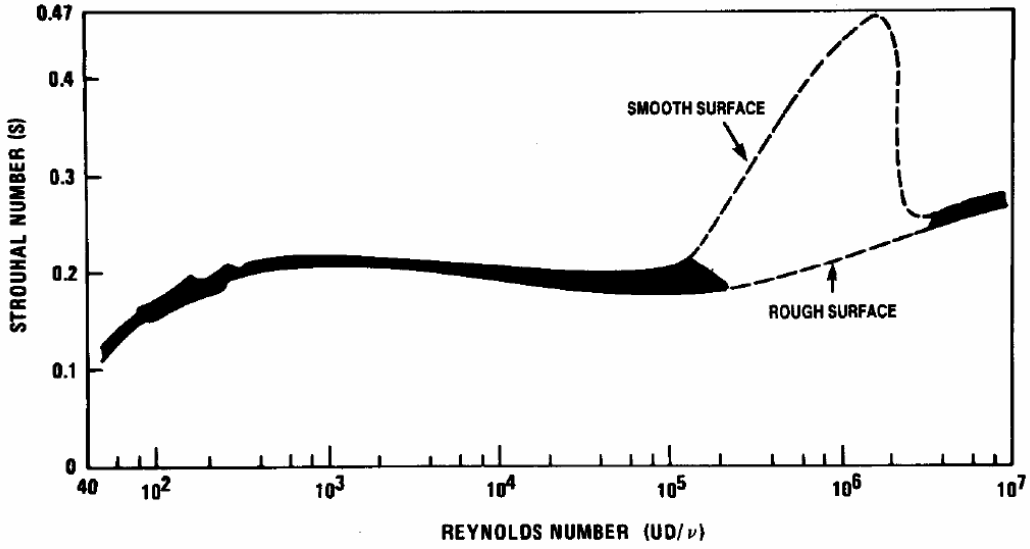

Figure 3.3 Strouhal number vs. Reynolds number for a circular, stationary cylinder (Blevins, R. D. 2001)

3.2 VORTEX-INDUCED VIBRATIONS

After a certain Reynolds number for a cylinder the laminar flow starts to become unsteady, Figure 3.1. The fluid starts to detach from the solid body at locations referred to as the separation point. At a higher Reynolds number, the flow becomes increasingly unsteady and the flow separation transitions to turbulent behavior. For a symmetrical body, the fluid will separate from the top and bottom and attempt to reattach to the body, as shown in Figure 3.4. When the fluid attempts to reattach, it will collapse onto itself, creating an oscillatory flow pattern in the wake of the solid body. This is called vortex shedding. This behavior is often observed in terms of pressure, where this oscillatory motion causes alternating regions of high and low pressure near the separation points (White 2009).

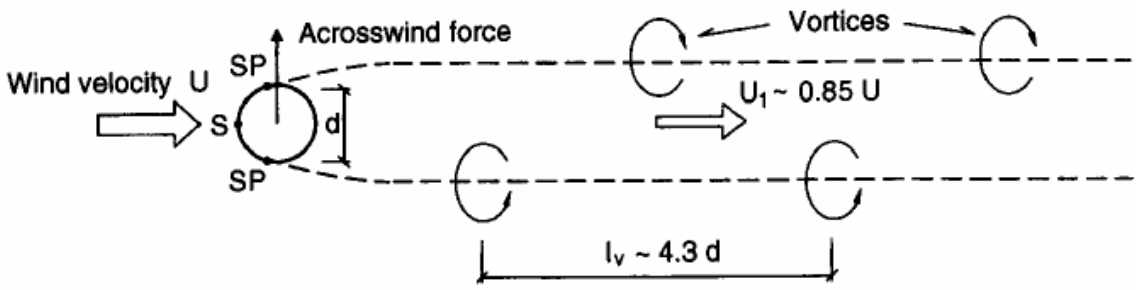

Figure 3.4 Vortex Shedding Behavior Passed a Stationary, Circular Cylinder (Blevins, R. D. 2001)

This oscillatory phenomenon is often studied and referred to as Vortex-Induced Vibrations (VIV) in literature, which refers to the vortex shedding behind a static object and the movement caused by the loading of vortex shedding on the object. In aerodynamic applications the flow speeds are often well above the laminar flow regime for many objects. Many structures and supports experience vortex shedding in one manner or another. The damage caused by vortex shedding is of great interest, with the two most common causes of damage being the cyclic loading from the vortex shedding and, to a lesser extent, harmonic oscillation.

For vortex shedding, the most important characteristic is with the shedding frequency or alternatively the Strouhal number. For a stationary circular cylinder, the most important characteristics to control for are the geometric scales, the forces, and surface roughness. These other factors can be described in terms of the Reynolds number, force coefficients, and the Strouhal number. Vortex shedding behavior can be influenced by controlling the flow parameters.

3.3 LOCK-IN RANGE AND OSCILLATORY FREQUENCY

For high speeds, the major interest for aerodynamic behaviors for supporting structures and wind is called the lock-in phenomenon. The lock-in phenomenon can be broadly defined as when the vortex shedding frequency matches the structural natural frequency, Equation 3.4. When this harmonic behavior occurs, it causes the supporting structure of interest to have the greatest movement compared to regular wind loading when there is little interaction between the structure motion and near-wind

dynamics (Simiu 1996). Expanding with the lock-in phenomenon, the stresses are amplified which leads to crack growth then to structural failure. From a safety standpoint, this may require mitigate of the effect to the structure.

$$\omega = \sqrt{\frac{k}{m}} \qquad \text{(Equation 3.4)}$$

Where:

ω = natural frequency (Radian/Sec),
k = equivalent spring constant (kg/m),
m = mass of the cylinder (m).

Before further discussion, there is a need to clarify the definition of the natural frequency of a structure, where the structure's stiffness is described in terms of *k* (kg/m) and the mass of the system is described in terms of *m* (kg). This is a relatively simple system to model with only a mass-spring system to be used to describe the object's motion. This system can be described in either one dimension along the parallel or tangential directions for the object or in one dimension for both coordinates. For the lock-in phenomenon, the only motion of interest is in the tangential direction going along the lift forces.

The lock-in phenomenon is the relationship of the natural frequency to the vortex shedding frequency of the fluid oscillation. This relationship can be used to determine the lock-in wind velocity for the structure. The lock-in velocity is developed as shown in Equation 3.5. For a certain range of velocities, the vortex shedding frequency will continue to match the natural frequency of the structure.

The lock-in velocity,

$$u_{lock-in} = \frac{f_{nD}}{S_t} \qquad \text{(Equation 3.5)}$$

Where:

f_n = natural frequency (Hz),
D = diameter length of the cylinder (m),
S_t = Strouhal number.

Figure 3.5 illustrates the relation of the frequency ratio of the vortex shedding frequency and the natural frequency compared to the flow velocity. The natural frequency dominate region, Figure 3.5, has very little motion when compared to the vortex shedding dominate range. The vortex shedding dominate range has greater motion. These two linear regions have a slope of 0.18-0.21 when discussing a circular cylinder called the Strouhal number. In the lock-in range, the frequency for both the vortex shedding and the structure match, which do not follow the linear trend between increasing velocity along with increase in shedding frequency. This lock-in range is where the greatest displacement and stresses on the cylinder occur.

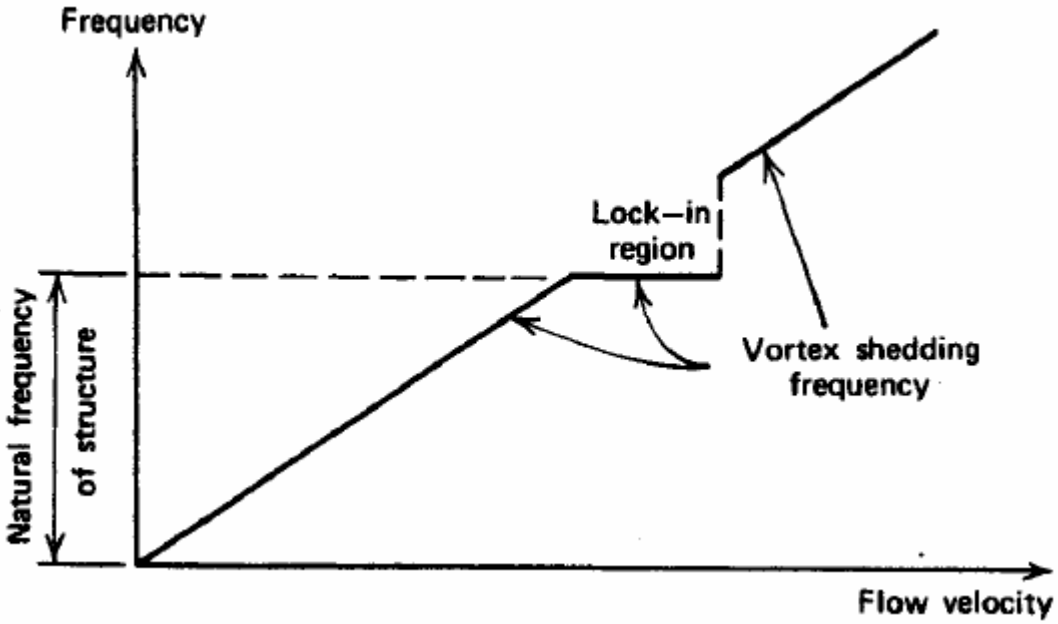

Figure 3.5 Frequency vs. Flow Velocity Chart (Simiu 1996)

Figure 3.6 shows the displacement ratio of the vertical displacement caused by the shedding frequency compared to the diameter of the cylindrical body alongside the frequency spectrum. There are three cases: 3.6a before lock-in, 3.6b during lock-in, and 3.6c after lock-in. The natural frequency is constant throughout all the cases, while the shedding frequency progressively increases in correlation

with increased velocity. The greatest displacement ratio is during lock-in followed by after lock-in. The smallest displacement ratio occurs before lock-in.

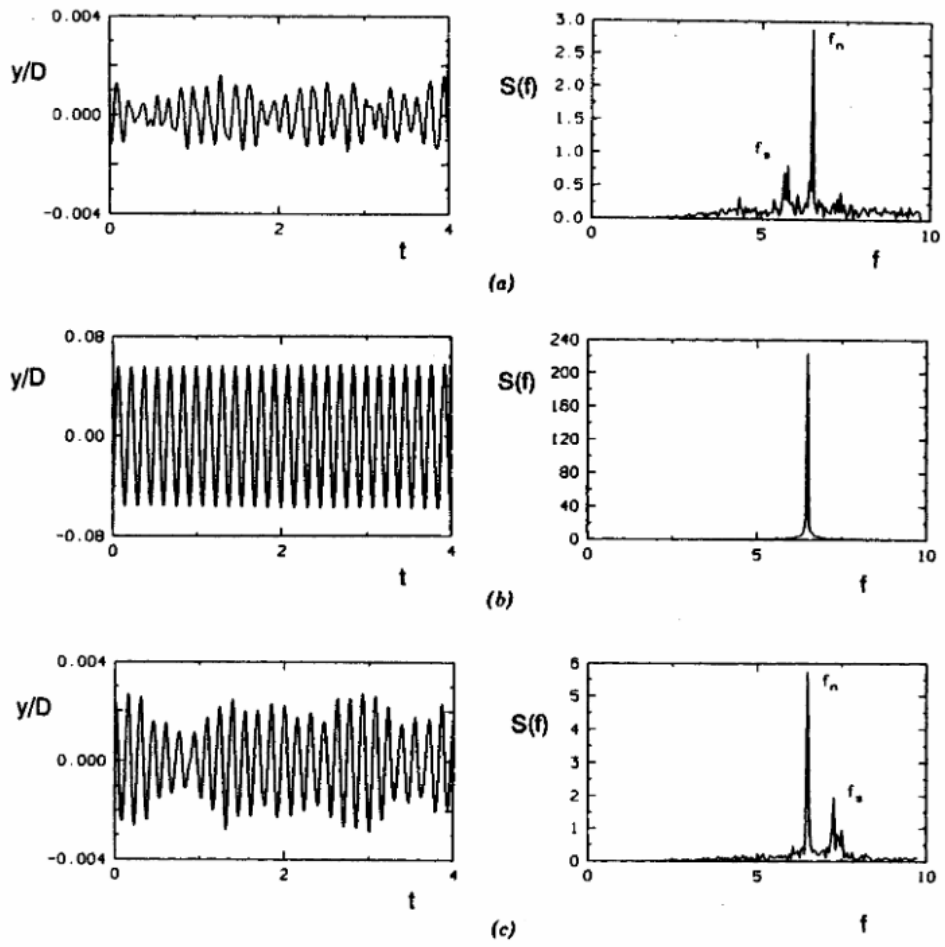

Figure 3.6 Oscillatory Cases of a Cylinder (a) Before Lock-in; (b) During Lock-in; (c) After Lock-in (Simiu 1996)

CHAPTER 4. COMPUTATIONAL FLUID DYNAMICS MODELING

4.1 SECTION INTRODUCTION

In the fields of engineering and physics, the study of fluid dynamics is of immense importance. For most engineering cases, fluid motion is not studied at microscopic levels. Instead, it is studied at considering large-scale flows. These areas of study are on a macroscale, where the bulk fluid motion is of more interest than particle motion. The macroscale assumption is called a continuum, where the Navier-Stokes equations are derived from the conservation laws found in Kundu, et al. (2015).

The Navier-Stokes equations were developed from conservation laws which are used to describe the full range of fluid motion. For simple problems at low speeds and non-geometric complex structures, the Navier-Stokes can yield exact solutions in some cases. Issue arises at higher speeds with the introduction of turbulence then develop of exact solutions using the Navier-Stokes equations becomes difficult. With the advent of Computational Fluid Dynamics (CFD), different methods have been developed to address the turbulence problem such as the computationally expensive Direct Numerical Simulation (DNS) or the Large Eddy Simulation (LES) and Reynolds-Average Navier-Stokes (RANS) modeling.

4.2 NAVIER-STOKES EQUATIONS

The Navier-Stokes equations permit description of fluid motion under the assumption of a continuum. It is assumed the bulk motion of a fluid system is greater than the free mean path of a fluid particle leading to the basis of a continuum. Fully expanded, the Navier-Stokes equations lead to five coupled equations with additional equations as needed for the physics. These equations describe the full fluid motion and associated properties.

The Navier-Stokes equations were derived from the conservation laws leading to a general statement which describes everything that enters or influences the boundaries of the fluid system. The

first conservation law is the Continuity Equation. It describes for an incompressible fluid how all mass entering the system will leave the system. If dealing with a compressible fluid, continuity will be conserved within the system and the boundaries. The derived Continuity Equation, Equation 4.1, is described in more detail in Kundu, et al. (2015).

The Continuity Equation is as follows,

$$\frac{\partial \rho}{\partial t} + \frac{\partial \rho u_i}{\partial x_i} = 0 \qquad \text{(Equation 4.1)}$$

Where:

ρ = fluid density,
u = fluid velocity.

The first term of the equation describes the time-dependent change of the density of the system. The second term of the Continuity Equation is known as the mass-density flux, as it can be interpreted as net loss at a point due to the divergence of the flux terms. These flux terms are known as the transport terms for the quantities moving from one region to another without making a net contribution to the entire field (Kundu, et al. 2015).

The Continuity Equation only describes two terms of density and velocity, which is insufficient to describe the full motion of the fluid flows. The next set of equations in Navier-Stokes is the Conservation of Momentum, which is where the Newton's Second Law of Motion is applied to a fluid flow. The Conservation of Momentum considers in three-dimensional calculations all of the body forces, viscous effects, and other influences on the moving fluid. The Conservation of Momentum (Anderson 1995) is described in Equation 4.2.

The Conservation of Linear Momentum Equation,

$$\frac{d\rho u_i}{dt} + \frac{\partial \rho u_i u_j}{\partial x_i} = -\frac{\partial p}{\partial x_i} + \mu \frac{\partial^2 u_i}{\partial {x_i}^2} + F_i \qquad \text{(Equation 4.2)}$$

Where:

ρ = fluid density,
u = fluid velocity,
p = pressure,
μ = dynamic viscosity,
F = Body Forces.

In the Conservation of Momentum equations, with a Cartesian coordinate system there are three nested equations. These corresponded with the (x, y, z)-components of the coordinate system. The three equations together, with the Continuity equation, become coupled through shared velocity terms. The terms of the Conservation of Momentum are in the following order: Temporal changes, fluid inertia terms, pressure forces, viscous effects of the fluid, and the body forces.

The Reynolds number is a ratio between the viscous and inertia terms of the fluid flow, which is often used to describe whether the fluid flow is laminar or turbulent. A low Reynolds number flow describes laminar properties of the fluid when the viscous term has very little influence compared to the inertia terms. This leads to the viscosity term being neglected for various solutions in low Reynolds number flow regimes. When the flow is considered high Reynolds number flow, the viscous term becomes dominate compared to the inertia term. The viscosity will then lead to the development of turbulence within the system, which adds additional complexity for developing a solution. This is termed the turbulence closure problem.

The final equation of Navier-Stokes is the Conservation of Energy, Equation 4.3. It is derived by developing the mathematical statement for all energy influences on a fluid particle in an inertial frame of reference (Kundu, et al. 2015). The first term of the equation is internal energy. The second term is the kinetic energy of the particle. Additional terms are in order: work, heat transfer, and work done by body forces. The energy term can be decomposed into the pressure and viscous surface-tension terms, as shown in Equation 4.4.

The Conservation of Energy Equation is,

$$\frac{d}{dt}[\rho(e+\frac{u_i u_j}{2})]+\frac{\partial}{\partial x_i}[\rho u_i(e+\frac{u_i u_j}{2})]=\frac{\partial u_i T_{ji}}{\partial x_i}-\frac{\partial q''}{\partial x_i}+\rho u_i F_i \qquad \text{(Equation 4.3)}$$

Where:

ρ = fluid density,
u = velocity,
ε = internal energy,
q'' = heat transfer flux,
T = Work component,
p = pressure,

The decomposed work term,

$$\nabla(uT)=-\nabla(pu)+\nabla(\tau u) \qquad \text{(Equation 4.4)}$$

Where:

p = pressure,
u = stream velocity,
T = work term,
τ = viscous work term.

For the Navier-Stokes equations, many of the terms are known. The known given terms depend on the type of fluid problem being analyzed, leaving several terms that need to be addressed within the equations themselves. For several terms related to the fluid's thermodynamic properties, additional equations are needed. The Equations of State, assuming an ideal gas, address thermodynamic fluid properties, Equations 4.5 and 4.6.

$$p=\rho RT \qquad \text{(Equation 4.5)}$$

Where:

p = pressure,
ρ = fluid density,
R = Gas Constant,
T = Temperature.

$$\varepsilon=h-pu \qquad \text{(Equation 4.6)}$$

Where:

ε = internal energy,
h = enthalpy,

p = pressure,
u = fluid velocity.

4.3 THE TURBULENCE PROBLEM

There is no analytical solution to describe all scales of fluid turbulence. This is one of the main challenges of Computational Fluid Dynamics (CFD). Turbulence is three-dimensional and collapses into smaller and often random time and length scales. The largest turbulence scales are defined by geometric boundaries impeding the flows, as describe by Pope (2000). The large temporal and spatial scales decrease to the Kolmogorov timescale as $Re^{-1/2}$ and the Kolmogorov length-scale as $Re^{-3/4}$. Mathematically, the largest difficulties for the Navier-Stokes equations are the nonlinear convection term and the pressure gradients.

The most common approaches for accounting for turbulence come in the form of 1) Reynolds-Averaged Navier-Stokes (RANS), 2) Large Eddy Simulation (LES), and 3) Direct Numerical Simulation (DNS). These are listed, from the least to most computationally intensive procedures. The RANS approach averages out all scales of the turbulence structures, which adds additional equations to be solved by additional transport equations to model the turbulence. RANS models can be applied to a full range of engineering problems. The LES approach models the larger geometric characteristic turbulence scales while using filtering approaches to average out the smaller scale (universal scale) turbulence eddies. DNS directly solves for all scales of turbulence leading to the need of very refined grids and temporal scales requiring long computational times. This approach is only applicable for a small sample of simple cases due to the large computation time and amount of resources needed.

The turbulence energy cascade theory proposed by Richardson and described in Pope (2000) is a dynamic, nonlinear system of turbulence that breaks larger turbulence scales down to the viscosity scale. These scales are used to describe the type of energy cascade ranges that the turbulence approaches handle, Figure 4.1. RANS model all length scales and time scales but can only describe a limited range of the

energy cascade. LES, only models the smaller scale eddies and can describe approximately 90% of the energy cascade. DNS is required to solve the entirety of the energy cascade.

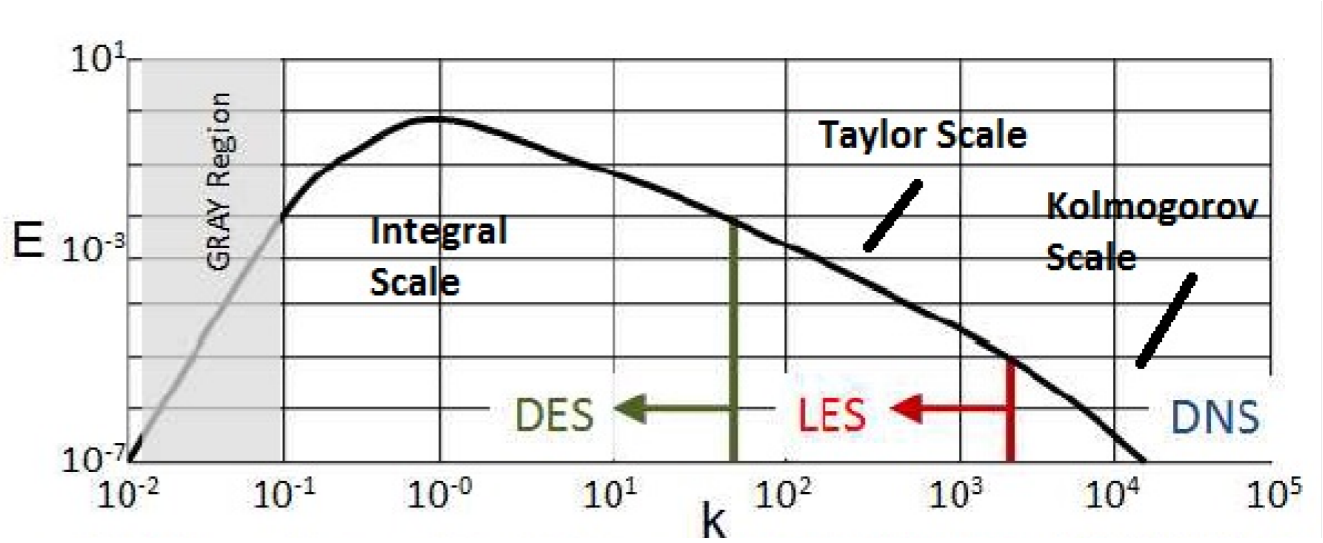

Figure 4.1 Turbulence Energy Cascade (Dudley 2016)

More resolved time and length scales lead to higher computational costs. Table 4.1 is a summarization of RANS, LES, and DNS methods with the estimated date of when the method might be readily applied, and the associated anticipated number of grid points and time steps required. The assumption given is for a reasonably high Reynolds flow number and a complex aerodynamic body (Dudley 2016). The number of grid points and time steps are calculated using the Kolmogorov time and length scales, based on the Reynolds number. The anticipated date described is based on the expected computational cost, which is based on the previously mentioned scales.

Table 4.1 Turbulence Approach Table (Dudley 2016)

Method	Grid Points	Time Steps	Date Ready
DES	10^{8}	10^{4}	Now
LES	$10^{11.5}$	$10^{6.7}$	2045
`DNS	10^{16}	$10^{7.7}$	2080

4.4 REYNOLDS-AVERAGING NAVIER-STOKES (RANS) MODELING

Turbulence is described as a chaotic, time dependent, three-dimensional flow field. This means the flow shows no predictable characteristics. Figure 4.2 shows an example of an unsteady time-dependent velocity signal. This demonstrates the chaotic nature of turbulence. Due to this behavior, there are no analytical solutions to describe the behavior of turbulence. One major approach to describe turbulence is by using the statistical behavior of the time to average out the turbulence noise in the signal. This is showed by the solid line in Figure 4.2. The mathematics of the Reynolds-Averaged Navier-Stokes (RANS) turbulence modeling approach is based on this technique.

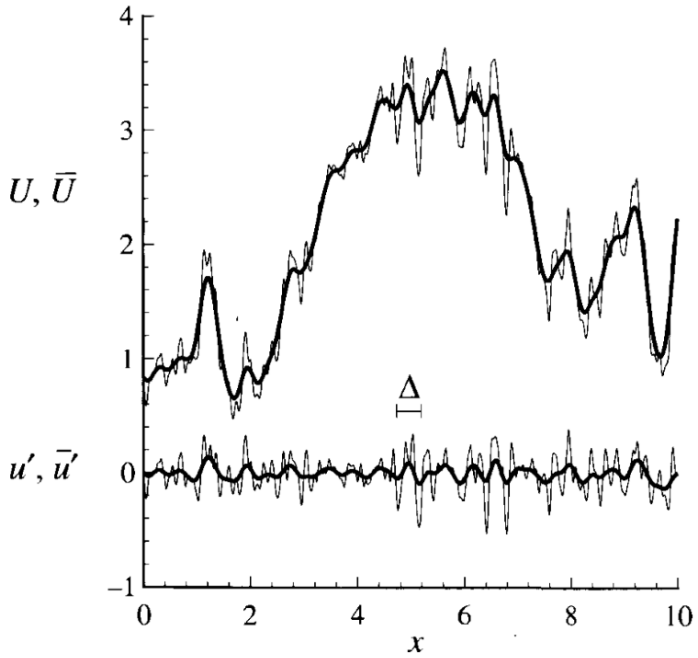

Figure 4.2 Turbulent Velocity vs. Time (Pope 2000)

The time-averaging can be seen in Equation 4.7 for the velocity, but a general form of the time-averaging can be used to describe all conservation parameters in the Navier-Stokes equations. The time-averaged approach is applied to the Navier-Stokes equations; Equations 4.1, 4.2, and 4.3, with the transformations show in Equations 4.8, 4.9, and 4.10. When comparing the original form of the Continuity (Equation 4.1) and Conservation of Energy (Equation 4.3) to the time-averaged form (Equation 4.7 and 4.8), the equations are similar. The same is not true of Equation 4.3 when compared

to the time-averaged form of the Momentum equation with an additional term (Equation 4.10). The full derivation is discussed in Wilcox (2000).

$$u_i(x,t) = U_i(x) + u_i'(x,t) \qquad \text{(Equation 4.7)}$$

$$\frac{\partial \bar{\rho}}{\partial t} + \frac{\partial \overline{\rho u_i}}{\partial x_i} = 0 \qquad \text{(Equation 4.8)}$$

$$\frac{d\overline{u_i}}{dt} + \frac{\partial \overline{\rho u_i u_j}}{\partial x_i} + \frac{\partial \overline{\rho u_i' u_j'}}{\partial x_i} = -\frac{\partial \bar{p}}{\partial x_i} + \mu \frac{\partial^2 \overline{u_i}}{\partial {x_i}^2} + \overline{F_i} \qquad \text{(Equation 4.9)}$$

$$\frac{d}{dt}\left[\left(\bar{e} + \frac{\overline{u_i u_j}}{2}\right)\right] + \frac{\partial}{\partial x_i}\left[\overline{\rho u_i}\left(\bar{e} + \frac{\overline{u_i u_j}}{2}\right)\right] = \frac{\partial \overline{u_i T_{ji}}}{\partial x_i} - \frac{\partial \overline{q''}}{\partial x_i} + \overline{\rho u_i F_i} \qquad \text{(Equation 4.10)}$$

The additional term shown in Equation 4.9 (third term) is known as the Reynolds stress term. It cannot be solved analytically because it leads to more unknowns than available equations, Wilcox (2000) and Pope (2000). This is known as the "turbulence closure problem." With the current increase in computing power to handle this closure problem, the use of additional equations allows for ways to model the turbulence.

These additional terms will need to resolve the convective and advective terms of the Navier-Stokes for developing the turbulence. With time averaging, there are additional terms that must be resolved for dealing the eddy structures in turbulent flow. These additional terms can be resolved with the use of different equation models to help mitigate the computations needed.

Two other equation models and similarly developed models are the more commonly used models and serve as the basis for numerical analyzes. These are the k-ε and models based on k-ω turbulence models. Such models are heavily used and were developed over decades, leading to different formulations. They use eddy viscosity as a term to resolve these two equation RANS approaches.

4.4.1 k-ε TWO-EQUATION MODEL

The k-ε two-equation model is one of the most commonly applied turbulence models in modern CFD, with k- ε uses two additional transport equations to solve for turbulence. The assumptions made for the standard model focus on the elements that affect the behavior of kinetic energy with using the mixing length scale model (Launder, B., and Sharma, B., 1974), Equations 4.11 – 4.13. The assumption for the flow behavior uses a ratio of both Reynolds stresses and the mean rate of deformation is equivalent. The model has been useful for planar shear slayers and recirculating flows. These generally do not have adverse pressure gradients (Bardina, J., et al. 1997). Internal flows in pipe bends would be an example. Modern versions of this model, such as the Realized k-ε model, attempt to handle the spreading rates to allow for improved pressure predictions (T.-H. Shih, et al. 1995), Equations 4.14 – 4.18. Another modified model is the Re-Normalized Group (RNG) k-ε model, Equations 4.19 – 4.23. This model is used to renormalize the Navier-Stokes equations in order to account for smaller scale motion (Yakhot, V., et al 1992).

Standard k-ε model

$$\frac{\partial \rho k}{\partial t} + \nabla(\rho k U) = \nabla\left(\frac{\mu_T}{\sigma_k}\nabla k\right) + 2\mu_T S_{ij} S_{ij} - \rho\varepsilon \qquad \text{(Equation 4.11)}$$

$$\frac{\partial \rho \varepsilon}{\partial t} + \nabla(\rho \varepsilon U) = \nabla\left(\frac{\mu_T}{\sigma_\varepsilon}\nabla \varepsilon\right) + C_{1\varepsilon}\frac{\varepsilon}{k} 2\mu_T S_{ij} S_{ij} - C_{2\varepsilon}\rho\frac{\varepsilon^2}{k} \qquad \text{(Equation 4.12)}$$

$$\mu_T = \rho C_\mu \frac{k^2}{\varepsilon} \qquad \text{(Equation 4.13)}$$

Where:

k = kinetic energy,

ε = eddy dissipation rate,

C_μ = 0.09,

σ_k = 100,

σ_ε= 1.33,

$C_{1\varepsilon}$ = 1.44,

$C_{2\varepsilon}$ = 1.92.

Realized k-ε model

$$\frac{\partial k\rho}{\partial t} + \frac{\partial k\rho u_j}{\partial x_j} = \frac{\partial}{\partial x_j}\left(\mu + \frac{\mu_T}{\sigma_k}\right)\frac{\partial k}{\partial x_j} + P_k + P_b - \rho\varepsilon - Y_M + S_k \quad \text{(Equation 4.14)}$$

$$\frac{\partial \varepsilon\rho}{\partial t} + \frac{\partial \varepsilon\rho u_j}{\partial x_j} = \frac{\partial}{\partial x_j}\left(\mu + \frac{\mu_T}{\sigma_\varepsilon}\right)\frac{\partial \varepsilon}{\partial x_j} + \rho C_1 S_\varepsilon + \rho C_2 \frac{\epsilon^2}{k+\sqrt{\nu\varepsilon}} + C_{1\varepsilon}\frac{\varepsilon}{k}C_{3\varepsilon}P_b + S_\varepsilon \quad \text{(Equation 4.15)}$$

$$C_1 = max[0.43, \frac{\eta}{\eta+5}] \quad \text{(Equation 4.16)}$$

$$\eta = S\frac{k}{\varepsilon} \quad \text{(Equation 4.17)}$$

$$S \equiv \sqrt{2S_{ij}S_{ij}} \quad \text{(Equation 4.18)}$$

Where:

P_k = turbulence kinetic energy generation,

P_b = turbulence energy due to buoyancy,

Y_M = compressible turbulence dissipation rate,

S = source terms.

RNG k-ε model

$$\frac{\partial k\rho}{\partial t} + \frac{\partial k\rho u_j}{\partial x_j} = \frac{\partial}{\partial x_j}\left(\mu + \frac{\mu_T}{\sigma_k}\right)\frac{\partial k}{\partial x_j} + P_k - \rho\varepsilon \quad \text{(Equation 4.19)}$$

$$\frac{\partial \varepsilon\rho}{\partial t} + \frac{\partial \varepsilon\rho u_j}{\partial x_j} = \frac{\partial}{\partial x_j}\left(\mu + \frac{\mu_T}{\sigma_\varepsilon}\right)\frac{\partial \varepsilon}{\partial x_j} + C_{1\varepsilon}\frac{\varepsilon}{k}P_k - \rho c_{2\varepsilon}^*\frac{\varepsilon^2}{k} \quad \text{(Equation 4.20)}$$

$$C_{2\varepsilon}^* = C_{2\varepsilon} + \frac{C_\mu\eta^3(1-\frac{\eta}{\eta_0})}{1+\beta\eta^3} \quad \text{(Equation 4.21)}$$

$$\eta = S\frac{k}{\varepsilon} \quad \text{(Equation 4.22)}$$

$$S \equiv \sqrt{2S_{ij}S_{ij}} \quad \text{(Equation 4.23)}$$

4.4.2 k-ω TWO-EQUATION MODEL

Continuing from the k-ε model, the k-ω turbulence model averages the smaller scale turbulence models with two additional transport equations. These equations allow the model to account for similar elements that affect the turbulent kinetic energy, where the ω term replaces Ɛ to account for specific dissipation rate. The k-ω model allows for improved modeling of problems with high-pressure gradients along walls. The most common modifications of this equation are the Wilcox k-ω (Wilcox 1989) and the Shear Stress Transport (Menter 1994) models, modified to better hand near wall treatments. The Wilcox k-ω, shown in Equations 4.24 – 4.26, was applied to low Re turbulent flows for bluff body

dynamics. The SST (Equations 4.27 – 4.29) has been noted in more recent studies to better handle near wall force calculations (Tominaga 2014), for higher Re values (12,000 < Re).

Wilcox k-ω model

$$\frac{\partial k}{\partial t} + u_j \frac{\partial k}{\partial x_j} = \frac{\partial}{\partial x_j}[(\nu + \sigma^* \nu_T)\frac{\partial k}{\partial x_j}] + \tau_{ij}\frac{\partial u_i}{\partial x_j} - \beta^* k\omega \quad \text{(Equation 4.24)}$$

$$\frac{\partial \omega}{\partial t} + u_j \frac{\partial \omega}{\partial x_j} = \frac{\partial}{\partial x_j}[(\nu + \sigma \nu_T)\frac{\partial \omega}{\partial x_j}] + \alpha\frac{\omega}{k}\tau_{ij}\frac{\partial u_i}{\partial x_j} - \beta\omega^2 \quad \text{(Equation 4.25)}$$

$$\nu_T = \frac{k^2}{\omega} \quad \text{(Equation 4.26)}$$

Where:

ω = turbulent frequency,

k= turbulent kinetic energy,

β^* = 0.09,

α = 5/9,

β = 0.075,

$\sigma^* = \sigma$ = 2.

Shear Stress Transport

$$\frac{\partial k}{\partial t} + u_j \frac{\partial k}{\partial x_j} = \frac{\partial}{\partial x_j}[(\nu + \sigma_k \nu_T)\frac{\partial k}{\partial x_j}] + P_k - \beta^* k\omega \quad \text{(Equation 4.27)}$$

$$\frac{\partial \omega}{\partial t} + u_j \frac{\partial \omega}{\partial x_j} = \frac{\partial}{\partial x_j}\left[(\nu + \sigma_\omega \nu_T)\frac{\partial \omega}{\partial x_j}\right] + \alpha S^3 - \beta\omega^2 + 2(1 - F_1)\sigma_{\omega^2}\frac{1}{\omega}\frac{\partial k}{\partial x_i}\frac{\partial \omega}{\partial x_i} \quad \text{(Equation 4.28)}$$

$$\nu_T = \frac{k^2}{\omega} \quad \text{(Equation 4.29)}$$

Where:

β^* = 0.09,

α = 5/9,

β = 0.075,

$\sigma_k = \sigma_\omega$ = 2,

σ_{ω^2}= 1/0.856,

F = a predefined blending function.

4.5 LARGE EDDY SIMULATION (LES)

Large Eddy Simulation (LES) models the larger eddies which are typically dependent on the geometric parameters impeding the flow. This is based on the Kolmogorov similarity scales, which describe the larger eddies. This allows the smaller or universal scales to be ignored or not modeled through a low-pass filtering of the Navier-Stokes equations. LES is a simulation approach like RANS, but only averages the length scale of the smaller scale eddies in the numerical solution. LES approaches have to resolve the integral. The most common approach for LES modeling is the Smagorinsky-Lilly model (Smagorinsky, J 1963), Equations 4.30 – 4.32. This model has been applied for fully turbulent low Re flows (Re < 5000) where the computational overhead is not as prohibitive, studies by Labbé, D.F.L. and Wilson, P.A. (2007) and Liang, C. and Papadakis, G. (2007).

Smagorinsky-Lilly Model

$$\tau_{ij} - \frac{1}{3}\tau_{kk}\delta_{ij} = -2(C_s\Delta)^2|\bar{S}|S_{ij} \quad \text{(Equation 4.30)}$$

$$\mu_{sgs} = \rho(C_s\Delta)^2|\bar{S}| \quad \text{(Equation 4.31)}$$

$$\mu_{eff} = \mu_{mol} + \mu_{sgs} \quad \text{(Equation 4.32)}$$

Where:

μ_{sgs}= eddy viscosity,
Δ = volume filter,
μ = viscosity terms,
C_s = 0.1 - 0.2.

4.6 DIRECT NUMERICAL MODELING (DNS)

The Direct Numerical Modeling approach does not attempt to model any of the turbulence length scales favoring to resolve all length and time scales as needed. This allows for the most accurate numerical approach. This is limited to only basic geometries and flows due to the need for large computational resources. The smallest turbulence scale is measured by the Kolmogorov length scale, which relates the kinematic viscosity to the kinetic energy dissipation rate. DNS resolves all spatial and temporal scales up to the Kolmogorov scales. This leads to the grid spacing being required to contain the

integral scale within the computational scale. The time scales then become dependent on the grid sizing through the Courant number. The Courant number describes the stability requirement of the numerical approach.

CHAPTER 5. PROBLEM METHODOLOGY

5.1 PROBLEM STATEMENT

The study sought to replicate wind tunnel experimental data (Chang 2010) for a dodecagonal cylinder by comparing the static force coefficients and dynamic cylindrical movement using CFD. In the static case, there are two extreme symmetrical cases for the drag coefficient: 1) the flat front and 2) the corner facing cylindrical orientation. The drag coefficient becomes insensitive at higher Reynolds numbers, where the static forces coefficient value starts to average out with 2%-variation. The lift coefficient is simulated at the similar range of Reynolds numbers at different angles of attack for the two orientations, leading to symmetrical looking curves depending on the orientation. In the dynamic case, the fluid velocity varied along the lock-in range, where the vortex shedding of the fluid matches the structural natural frequency.

Computational Fluid Dynamics (CFD) is relatively cheap in cost of setup and with the ability to replicate the relevant physics involved. When both CFD and experimental results are available there is a confirmation of data. Experimental data can be used to validate the CFD generated data. Once the CFD simulation setup is validated against wind tunnel results, it is possible to simulate further conditions without the need for expensive field testing. Further CFD work can be used to simulate more extreme or rare wind conditions to evaluate how a High-Light Mast-Pole (HLMP) responses and handles conditions like buffeting.

5.2 WIND TUNNEL EXPERIMENT DIMENSIONS AND CONDITIONS

Wind tunnel experiments have been conducted to study the aerodynamic characteristics of fluid flow pass a dodecagonal cylinder. At the Iowa State University, there is a Wind Simulation and Testing Laboratory (WiST Lab) of the subsonic, suction type with a max speed of approximately 80 m/s (Figure

5.1). The test chamber of the tunnel is 0.91×0.76 (3ft × 2.5ft) meters, with a length of 2.44 meters (8ft) following the exit.

Figure 5.1 Iowa University WiST Lab (Chang 2010)

The test model developed for the wind tunnel experiments at WiST was a wooden cylindric dodecagonal (12-sided). It had a cross-section diameter of 0.1016 meters (4-inches). The span-wise length for the cylinder was 0.508 meters (20-inches). The full static model can be seen in Figure 5.2a. The wooden model was reinforced by an aluminum rod, allowing the model to be treated as a rigid body. For the dynamic case, the rigid supports were replaced by 8 springs and 2 leaf springs (Figure 5.2b). The spring combinations had a total stiffness of 5786.5 N/m (396.5 lbs./ft) and limited the movement of the

cylinder to the y-direction (tangential to the wind inlet flow). The inertial mass of the system was 2.78 kg (6.13 lbs.) with the structure having a natural frequency of 7.25 Hz.

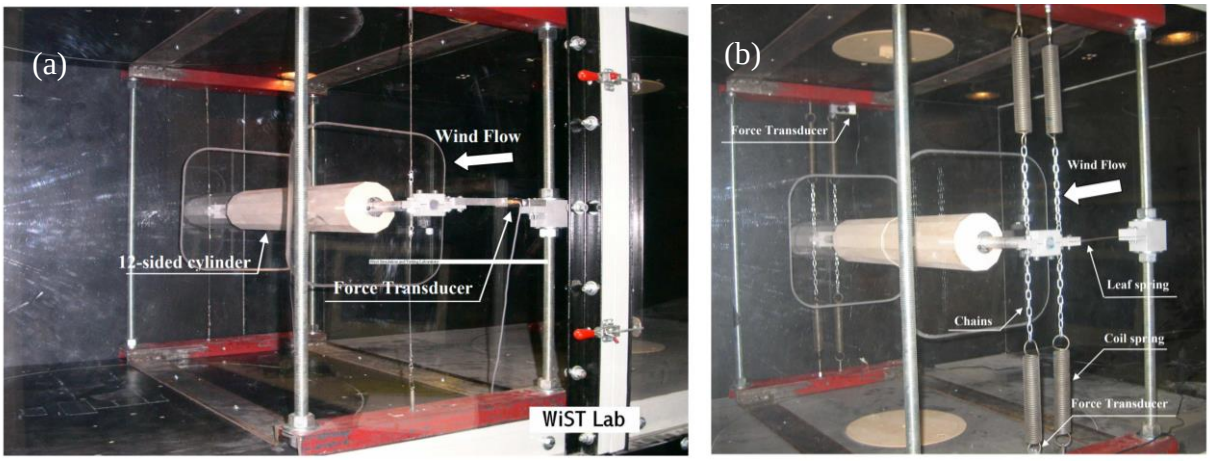

Figure 5.2 (a) Static Wind Tunnel Model; (b) Dynamic Wind Tunnel Model (Chang 2010)

5.3 GEOMETRIC CONDITIONS

Shown in Figure 5.3a is a two-dimensional cross section of the fluid control volume for the CFD simulation work, with a three-dimensional extrusion, as shown in Figure 5.3b. The diameter of the dodecagonal (12-sided) cylinder was approximately 0.1016 meters (4-inches) with a control volume height of 3 ft (0.91-meters) and a depth of 2.5 ft (0.91-meters). While the wind tunnel cylinder model was 0.508-meters (20-inches), the CFD control volume is longer in the span-wise direction to match the full spanwise length of the wind tunnel. This is to take into greater account of the three-dimensional turbulence eddy structures. In the case of wind tunnels, the air intake is sufficiently long for the wind to fully develop with no consideration for the outlet length. The only consideration is convenient exhausting of the air mass. The full length of the CFD control volume was 5.08-meters (200-inches).

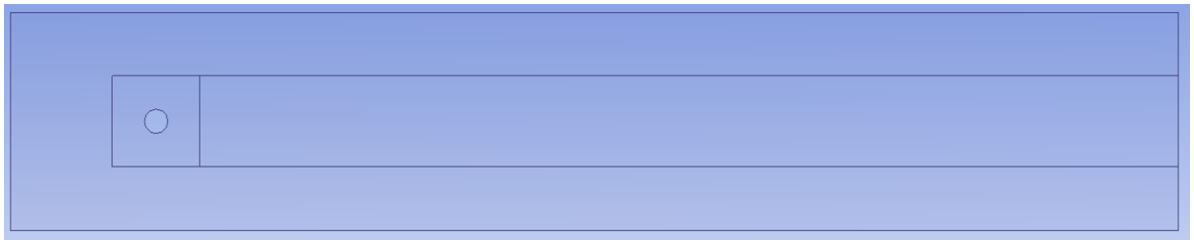

(a)

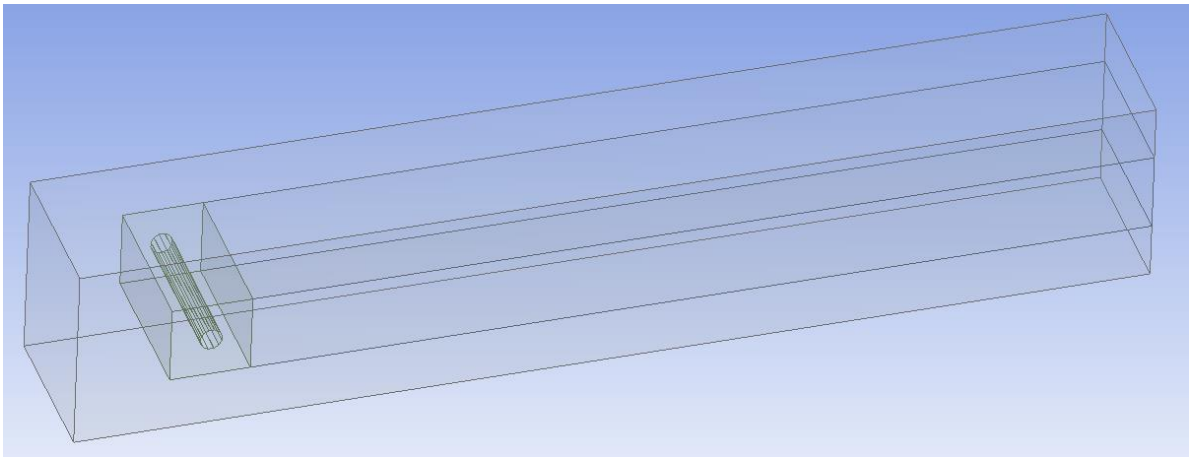

(b)

Figure 5.3 (a) 2D Control Volume; (b) 3D Extrusion of Control Volume

The height and span-wise extrusion were extended to match the dimensions used for the wind tunnel test chamber, with the location of the dodecagonal cylinder being 4.5-diameters from the top and bottom of the control volume. The frontal distance of the cylinder from the inlet was 6.25-Diameters, this allowed the fluid flow to develop without interference from the boundary conditions. The outlet condition was 44-diameters from the upstream cylinder. The downstream length was not sufficiently long enough to fully model the wake. However, according to Patel (2010) the minimum distance was considered satisfy and would minimize the wake effects on the test results. Another factor that limited the downstream distance was the increased computational cost and the time required to resolve the full wake. The three-dimensional length was 7.5-diameters. All lengths are shown in Figure 5.4.

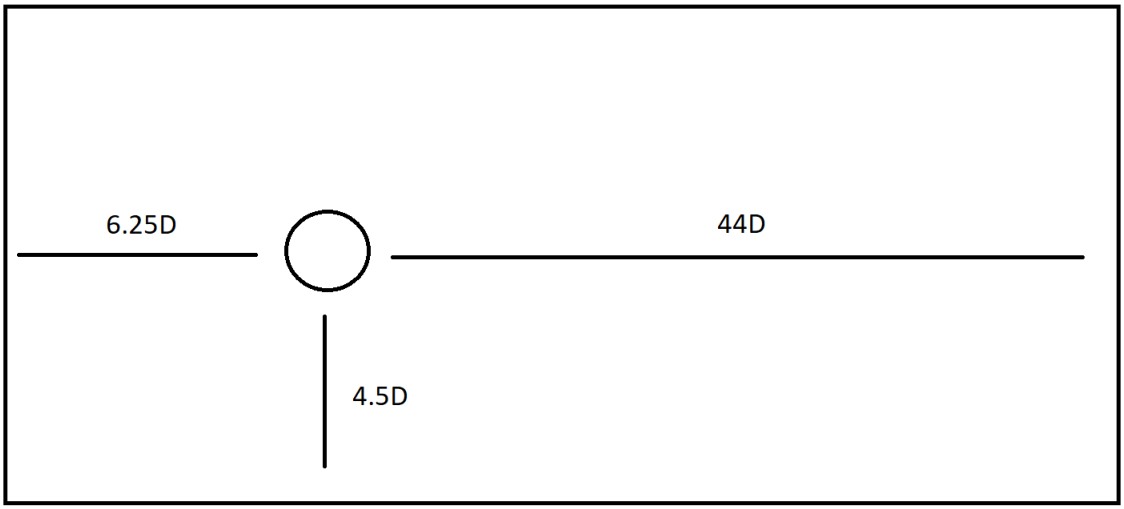

Figure 5.4 Control Volume Dimensions

5.4 MESHING

The control volume, shown in Figure 5.3a, was subdivided into three regions where three separate meshing methods were applied using the ANSYS® mesh generation tool. In a two-dimensional slice, mesh can be seen in Figure 5.5. For the region around the cylinder, a quad-only swept method allowed for better mesh quality around the area of greatest importance. The wake of the cylinder used a structured quad method to provide sufficient resolution to capture the three-dimensional wake effects. For the remainder of the control volume, an uncontrolled structured-quad mesh was used because there was no need to refine the region, as it is an area of little importance for the overall CFD simulation.

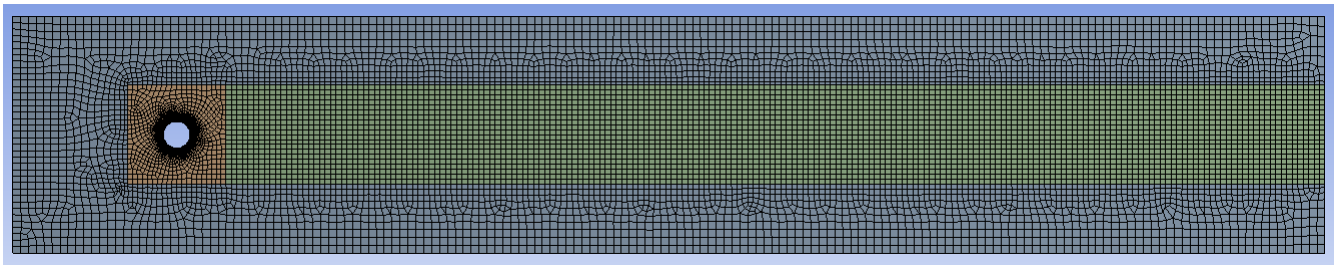
Figure 5.5 2D Slice, Wireframe Mesh

In the span-wise direction of the cylinder, an initial number division of 50 was used for the lower threshold with increasing values as needed, for the mesh studies. Following the circumference of the cylinder, an initial total of 360 divisions were used on the cylinder with 30 divisions on each of the flat

front faces of the dodecagonal. These values were used for the lower threshold of the mesh for most cases of the simulation. The average for upper span-wise divisions was 70 and the average face divisions being closer to 50.

According to ANSYS® documentation (ANSYS® 2017), for accurate results the near wall treatment needs to be considered for developing the boundary layer around the dodecagonal cylinder. A general approach for handling the near-wall treatment is the use of a logarithmic wall function that models the boundary layer, with the requirement of a first layer wall thickness of approximately 30 in terms of the y+. Use of a near wall treatment for a y+ value approximately 1 is needed to resolve the boundary layer without a wall function. The disadvantage of using such a small first layer wall thickness as 1 is the increased meshing needed, which the larger mesh increases the computational time. The chosen turbulence model was the k-ω SAS-SST. This model requires the first layer wall y+ thickness to be approximately 1 to model the wall forces accurately. The modeling of the near wall treatment is described further by the Law of the Wall in the next section.

5.5 LAW OF THE WALL

The Law of the Wall was developed to better understand the boundary layer near a smooth solid for the case of a flat plate. Turbulence typically develops due to the presence of walls with the Law of the Wall being developed on the assumption that near wall turbulence is dependent of flow conditions with no interference from the flow conditions far away from the wall (Pope 2000). The development of the relations is shown by Equations 5.1 - 5.3. With the introduction of frictional velocity, two dimensionless values of dimensionless length and dimensionless velocity are developed. With no other observable properties to influence the frictional velocity, the u+ becomes dependent on only the y+, based on the shear rate for the laminar layer near the wall.

The friction velocity is defined as,

$$u_\tau = \sqrt{\frac{\tau_w}{\rho}} \quad \text{(Equation 5.1)}$$

Where:

τ_w= Shear rate,
ρ = density.

The dimensionless wall distance is defined as,

$$y^+ = \frac{u_\tau y}{\nu} \quad \text{(Equation 5.2)}$$

Where:

y = distance from wall,
ν = kinematic viscosity.

The dimensionless velocity is defined as,

$$u^+ = \bar{u}\sqrt{\frac{\tau_w}{\rho}} \quad \text{(Equation 5.3)}$$

Where:

$\bar{u}$ = time averaged velocity.

The assumptions used for the development of the boundary layer are smooth walls with a condition of 0 velocity (no-slip). This will lead to the flow near the wall being treated as laminar, which this section of the boundary layer being normally referred to as the laminar sub-layer (Pope 2000). It will determine how deep turbulence perturbation will penetrate this layer and in turn determines the layer's thickness. Prandtl's mixing length model (Equation 5.4) is used to model the turbulence scales. This model is compared to experimental data of the universal properties of the turbulent flow near a solid boundary was created, as seen in Figure 5.6. The three layers for a turbulent flow: viscous sub-layer y+ = 5, transitional "buffer zone" = 5 < y+ < 30, and the fully turbulent region y+ >=30 (ANSYS® 2017).

$$u^+ = \frac{\bar{u}}{u_\tau} \qquad \text{(Equation 5.4)}$$

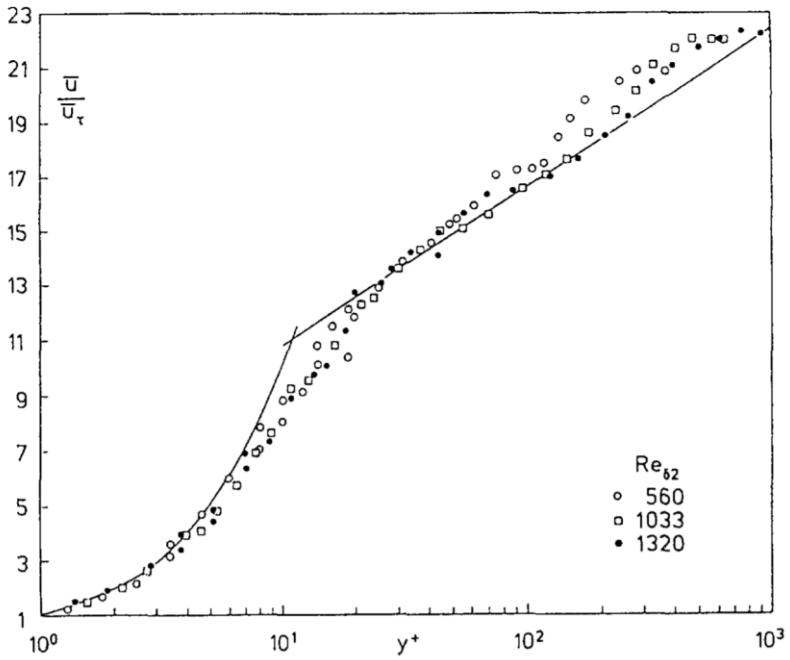

Figure 5.6 Non-Dimensionalized Behavior of the Boundary Layer (Fernholz, H. and Finleyt, P. 1996 with LDV measurement from Djenidi and Antonia 1993)

5.6 BOUNDARY CONDITIONS

The highest velocity corresponding to the speed of sound (Mach number where Mach 1 is 343 m/s) is less than 0.2. This means that the general flow is considered incompressible flow, allowing neglection of the energy equation and changing bulk density. The boundary condition for the study includes three non-velocity (no-slip) walls and the top and bottom of the two-dimensional slice with the body of the cylinder. The no-slip walls allow development of the boundary layer. The inlet is considered a constant velocity and can be considered similar to a free-stream flow while the outlet was selected to be a pressure opening while the control volume cannot be considered long enough to resolve the entire wake due to recirculation of the flow at the outflow boundary. The opening boundary condition was applied to allow for flow calculations to cross the outlet. For three-dimensional consideration, the z-direction (span-wise direction) boundaries are linked by a periodic and translation boundary condition.

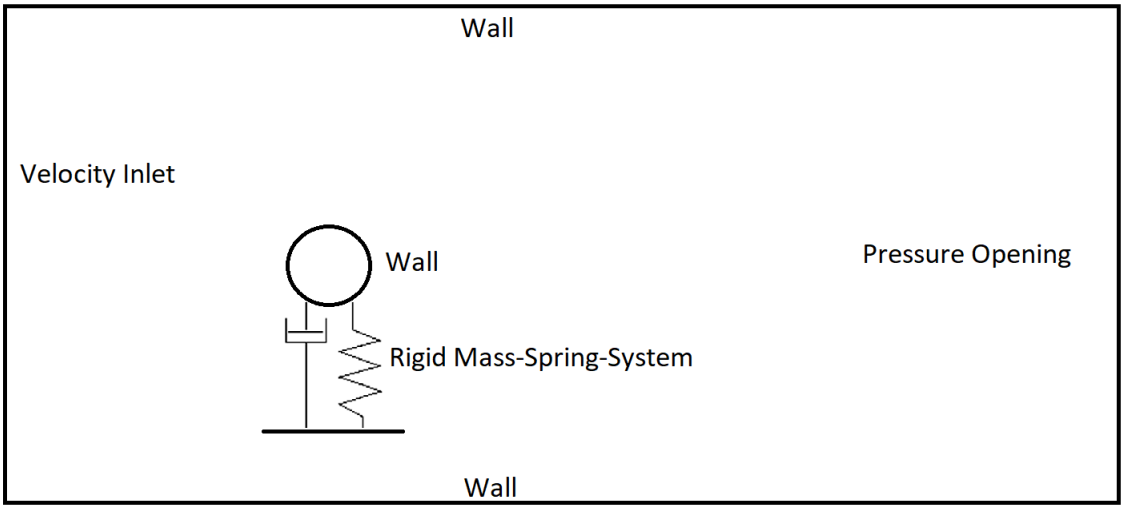

Figure 5.7 Boundary Conditions

For the dynamic case, the dynamic mesh option was set to allow the ANSYS® CFX package to solve for the overall fluid field and then use that information to calculate the displacement of the rigid body cylinder. The initial position of the cylinder was set to the original position of the static cylinder. For a rigid body setup in CFX, several conditions and terms had to be defined. The moments of inertia terms had to be set to 0 to prevent rotation of the body. The initial mass is given as 2.78 kg (6.13 lbs.). The movement of the cylinder was restricted to only the y-direction (vertical direction or tangential to the flow) using a standard Cartesian orientation with a spring constant of 5786.5 N/m (4267.9 lb/ft), similar to the experimental conditions.

5.7 TEMPORAL AND INITIALIZATION CONDITIONS

There are two steps to set the initialization conditions for the CFD simulation. The first step has an initialization condition where the flow field can be considered non-moving (0 m/s velocity) or with a flow conditions that match the inlet velocity value. The simulation was set to solve as a steady state case. The intended tolerance was set to 1×10^{-4} as an acceptable convergence criterion. The solution in lower flow regimes ($Re < 10^5$) were able to converge at tighter tolerances of 1×10^{-6}. In the higher flow regimes

(10^5 < Re), the solution did not converge to 1×10^{-6}. Instead, the solution could converge at 1×10^{-5} within the same iteration limit (Figure 5.8). Other examples of convergence can be seen in Appendix A. The converged steady-state solutions offered lower results than expected when compared to experimental results. However, this converged solution would be used to initialization the transient solution. This allowed for the transient solution to develop further due to an already solved steady-state solution. From the steady-state condition, transient flow can be observed to develop from the oscillating monitors.

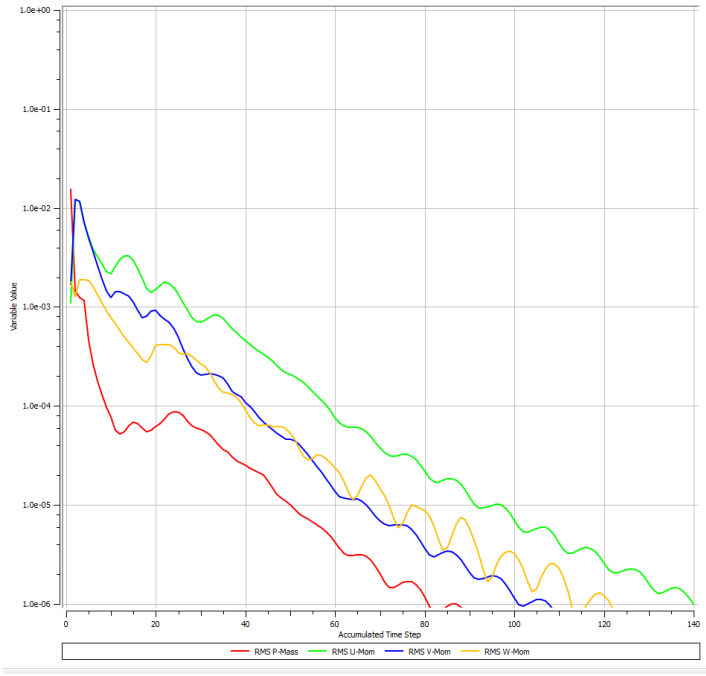

Figure 5.8 Convergence for Velocity of 5 m/s

For transient solutions, there needs to be consideration of simulation stability (Anderson 2000). This can be described by the Courant-Friedrichs-Lewy (CFL) condition (Courant number), shown in Equation 5.5. The CFL condition is a dimensionless number. It relates the freestream velocity to the time-step and the grid spacing, where a CFL number close to 1 is considered stable and accurate. The implementation used by ANSYS® CFX does not need a global CFL condition of 1 and can rely on higher CFL numbers to remain stable. This is not always accurate (ANSYS® 2017). There needs to be consideration about a sufficiently small time-step needed for accuracy.

The CFL (Courant number) is defined as,

$$C = \frac{\Delta t}{\Delta x_{cell}} u_{\infty} \quad \text{(Equation 5.5)}$$

Where:

C = Courant number
Δt = Change in time (seconds)
Δx_{cell} = Minimum cell length (meters)
u_{∞} = Freestream velocity (m/s)

As general rule of thumb, the time-step for the overall simulation should be initially 1,000 samples or more depending on the expected shedding frequency and unsteadiness of the problem. The initially given sampling rate of 1,000 was able to capture the necessary physics for low to mid-Reynolds number flows. The time-step should be small enough to prevent "jumps", so the fluid volumes do not skip any cells. This keeps the problem within the physical realm, reducing numerical noise. The initial time-step is determined by dividing the reference length, which for this case was 0.1016 meters, of the cylinder by the free stream velocity by 10 (Equation 5.6). The calculated time-step would be used as an initial value with, additional lower time-steps to consider the results temporal independent.

$$\Delta t = \frac{D}{10 u_{\infty}} \quad \text{(Equation 5.6)}$$

Where:

D = Diameter.

5.8 RESIDUAL HANDLING

The ANSYS® CFX program handles convergence, using the of Root Mean Square (RMS) method. CFX monitors the residual difference of the physical properties between the previous iteration/time-step to the current iteration before proceeding to the next solver step. There is little handling from the user at the run step except to monitor the physical characteristics of interest which are defined during simulation setup. The monitored values for the static case are the drag and lift force with the amplitude displacement monitored for the dynamic case. The mean value of the drag and lift forces are averaged for the mean

value, with only the maximum displacements averaged for the dynamic case. Lift force is shown as an example in Figure 5.9. The accuracy of CFD result were compared to the experimental results using the percent difference method, Equation 5.7.

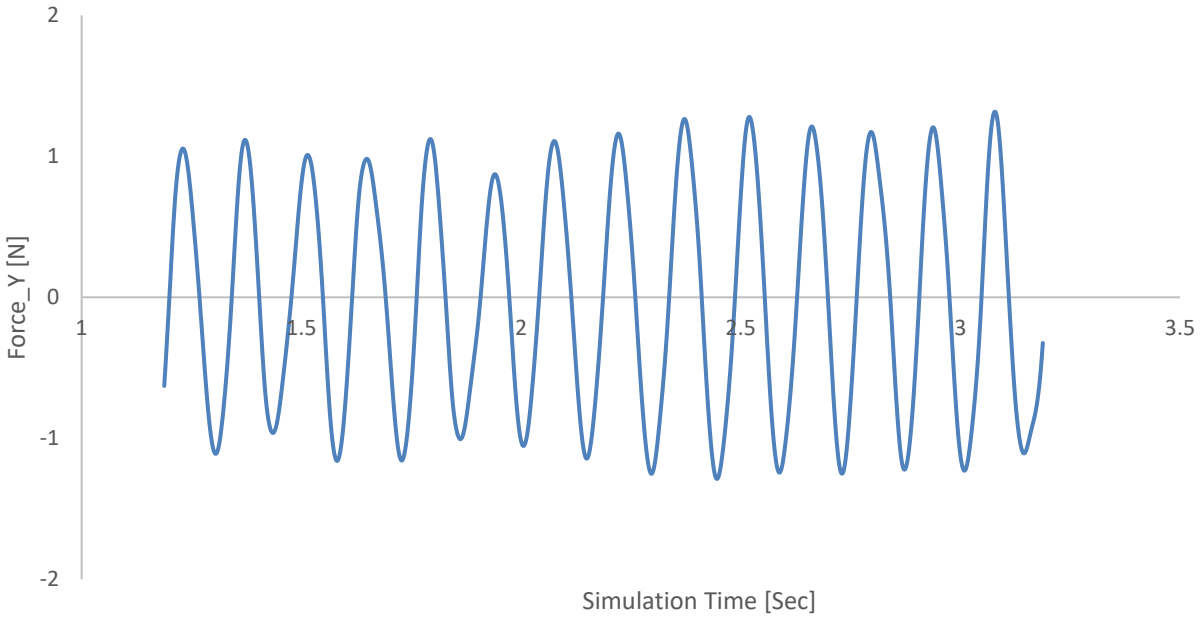

Figure 5.9 Lift Force Temporal Oscillation

The %-difference is defined as,

$$\%_{difference} = 100 \times \left| \frac{Experimental\ Value - Computational\ Value}{Experimental\ Value} \right| \qquad \text{(Equation 5.7)}$$

CHAPTER 6. RESULTS AND DISCUSSION

6.1 BACKGROUND INFORMATION

The main goal of the study was to replicate wind tunnel experiments with Computational Fluid Dynamics (CFD) and validate the accuracy of the computations. Two overarching flows over a dodecagonal cylinder cases were replicated. The first case was a statically rigid cylinder. The drag coefficient for both flat, front facing and corner facing cylinders were considered along with the lift coefficient at varying angles of attack. The dynamic case was considered only for a face-oriented dodecagonal cylinder with a mass-spring system. The cylinder was restricted to move only tangential to the fluid flow, while being subjected to the lock-in range for vortex shedding.

6.2 TURBULENCE MODEL COMPARISON

Over a large range of Reynolds numbers, the mean drag coefficient for a dodecagonal (12-sided) cylinder showed little variation from the experimental value of 1.56. The flow was fully turbulent for Reynolds numbers above 300 and to properly simulate the turbulence without the use of Direct Numerical Simulation (DNS) the use of turbulence models was needed. The near wall forces which acted on the dodecagonal cylinder were sensitive to the near wall treatments handled by the turbulence models. It is recommended not to use the logarithmic wall function typically used by k-ε turbulence models and instead to fully resolve the boundary layer with a y+ value of 1. The following turbulence models are based on the k-ω which handles the full boundary layer and were used: Shear Stress Transport (SST), Scale-Adaptive Simulation (SAS) SST, and the Detached-Eddy Simulation (DES). Table 6.1 shows a comparison between the simulation results and the experimental values at a Re of 7.5×10^4. The flow velocity was under the Mach number < 0.2, where the flow was considered incompressible and the energy equation was neglected.

The SAS-SST and DES turbulence approaches provided the most accurate results when compared to the experimental values at the given mesh sizing and time step. The SAS-SST turbulence model was selected due to it being relatively cheaper in terms of computational time, when compared to DES. This was only an observational point when comparing the CPU wall clock as it completes a similar time of computational run time of 5 seconds. Further mesh and temporal studies would be required to fully justify this statement, but that is beyond the scope of this study.

Table 6.1 Turbulence Model Comparison for a Dodecagonal Cylinder Comparison to Experiment

Turbulence Model	Grid Size	Time-step (s)	Mean C_D (Exp.) (Chang, 2010)	Mean C_D (CFD)	Strouhal (Exp.)	Strouhal (CFD)
SST	810835	0.002	1.56 (+/- 2%)	1.24 (20.5%)	0.20	0.18 (10%)
SAS-SST	787760	0.002	1.56 (+/- 2%)	1.57 (0.6%)	0.20	0.21 (5%)
DES	820347	0.001	1.56 (+/- 2%)	1.58 (1.2%)	0.20	0.2 (0%)

6.3 STATIC DRAG COEFFICIENT

Two drag cases were studied for a dodecagonal (12-sided) cylinder shown in the experimental results. The higher drag for a dodecagonal cylinder is 1.56 with a 2% variation in value at higher Reynolds number of 1×10^5 to 3.5×10^5 for the flat front orientation of the cylinder. For a corner facing orientation, the drag was approximately 1.40 with a similar variation of 2% from experimental results at similar range Reynolds numbers. This deviation in values between the cases can be defined by how a flat face orientation is more of a blunt body which leads to higher stagnation pressure. The corner orientation can be described as more aerodynamic in shape, with a smaller drag.

The mean drag force was monitored in the CFD simulations and used to calculate the mean drag coefficient for a dodecagonal cylinder, with the lift force being monitored to determine the frequency to calculate the Strouhal number. The results for the drag coefficient and Strouhal number were taken at three different Reynolds numbers of 1.0×10^5, 1.35×10^5, and 1.6×10^5 with corresponding velocities of 15, 20, and 24 m/s, respectfully. The highest velocity was under a Mach number of 0.2 (Mach 1 = 343 m/s), where the flow was considered incompressible at ground level and the energy equation can be neglected.

Shown in Table 6.2 is a comparison of the drag coefficient and Strouhal number results for a flat facing cylinder at different mesh densities against the experimental results. The chosen tolerance was 10% or less for variation against experimental results. For the initial mesh cases, the largest error against experimental results was 7% for the case at 1.63×10^5 with increased mesh density having less than 4%. For either case, the deviation was under 10%, with similar mesh densities that fall within the cases shown in Table 6.2 showed acceptable results.

Table 6.2 Flat Facing Orientation Drag Mesh Study (Experiments from Chang 2010)

Re	Grid Size #1	Mean C_D (Exp.)	Mean C_D (CFD)	%-diff	Grid Size #2	Mean C_D (Exp.)	Mean C_D (CFD)	%-diff
1.0×10^5	380769	1.56 (+/- 2%)	1.65	5.8%	1185847	1.56 (+/- 2%)	1.61	3.21%
1.35×10^5	405206	1.56 (+/- 2%)	1.61	3.2%	1210169	1.56 (+/- 2%)	1.57	0.64%
1.6×10^5	455368	1.56 (+/- 2%)	1.45	7.1%	1217235	1.56 (+/- 2%)	1.57	0.64%

Shown in Table 6.3 is a mesh study for a corner orientation at a Reynolds number of 1.6×10^5, with the highest values for drag at the smallest listed mesh of 12.9%. While with increasing mesh density the value becomes closer to experimental values, the decreases in values was considered "extreme" for a large deviation from experimental values, so other factors were explored. The sensitivity of the time-step shown in Table 6.4 for a grid density of 756834 nodes at Reynolds numbers of 1.6×10^5. The results for the change in time-step showed closer agreement to experimental results, showing the time-step has a large influence on certain results. Shown in Table 6.5 is the drag results at a mesh density of 756,834 nodes at different Reynolds numbers.

Table 6.3 Corner Orientation Mesh Study (Reynolds number of 1.6×10^5 with Experiment from Chang 2010)

Grid Size #1	Mean C_D (Exp.)	Mean C_D (CFD)	%-diff
756834	1.40 (+/- 2%)	1.58	12.9%
1025014	1.40 (+/- 2%)	1.50	7.1%
1293788	1.40 (+/- 2%)	1.47	5.0%

Table 6.4 Temporal Dependency Study for (Mesh Density 756834 Nodes and Reynolds of 1.6×10^5 with Experiments from Chang 2010)

Time-step (s)	Mean C_D (Exp.)	Mean C_D (CFD)	%-diff
0.01	1.40 (+/- 2%)	1.58	12.9%
0.002	1.40 (+/- 2%)	1.43	2.1%
0.001	1.40 (+/- 2%)	1.42	1.4%

Table 6.5 Drag Results for Corner Orientation (Mesh Density of 756834 Nodes and a Time-step of 0.002 seconds with Experiments from Chang 2010)

Re	Mean C_D (Exp.)	Mean C_D (CFD)	%-diff
1.0×10^5	1.40 (+/- 2%)	1.38	1.4%
1.35×10^5	1.40 (+/- 2%)	1.43	2.1%
1.6×10^5	1.40 (+/- 2%)	1.39	0.7%

The flat facing orientation drag results from Table 6.4 at the grid sizing #2 and drag for corner orientation from Table 6.5 were compared to the experimental results shown in Figure 6.1. There was reasonable agreement between experimental results and CFD results. This demonstrates that the current CFD tools produce sufficiently accurate simulation results for flow over a dodecagonal cylinder in fully turbulent flow regime at high Reynolds numbers.

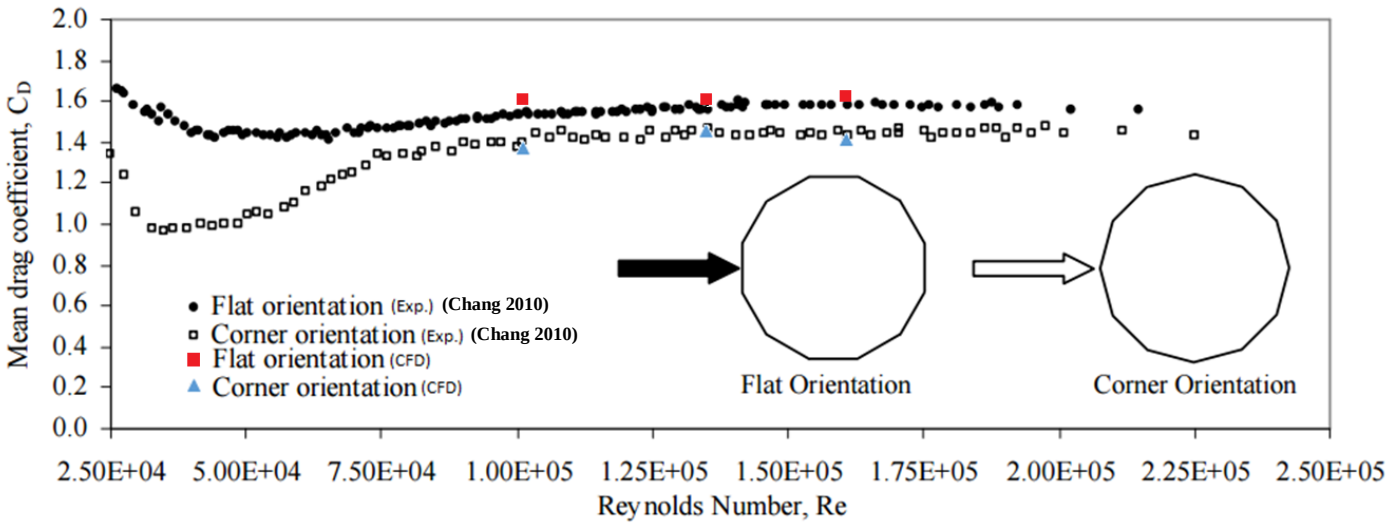

Figure 6.1 CFD Results compared to Experimental Results

Figure 6.2 illustrates the velocity contours of the flat front and corner facing orientations at a Re number of 1.6×10^5. The flow was initialized at a time-step of 0 seconds from a solved steady-state solution. Then, the flow developed shear layers at approximately 0.1 seconds of simulation time before the downstream wake becomes fully turbulent prior to 0.3 seconds for flows at a Re number of 1.6×10^5. The shear layer for a symmetrical body is termed von-Karman vortex shedding and can be seen in both Figure 6.2 cases. The von-Karman sheets began to dissipate at 20-25 diameters from the upstream cylinder, which could be caused by the high velocity stream and the vortexes breaking down to its smaller eddies.

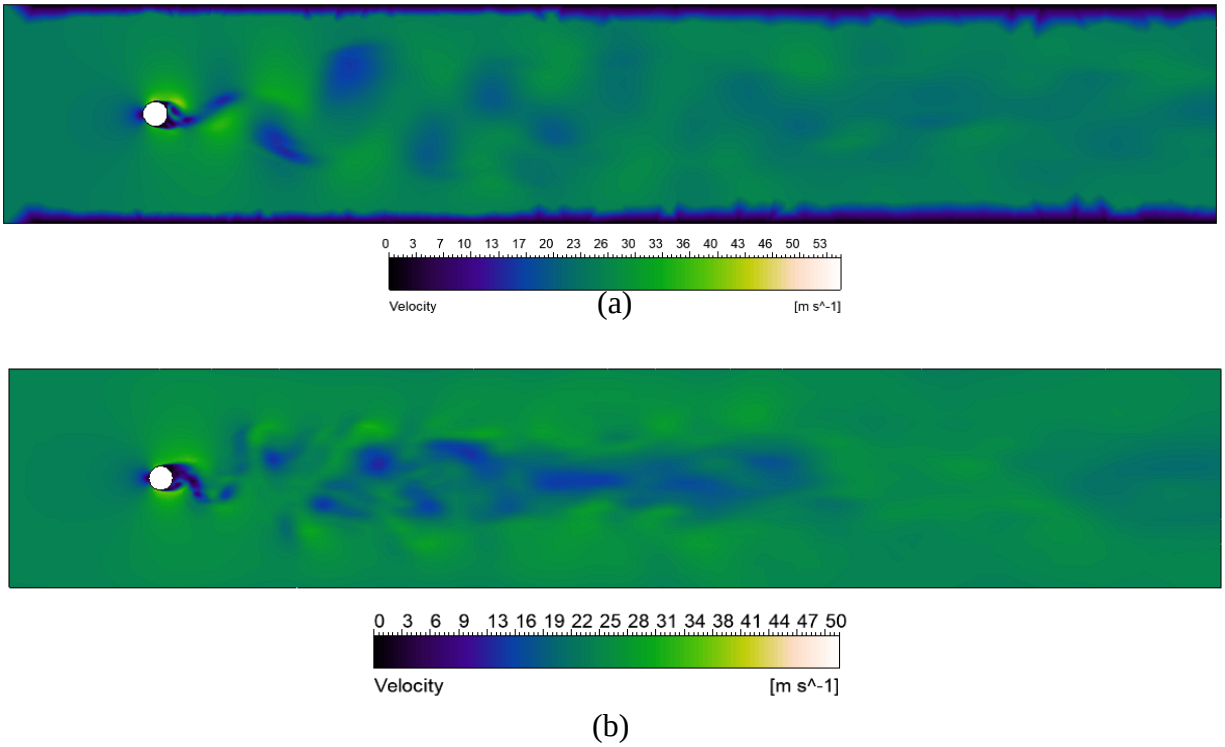

Figure 6.2 Velocity Contours at Re = 1.6×10^5 (a) Flat Front Orientation @ 11.4 Seconds (b) Corner Orientation @ 0.838 Seconds

For a circular cylinder, when the flow becomes unsteady, shear layers begin to develop at a point near the back of the cylinder. When the flow grows in Reynolds numbers and becomes increasingly turbulent, the shear layer separation begins to occur closer to the front area of the cylinder. This was not the case seen for a dodecagonal cylinder at high Reynolds number flows. The separation point was

"tripped" at one of the leading sharp corners for the dodecagonal cylinder. This was the same for all simulated cases at high Reynolds numbers. Shown in Figure 6.3 are the separation points for corner and flat front orientations.

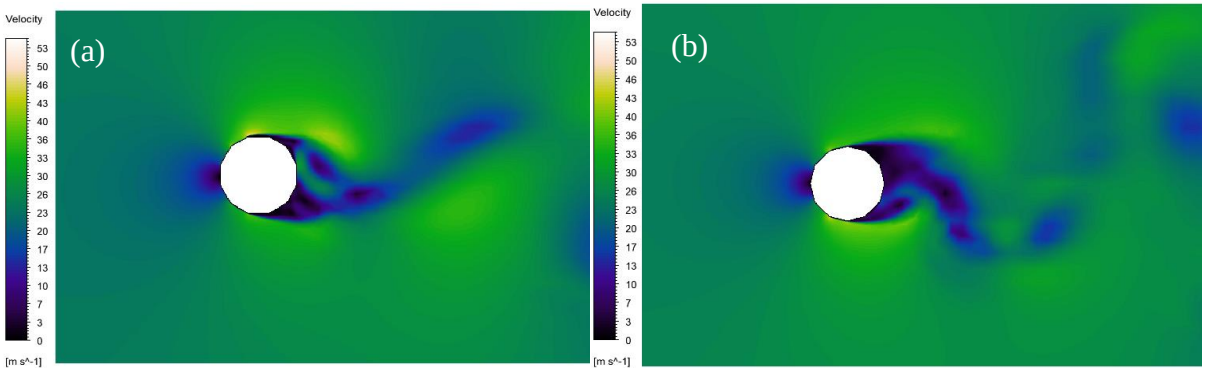

Figure 6.3 (a) Flat Front Orientation Separation Point (b) Corner Orientation Separation Point

6.4 LIFT COEFFICIENT

For both the flat and corner orientation cases, the mean lift coefficient was at 0 for 0° angle of attack, an expected behavior for symmetrical bodies. For a flat orientation, the angle of attack was changed to -6°, with a lift coefficient of 0.21 at a mesh density of approximately 600,000 nodes and time-step of 0.002 seconds. Based on the principle of symmetry for an angle of attack 6° the lift coefficient was determined to be -0.21. The lift coefficient for the corner orientation at angle of attack of -5° was found to be -0.12 with a mesh density of approximately 700,000 nodes at a time-step of 0.002 seconds. Similarly, based on the principle of symmetry, the lift coefficient for 5° was determined to be 0.12. The lift coefficients for both cases are compared to the slope of the experimental results in Figure 6.4. The slope for the flat orientation experimental resulted was -0.7π with the CFD at a slope of -0.64π the difference was 9%. The slope for the experimental results for the corner orientation was 0.5π with the CFD results slope being 0.44π a difference of 12%. The lift values were close in value, within an acceptable margin.

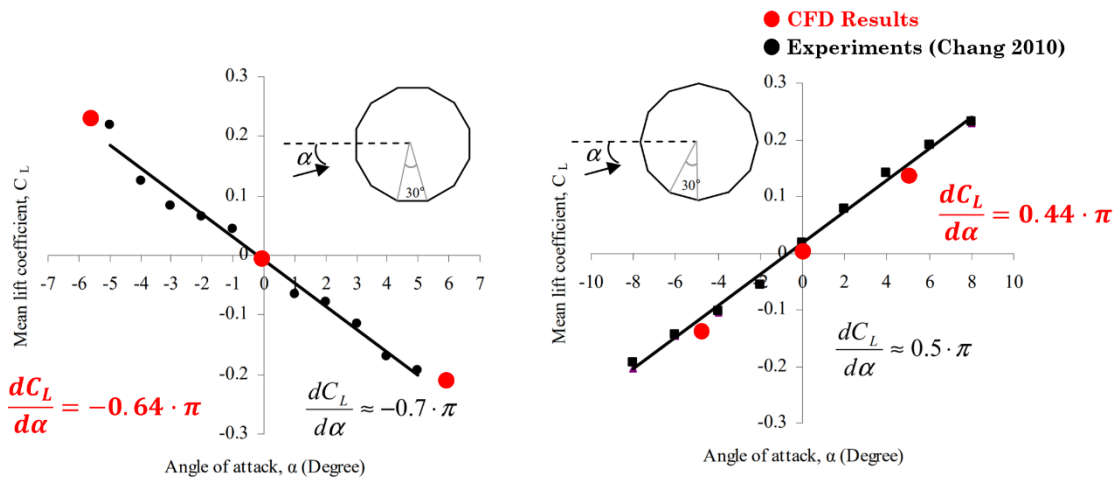

(a) Flat orientation (b) Corner orientation

Figure 6.4 CFD Lift Coefficient Compared to Experimental Results

6.5 DYNAMIC CASE

The dynamic case was a mass-spring system with limited motion in the longitudinal direction to the fluid flow, this orientation subjected the dodecagonal cylinder to unsteady loading. The experimental cylinder results had an applied weight of 2.78 kg (6.13 lb) with a system stiffness of 5786.5 N/m (396.5 lb_f/ft). The fluid regime mimicked the wind tunnel test chamber, used a cylinder height of 0.914-meters (36-inches) and a span-wise distance of 0.762-meters (30-inches). The full three-dimensional effects must be considered for the loading on the cylinder as turbulence is a three-dimensional phenomenon. Additionally, the CFX rigid body solver used a moving/deforming mesh tool, to solve the displacement caused by the oscillatory motion. This was due to the turbulent fluid flow with no rotation being taken into consideration and movement limited to the tangential direction. The mass and system stiffness were equivalent to the measurements from the previous experimental results.

The most extreme case was the flat facing orientation due to the higher drag force, when compared to corner orientation orientations. Similar conditions for mesh density, initial conditions, and boundary conditions to the flat front facing orientation drag coefficient cases were used for all cases. The only

changing variable for the mesh was the first cell height to accommodate y+ for the lower Reynolds number range. The corresponding velocity range of 2.5 m/s to 6 m/s corresponding to 3 and 9 reduced velocity for a 0.1016-meter dodecagonal cylinder. This flow regime was considered incompressible and the thermodynamic considerations can be neglected.

Shown in Figure 6.5 is the comparison of experimental results to the CFD results for a mass-spring cylinder displacement ratio, lock-in conditions. There was agreement for the general behavior between the experimental and computational results for the displacement ratio. However, the amplitudes for outside the lock-in range did not maintain a noticeable displacement and went to 0. The greatest displacement for the computational results was at a reduced velocity of 5.75, which had a displacement ratio of 0.164. The reduced velocity is the ratio between the freestream velocity to the unsteady oscillation frequency multiplied by the diameter, with the reduced frequency being the ratio between the shedding frequency and natural frequency. A visualization of the cylinder movement can be seen in Figure 6.6. When compared to the experimental displacement ratio of 0.159, there was less than a 5% difference. For the computational results, the displacement for lock-in occurred between 4 and 6 reduced velocities. After the value of 6, the displacement ratio for computational results began to level out to less than 0.05. The general behavior was similar, but a physical consideration for the variation in behavior between experimental and computational results could be the wind tunnel model might not have a uniform displacement across the cylinder. This could have added additional unsteadiness to the experimental results.

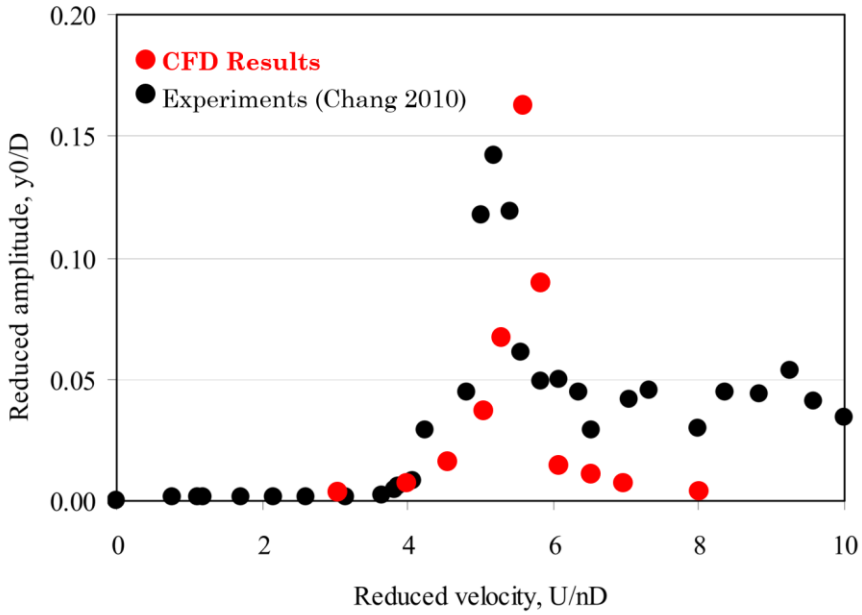

Figure 6.5 CFD vs. Experimental Reduced Amplitude Ratio

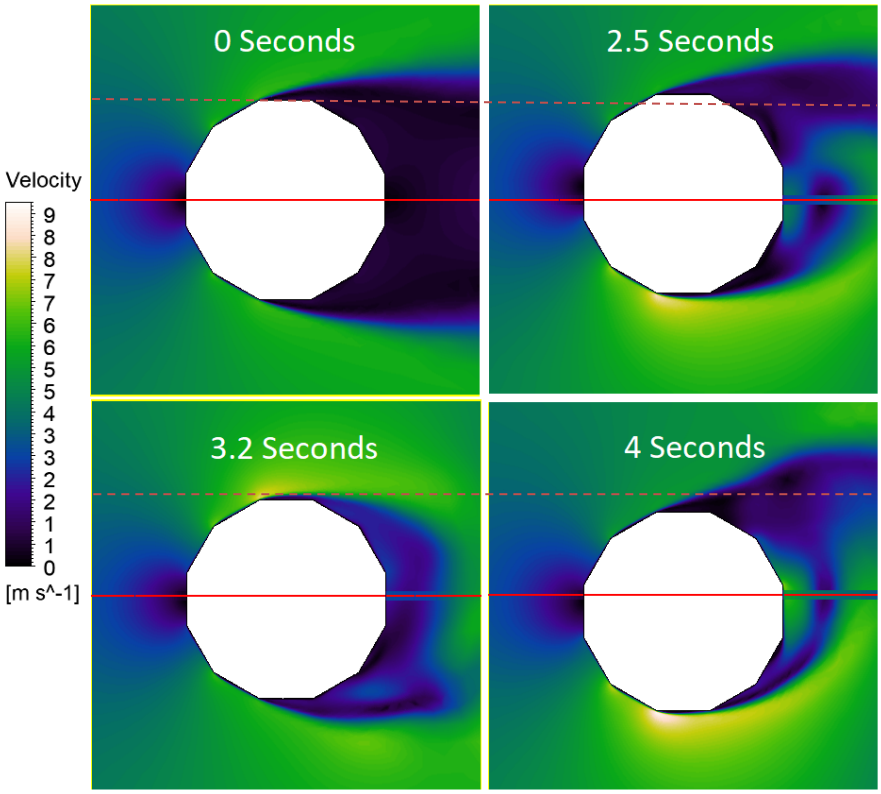

Figure 6.6 Displacement Visualization (Ur = 5.75)

The frequency comparison between the computational and experimental results for the reduced velocity can be seen in Figure 6.7. From the experiments results, the lock-in frequency, when the vortex

shedding frequency matches the natural frequency of the system, is between the values of the reduced velocity of 5 to 7 with a Strouhal number of 0.2. The CFD results, when just comparing the linear portion of the results had a Strouhal number of 0.2, like the experimental results. The lock-in frequencies for the computational results can be observed between 5 and 6 reduced velocity, with some noticeable increase at reduced velocities of 6.25 and 6.5 before there is return to the linear range at 7. The increase started, from reduced velocity of 6.25, this can be a factor due to the limitations of the turbulence model used as Reynold-Averaged Navier-Stokes (RANS) based approaches are temporal averaged.

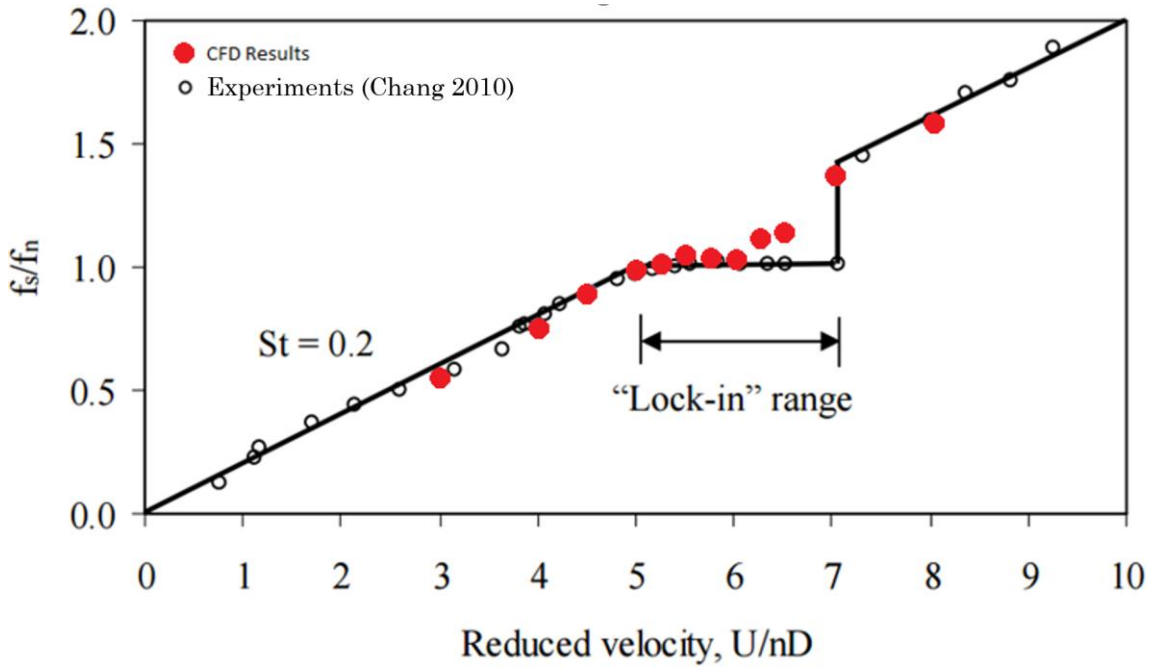

Figure 6.7 Reduced Frequency vs. Reduced Velocity Comparison

There were considerations for the dependencies on mesh and time-step sizes. However, cases showed little variation for not capturing the full lock-in range. The used time-step of 0.002 seconds might not be sufficiently small to capture the full temporal dependencies. Lower time-step cases examined the frequency ratio and showed little variation. Full temporal dependencies could not be fully investigated due to limitation of research time. This is something to consider for further investigation. The SAS-SST turbulence model proved suitable for predicting drag and lift for a dodecagonal cylinder at a subcritical Reynolds number. It had the ability to capture expected frequency for a portion of the

lock-in behavior. The SAS-SST turbulence model based on the RANS SST model might permit capture of full turbulence behavior. For further investigations more "true" hybrid approaches should be considered for the possibility of LES models.

6.6 SCRUTON NUMBER AND ADDED MASS

The Scruton number is an important number for wind engineering purposes as it considers the structural response due to wind loading. The Scruton number is described by Equation 6.1 (Simiu 1996), the formulation takes into consideration the damping ratio, inertial mass, stiffness, and natural frequency.

$$S_c = \frac{m\zeta}{pD^2} \qquad \text{(Equation 6.1)}$$

Where:

m = mass (kg)

ζ = Damping ratio

p = Density (kg/m^3)

D = Cylinder Cross-Section (m)

An initial work the use CFD to study the lock-in behavior at different masses to get the displacement ratios for the Scruton number. The CFD frequencies can be seen in Table 6.6 compared the natural frequencies of the masses used from experimental results. The experimental damping ratios were used with the frequencies achieved from CFD to calculate the Scruton number. The damping ratios were compiled from the CFD results in Table 6.6.

The fitted curved, with a similar format to previous a study (Chang 2010), was applied to the CFD results for Scruton number and displacement ratio, as shown in Figure 6.8. The fitted curve data for most values, except for an added mass case of 0 kg (base case), resemble the curve for a circular cylinder. The most likely consideration for each mass damping cases is that the max displacement occurs at different lock-in velocities than the chosen. This would lead to the need for further investigations of maximum

displacements. For most cases, the lock-in range occurs at a reduced velocity between 5 and 7, with a maximum displacement occurring at 5.75 for the base case. A reduced velocity of 5.75 was used for each mass, but there could be different maximum displacement case for the associated Scruton number. The matter must be further investigated.

Table 6.6 Added Mass (Experiments from Chang 2010)

Mass (kg)	Added Mass (kg)	Experimental Damping Ratio	Natural Frequency (Hz)	CFD Shedding Frequency (Hz)	Sc	CFD Displacement Ratio
2.79	0	0.001952	7.25	7.20	0.86	0.610
4.43	1.65	0.001465	5.75	5.90	1.02	0.072
6.64	3.85	0.001534	4.70	5.00	1.62	0.022
8.31	5.52	0.001666	4.20	4.34	2.18	0.007
10.26	7.47	0.001775	3.78	4.00	2.87	0.009
12.26	9.47	0.001873	3.46	3.60	3.62	0.003
14.17	11.38	0.002135	3.22	3.30	4.78	0.001

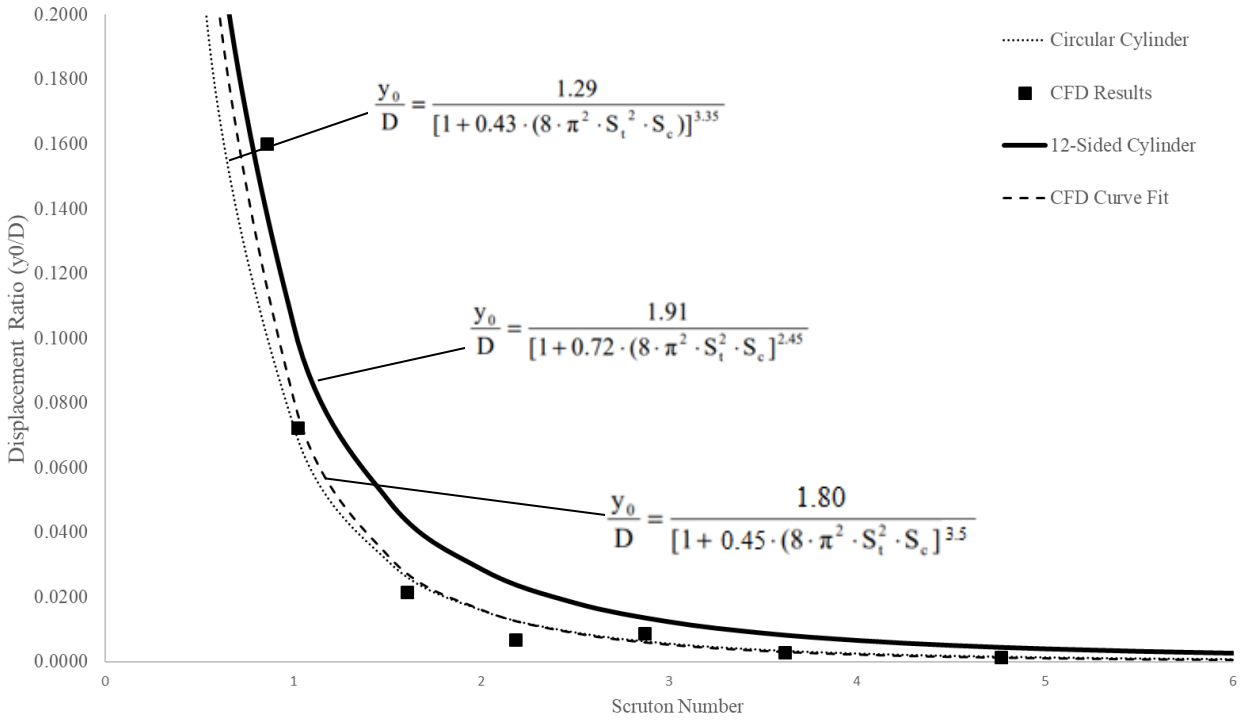

Figure 6.8 Scruton number vs. Displacement Ratio

As noted by Simiu, et al. (1996), various empirical and analytical models have been developed to represent the vortex shedding response of bluff bodies. Examples can be seen in Figure 6.8, with displacement as a function of the natural frequency in terms of Scruton number. The compared relations were derived using previous fitted curves to experimental data. The curve fitted to the computational results is shown in Equation 6.2. All the results were taken at a single lock-in value of a reduced velocity of 5.75. The case of 5.75 may be close to the maximum displacement, but the maximum displacement may have some variation for each added mass damping case. The curve fitted to the computational results is similar to that for a circular cylinder. However, this could be because the maximum lock-in amplitude velocity was not known for all the tested cases.

$$\frac{y_0}{D} = \frac{1.80}{[1+0.45(8\pi^2 {S_t}^2 S_c)]^{3.5}} \qquad \text{(Equation 6.2)}$$

The derivation of the relation starts with the convention to separate the force into three components for self-oscillation (se), buffeting (b) and vortex shedding (v) given by the following equation:

$$F^y = F_{se}^y + F_b^y + F_v^y \qquad \text{(Equation 6.3)}$$

The expression for buffeting is shown in Equation 6.4 (Sarkar 1992):

$$F_b^y(s) = -\frac{1}{2}\rho UD(C_D + C_L') \int_0^s [w(\sigma)\varphi_w'(s-\sigma)]d\sigma \qquad \text{(Equation 6.4)}$$

Where:

φ_w' = derivative of buffeting indicial function.

Self-exciting is shown in Equation 6.5.

$$F_{se}^y(t) = \frac{1}{2}\rho UD(KH_1^* \frac{\dot{y}}{U}) \qquad \text{(Equation 6.5)}$$

Where:

K = reduced frequency,

H_1^* = non-dimensional function of reduced frequency or reduced velocity known as flutter derivative in Quasi-steady form.

Scanlan's Van-Der Pole Oscillator Model (Simiu 1996) was used for the calculating the vortex-shedding force.

$$F_v^y(t) = \frac{1}{2}\rho U U^2 D[Y_1\left(1-\varepsilon\frac{y^2}{D^2}\right)\frac{\dot{y}}{U} + Y_2\frac{y}{D} + \widetilde{C_L}\,sin(\omega_n t + \varphi)] \qquad \text{(Equation 6.6)}$$

Where:

Y_1 and ε = self-exited damping parameters,

Y_2 = linear aeroelastic stiffness parameter,

$\widetilde{C_L}$ = RMS of the lift coefficient.

The self-oscillatory behavior is a complex phenomenon. According to Simiu, et al. (1996), there have been attempted to model the behavior using two different equations; one for the structural response and another for the wake oscillations. Equation 6.3 shows the full approach to model the oscillatory behavior. The Y_1, ε, Y_2, and $\widetilde{C_L}$ in Equation 6.6 are functions of the unsteady aerodynamic behavior of the reduced velocity, where Y_2 and $\widetilde{C_L}$ can ignored due to having negligible effects on the response (Simiu 1996). The total Equation 6.3 and all the terms reduce to Equation 6.7, where a single-degree-of freedom model with parameters of Y_1 and ε can be developed. Both Y_1 and ε are observable aerodynamic damping parameters from the experimental models. With the use of the fitted Equation 6.2, the aerodynamic damping parameters were extracted using Equation 6.7 and plotted for a range of Scruton numbers. The Y_1 and ε equations shown in Equation 6.8 and 6.9, respectfully (Simiu, et al. 1996).

$$\frac{y_0}{D} = 2\sqrt{\frac{Y_1 - 8\pi S_c S_t}{Y_1 \varepsilon}} \qquad \text{(Equation 6.7)}$$

$$Y_1 = \frac{8\pi S_c S_t}{1-\varepsilon\frac{\Delta^2}{4}} \qquad \text{(Equation 6.8)}$$

Where:

$$\Delta = \frac{y_0}{D}.$$

$$\varepsilon = \frac{4(S_{c1} - S_{c2})}{\Delta_2{}^2 S_{c1} - \Delta_1{}^2 S_{c2}} \qquad \text{(Equation 6.9)}$$

Where:

S_{c1} = previous Scruton number,

S_{c2} = current Scruton number,

Δ_1 = previous displacement ratio,

Δ_2= current displacement ratio.

The aerodynamic parameters are plotted in Figure 6.9, with the Y_1 plotted against the Scruton number. In figure 6.9 the ε was logarithmically plotted against the Scruton number. The behavioral trends were like experimental results but were with a lower value. These values were non-linear aspects of the self-oscillatory amplitude from the harmonic motion caused by the vortex shedding in wake of the bluff-body. The Y_1 described the amplitude decay response until it reaches a steady-state response within the lock-in range. The ε described the damping response caused by the fluid.

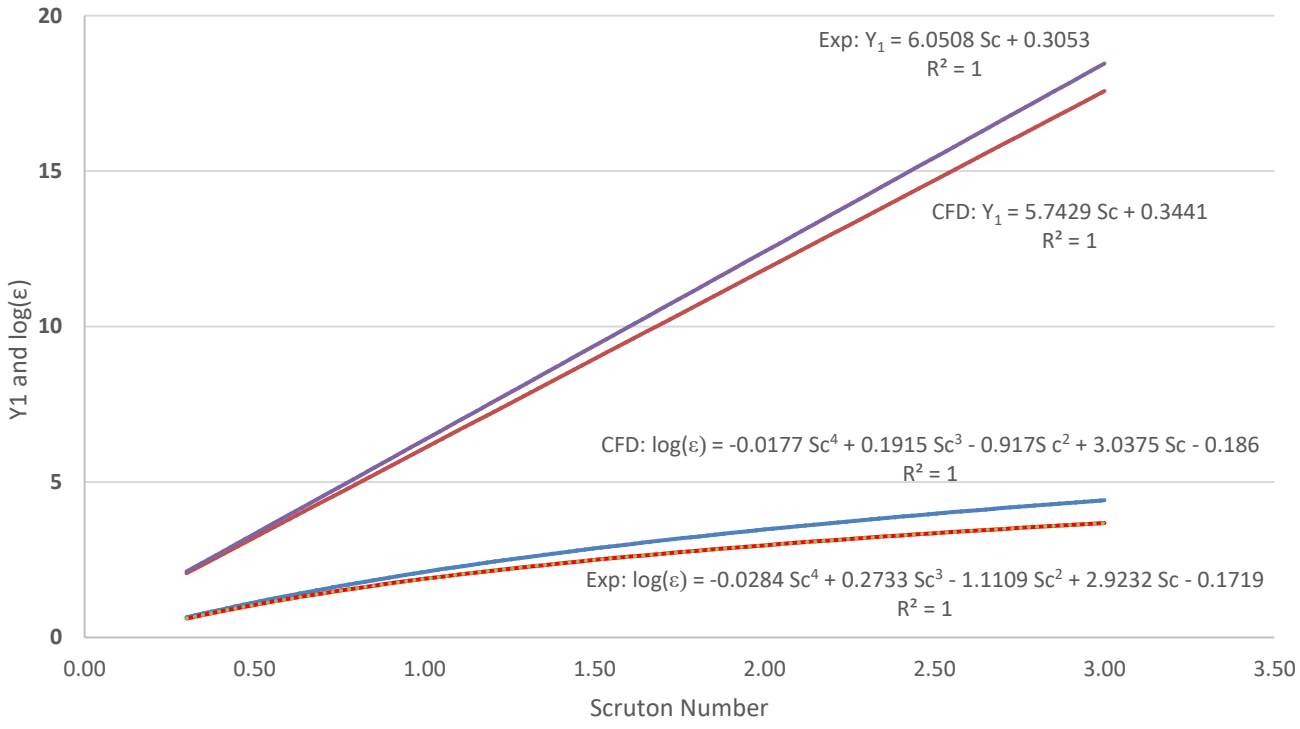

Figure 6.9 Aerodynamic Parameters at Lock-in

CHAPTER 7. SUMMARY, CONCLUSIONS, AND FUTURE WORK

This work sought to validate the use of CFD modeling for determining the aerodynamic parameters of a dodecagonal cylinder. The static cases for drag and lift for fully turbulent, high Reynolds number flows were conducted to investigate the fluid-structural behavior of a dynamic system cylinder. The aerodynamic parameters were compared against wind tunnel experiments to validate the CFD modeling of structural behavior.

Significant findings:

- The lift coefficients for a static dodecagonal cylinder at flat and corner orientations were found at a high Reynolds numbers (Re) with varying angles of attack with reasonable accuracy (less than 15% difference between the computational and wind tunnel experimental results).
- The drag coefficients for flat and corner orientations were compared against wind tunnel experimental values for a range of subcritical Re. The difference in values was less than 10%. With increased mesh density associated with increased spanwise divisions and decreased cell size around the dodecagonal cylinder wall, the difference decreased to 5%. Additional consideration was taken in terms of time-step.
- The linear frequency range before and after the lock-in phenomenon was determined to have little variation from the wind tunnel tests (S_t of 0.2).
- The lock-in frequency ranged between the reduced velocity of 5 and 6 in CFD, while the lock-in frequency ranged between the reduced velocity of 5 and 7 in wind tunnel tests.
- Structural responses with added mass in terms of Scruton number were developed and compared to the wind tunnel experimental results. The responses in CFD for the 12-sided cylinder was similar to the wind tunnel experimental response of circular cylinders.
- The aerodynamic damping that describes the non-linear, self-excited behavior is similar to the wind tunnel experimental results.

The recommendation for the Scruton number is to investigate the full dependencies of the cases and find the maximum displacement for each case, instead of relying on the base case value. This would serve as a more thorough investigation for the effects of added mass and how it changes the displacement ratio. This would have a greater resemblance to reality.

The SAS-SST was shown to be a reasonable turbulence model when dealing with the static cases and determining the vortex shedding frequency. However, higher order turbulence models should be investigated to see if the full lock-in frequencies can be determined for high Reynolds number values. Another consideration is investigating the rigid body solver used in ANSYS® CFX to determine the limitations for rigid cylinder movements. Otherwise, the SAS-SST should be a reasonable turbulence model for a full scale High-Light Mast-Pole (HLMP) due to the validation provided by this study.

Further investigation against wind tunnel experiments could be conducted regarding buffeting, which is the irregular oscillation of an object caused by turbulence. This relation can be expanded upon by the frequency domain and the power spectral density of turbulence in the upstream flow. This behavior can be further defined in terms of aerodynamic admittance, which is a function of the reduced frequency.

REFERENCES

Abdullah, M., et al., “Modeling Flow around Bluff Bodies”, Journal of Computing in Civil Engineering (2005), 19, 104-107.

Alawadhi, E., “Numerical Simulation of Fluid Flow past an Oscillating Triangular Cylinder in a Channel”, Journal of Fluids Engineering (2013), 135.

Anderson, J., “Computational Fluid Dynamics: The Basics with Applications”, McGraw-Hill, Inc. (1995).

ANSYS®, “CFX-Pre User’s Guide”. ANSYS® (2017).

Attia, W., and Ahmed, A., “Aeroelastic Investigation of Long Span Suspension Bridge Decks by Numerical CFD and FSI Analyses”, Civil and Environmental Research (2016), 8.

Bardina, J.E., Huang, P.G., Coakley, T.J., "Turbulence Modeling Validation, Testing, and Development", NASA Technical Memorandum 110446 (1997).

Blevins, Robert D., Flow-induced vibration, Reprint, Krieger Pub Co (2001), Florida.

Blocken, B., Carmeliet, J., and Stathopoulos, T., “CFD evaluation of wind speed conditions in passages between parallel buildings—effects of wall-function roughness modifications for the atmospheric boundary layer flow”, Journal of Wind and Industrial Aerodynamics (2007), 95. 941-962.

Bruno, et al., “3D flow around a rectangular cylinder: A computational study”, Journal of Wind Engineering and Industrial Aerodynamics (2010), Volume 98, Issues 6–7, Pages 263-276, ISSN 0167-6105,

Brusiani, F., Miranda, S., Patruno, L., Ubertini, F., and Vaona, P., “On the evaluation of bridge deck flutter derivatives using RANS turbulence models”, Journal of Wind Engineering and Industrial Aerodynamic (2013), 119, 39-47.

Bourguet, R, et al, “Vortex-induced vibrations of a long flexible cylinder in shear flow”, Journal of Fluid Mechanics (2011), 677, 342-382.

Bunge, U., Gurr, A., and Thiele, F., “Numerical aspects of simulating the flow-induced oscillations of a rectangular bluff body”, Journal of Fluids and Structures (2003), 18, 405-424.

Cao, S., Ozono, S., Tamura, Y., Ge, Y. and Kikugawa, H., “Numerical simulation of Reynolds number effects on velocity shear flow around a circular cylinder”, Journal of Fluids and Structures (2010). 26(5), 685-702.

Cao, S. and Tamura, Y., “Flow around a circular cylinder in linear shear flows at subcritical Reynolds number”, Journal of Wind Engineering and Industrial Aerodynamics (2008). 96(10–11), 1961-1973.

Caracoglia, L., “Analysis of light pole vibration in Illinois”. http://cee.uiuc.edu/nsel/proj/luca.htm. Accessed on November 16th, 2007.

Carassale, L. and Solari, G., “Monte Carlo simulation of wind velocity fields on complex structures”, Journal of Wind Engineering and Industrial Aerodynamics (2006). 94(5), 323-339.

Catalano, P., Wang, M., Iaccarino, G. and Moin, P., “Numerical simulation of the flow around a circular cylinder at high Reynolds numbers”, International Journal of Heat and Fluid Flow (2003). 24(4), 463-469.

Chang, B., Sarkar, P. P., and Phares, B. M., "Aerodynamic Model in Time-domain for Predicting Aerodynamic Loads on a Slender Support Structure”, The ASCE Journal of Engineering Mechanics (2010), Vol. 136, No. 6, pp. 736-746.

Chen, X. and Kareem, A., “Nonlinear response analysis of long-span bridges under turbulent winds”, Journal of Wind Engineering and Industrial Aerodynamics (2001). 89(14–15), 1335-1350.

Chen, W. and Li , “Vortex-induced vibration of stay cable under velocity using CFD numerical simulation method”, Front. Archit. Civ. Eng. China (2009), 3(4): 357-363.

Cheng, M., Whyte, D.S. and Lou, J., “Numerical simulation of flow around a square cylinder in uniform-shear flow”, Journal of Fluids and Structures (2007). 23(2), 207-226.

Chern, M., Kuan, Y., Nugroho, G., Lu, G., and Horng, T., "Direct-forcing immersed boundary modeling of vortex-induced vibration of a circular cylinder", Journal of Wind Engineering and Industrial Aerodynamics (2014), 134, 109-121.

Chern, M., Chakraborty, S., Kuan, Y., Nugroho, G., Liao, C., Lu, G., and Horng, T., "Numerical Study of Vortex-Induced Vibration of Circular Cylinder Adjacent to Plane Boundary using Direct-Forcing Immersed Boundary Method", Journal Mechanics (2017).

Choi, H., "Distributed Forcing for Flow Over a Bluff Body". 2nd AIAA Flow Control Conference (2004).

Cimarelli, A., Leonforte, A., and Angeli, D., "Direct numerical simulation of the flow around a rectangular cylinder at a moderately high Reynolds number", Journal of Wind Engineering & Industrial Aerodynamics (2018), 174, 39-49.

Costa, C. and Borri, C., "Application of indicial functions in bridge deck aeroelasticity", Journal of Wind Engineering and Industrial Aerodynamics (2006), 94(11), 859-881.

CRIACIV (Patruno, et al. Contacted), University of Florence, January 2015

CSA International, Canadian Highway Bridge Design Code. Toronto, Canada, 2000

De, A.K., Dalal, A., "Numerical simulation of unconfined flow past a triangular cylinder", Int. J. Numer. Methods Fluids (2006), 52 (7), 801–821.

Dexter, R., "Investigation of Cracking of High-Mast Lighting Towers", Final report to Iowa Department of Transportation (2004).

Djenidi, L. and Antonia, R. A. "LDA measurements in low Reynolds-number turbulent boundary layers, Exp. Fluids (1993), 14, 280-283.

Dong, S., and Karniadakis, G., "DNS of flow past a stationary and oscillating cylinder at Re = 10000", Journal of Fluids and Structures (2009), 20, 519 – 531.

Dudley, J., "Introduction to RANS Modeling", University of New Haven, Computational Fluid Dynamics and Heat Transfer Lecture (2016).

Elmiligui, A., et al., “Numerical Study of Flow Past a Circular Cylinder using RANS, Hybrid RANS/LES and PANS Formulations”, American Institute of Aeronautics and Astronautics (2004).

Fernholz, H. and Finleyt, P., “The incompressible zero-pressure-gradient turbulent boundary layer: An assessment of the data”, Progress in Aerospace Sciences (1996), 32(4), 245-311.

Frandsen, J.B., “Numerical bridge deck studies using finite elements. Part I: flutter”, Journal of Fluids and Structures (2004), 19(2), 171-191.

Franke, J. and Frank, W., “Large eddy simulation of the flow past a circular cylinder at ReD=3900”, Journal of Wind Engineering and Industrial Aerodynamics (2002), 90(10), 1191-1206.

Graham, J.M.R.. Flow Around Circular Cylinders. Vol. 2: Applications: M.M. Zdravkovich, Oxford Science Publications (Oxford University Press), Journal of Fluids and Structures (2003), 18, 146.

Gopalkrishnan, R. “Vortex-induced forces on oscillating bluff cylinders”, Ph.D. Thesis, Department of Ocean Engineering (1993), MIT, Cambridge, MA, USA.

Grozescu, L. Bruno, D. Fransos, M.V. Salvetti, “Large-eddy simulations of a Benchmark on the Aerodynamics of a Rectangular 5:1 Cylinder”, Proceedings XX Congresso dell'Associazione Italiana di Meccanica Teorica e Applicata (AIMETA 2011), Bologna.

Huang, M.F., Lau, I.W.H., Chan, C.M., Kwok, K.C.S. and Li, G., “A hybrid RANS and kinematic simulation of wind load effects on full-scale tall buildings”, Journal of Wind Engineering and Industrial Aerodynamics, 99(11), 1126-1138.

Jeong, U.Y., Koh, H.-M. and Lee, H.S., “Finite element formulation for the analysis of turbulent wind flow passing bluff structures using the RNG k−ε model”, Journal of Wind Engineering and Industrial Aerodynamics (2002), 90(3), 151-169.

Jus, Y., et al., “Low Mass-Damping Vortex-Induced Vibrations of a Single Cylinder at Moderate Reynolds Number”, Journal of Pressure Vessel Technology (2014), 136.

Kundu, P.K. and Cohen, I.M. and Dowling, D.R., Fluid Mechanics, Fifth Edition, Academic Press (2012).

Labbé, D.F.L. and Wilson, P.A., “A numerical investigation of the effects of the span-wise length on the 3-D wake of a circular cylinder”, Journal of Fluids and Structures (2007), 23(8), 1168-1188.

Lakshmipathy, S., and Girimaji, S., “Partially Averaged Navier-Stokes (PANS) Method for Turbulence Simulations: Flow Past a Circular Cylinder”, Journal of Fluids Engineering (2010), 132.

Launder, B. E., and Sharma, B. I., "Application of the Energy Dissipation Model of Turbulence to the Calculation of Flow Near a Spinning Disc", Letters in Heat and Mass Transfer (1974), vol. 1, no. 2, pp. 131-138.

Lee, A.H., et al., “Coupled delayed-detached-eddy simulation and structural vibration of a self-oscillating cylinder due to vortex-shedding”, Journal of Fluids and Structures (2014), http://dx.doi.org/10.1016/j. jfluidstructs.2014.02.019

Lee, N., Lee, H., Baek, C., and Lee, S., “Aeroelastic of bridge deck flutter with modified implicit coupling method”, Journal of Wind Engineering and Industrial Aerodynamics (2016), 155, 11-22.

Leontini, J.S., and Thompson, M.C., “Vortex-induced vibrations of a diamond cross-section: Sensitivity to corner sharpness” Journal of Fluids and Structures (2013), Volume 39, May 2013, 371-390, http://dx.doi.org/10.1016/ j.jfluidstructs.2013.01.002i

Liang, C. and Papadakis, G., “Large eddy simulation of pulsating flow over a circular cylinder at subcritical Reynolds number”, Computers & Fluids (2007), 36(2), 299-312.

Lu, C.L., Li, Q.S., Huang, S.H., Chen, F.B. and Fu, X.Y. (2012), “Large eddy simulation of wind effects on a long-span complex roof structure”, Journal of Wind Engineering and Industrial Aerodynamics, 100(1), 1-18.

Mannini, C., Soda, A., and Schewe, G., “Numerical investigation on the three-dimensional unsteady flow past a 5:1 rectangular cylinder”, Journal of Wind Engineering and Industrial Aerodynamics (2011), 99, 469-482.

Manzoor, P. Hernon and X.Amandolese. “Vortex-induced Vibrations of a square cylinder in a wind tunnel”, 3'd Fluids Engineering Summer Meeting, Canada 2010.

Menter, F. R., "Two-Equation Eddy-Viscosity Turbulence Models for Engineering Applications", AIAA Journal (1994), vol. 32, no 8. pp. 1598-1605.

Murakami, S., Mochida, A., and Sakamoto, S., “CFD analysis of wind-structure interaction for oscillating square cylinders”, Journal of Wind Engineering & Industrial Aerodynamics (1997), 72, 33-46.

Ng, Z., Vo, T., Hussam, K., and Sheard, G., “Two-dimensional wake dynamics behind cylinders with triangular cross-section under incidence angle variation”, Journal of Fluids and Structures (2016), 63, 302-324.

Oñate, E., Vallis, A., and Julio, Garcia., “Modeling incompressible flows at low and high Reynolds numbers via a finite calculus-finite element approach”, Journal of Computational Physics (2007), 244, 332-351.

Ong, L., and Wallace, J. “The velocity field of the turbulent very near wake of a circular cylinder”, Exp. Fluids 20 (1996), 441–453.

Panton, Ronald, Incompressible Flow: Chapter 14, Wiley-Interscience (2013), New York.

Patel, Y. “Numerical Investigation of Flow Past a Circular Cylinder and in a Staggered Tube Bundle Using Various Turbulence Models”, Lappeenranta University of Technology (2010).

Patruno, L., Ricci, M., Miranda, S., and Ubertini, F., “Numerical Simulation of a 5:1 rectangular cylinder at non-null angles of attack”, Journal of Wind Engineering and Industrial Aerodynamics (2016), 151, 146-157.

Pope, S., Turbulent Flows, Cambridge: Cambridge University Press (2000), doi:10.1017/CBO9780511840531

R. M. Darekar and S. J. Sherwin, “Flow past a square-section cylinder with a wavy stagnation face,” J. Fluid Mech ((2001), 426, 263–295.

Rohde, A., “Numerical Investigation of the Evolution of Vortex Instability in a 2-D Compressible Flow over a Cylinder”, 20th AIAA Computational Fluid Dynamics Conference (2011).

Rosetti, G., Vaz, G., and Fujarra, A., “URANS Calculations for Smooth Circular Cylinder Flow in a Wide Range of Reynolds Numbers: Solutions Verification and Validation”, Journal of Fluids Engineering (2012), 134.

Roshko, A. "Experiments on the Flow Past a Circular Cylinder at Very High Reynolds Number." J. Fluid Mech (1961), 10, 345-356.

Saeedi, M., et al, “Direct numerical simulation of turbulent wake behind a surface-mounted square cylinder”, Journal of Fluids and Structures (2014), http://dx.doi.org/10.1016/j.jfluidstructs.2014.06.021

Sarkar P., “New identification methods applied to the response of flexible bridges to wind”, Ph.D. dissertation, Johns Hopkins University (1992).

Sarkic, A., et al. “Bridge flutter derivatives based on computing, validated pressure fields”, Journal of Wind Engineering and Industrial Aerodynamics (2012), 104-106, 141-151.

Schewe, G., “Reynolds-number-effects in flow around a rectangular cylinder with aspect ratio 1:5”, Journal of Fluids and Structures, Volume 39, 2013, Pages 15-26, ISSN 0889-9746, https://doi.org/10.1016/j.jfluidstructs.2013.02.013.

Selvam, R., and Govindswamy, S., “Aeroelastic Analysis of Bridge Girder Section Using Computer Modeling”, University of Arkansas (2001).

Sharma, A., and Eswaran, V., “Heat and fluid flow across a square cylinder in the two-dimensional laminar flow regime,” Numer. Heat Transfer (2004), Part A 45, 247–269.

Shih, et al., “Experiments on flow past rough circular cylinders at large Reynolds numbers”, J. Wind Eng. Indust. Aerodyn (1993), 49, 351–368.

Shimada, K. and Ishihara, T., “Predictability of unsteady two-dimensional k−ε model on the aerodynamic instabilities of some rectangular prisms”, Journal of Fluids and Structures (2012). 28(0), 20-39.

Simiu, E. and Scanlan, R. H., Wind Effects on Structures, Fundamentals and Applications to Design, 3rd ed., John Wiley & Sons, New York, NY (1996).

Singh, S., and Biswas, G., “Vortex induced vibrations of a square cylinder at subcritical Reynolds numbers”, Journal of Fluids and Structures (2013), 41, 146-155.

Smagorinsky, J, "General circulation experiments with the primitive equations, i. the basic experiment. Monthly Weather Review", 91: pp 99-164, 1963.

Szabó, G., and Györgyi, J., “Three-dimensional Fluid-Structure Interaction Analysis for Bridge Aeroelasticity”, Proceedings of the World Congress on Engineering and Computer Science Volume II (2009).

Tang, Y., Shixiong, S., and Li, M., “A numerical investigation on galloping of an inclined square cylinder in a smooth flow”, Journal of Wind Engineering and Industrial Aerodynamics (2015), 144, 165-171.

Tayyaba Bano, N.A.S., S. Manzoor, Shahab Khushnood, “Numerical Simulation of Flow past a Square Cylinder”, Proceedings of 2012 9th International Bhurban Conference on Applied Sciences & Technology (IBCAST), (Islamabad, Pakistan, 9th - 12th January, 2012).

T.-H. Shih, W. W. Liou, A. Shabbir, Z. Yang, and J. Zhu. "A New k- ϵ Eddy-Viscosity Model for High Reynolds Number Turbulent Flows - Model Development and Validation", Computers Fluids (1995), 4(3):227-238.

Tu, J., Zhou, D., Bao, Y., Han, Z., Li, R., “Flow characteristics and flow-induced forces of a stationary and rotating triangular cylinder with different incidence angles at low Reynolds numbers”, J. Fluids Struct (2014), 45, 107–123.

Wang, H., Zhao, D., Yang, W., Yu, G., “Numerical investigation on flow-induced vibration of a triangular cylinder at a low Reynolds number”, Fluid Dyn (2014), Res. 47, 015501.

Wilcox, D.C., "Re-assessment of the scale-determining equation for advanced turbulence models", AIAA Journal (1988), vol. 26, no. 11, pp. 1299-1310.

Wilcox, D. C., Turbulence modeling for CFD. La Cãnada, CA: DCW Industries, Inc (1994).

White, F. M. Fluid mechanics 5th Edition. Boston, Mass: WCB/McGraw-Hill (2015).

Williamson, C.H.K., “Vortex dynamics in the cylinder wake”, Annual Review of Fluid Mechanics (1996), 28, 477–539.

Xie, Deng, Xiao and Yao, “A numerical simulation of VIV on a flexible circular cylinder”, The Japan Society of Fluid Mechanics and IOP Publishing Ltd (2012), 44(4).

Yakhot, V., Orszag, S.A., Thangam, S., Gatski, T.B. & Speziale, C.G., "Development of turbulence models for shear flows by a double expansion technique", Physics of Fluids A (1992), Vol. 4, No. 7, pp1510-1520.

Ying Zhou, Q.-L.Z., Zhen-Hua Liu, “Numerical Simulation of Fluid-Structure Interaction for Wind-induced Dynamic Response of Jinan Yellow River Cable-stayed Bridge in Cantilever State”, 2009 International Conference on Engineering Computation (2009), 51-54.

Yoshihide Tominaga, “Flow around a high-rise building using steady and unsteady RANS CFD: Effect of large-scale fluctuations on the velocity statistics”, Journal of Wind Engineering and Industrial Aerodynamics (2014), Volume 142, Pages 93-103, ISSN 0167-6105, https://doi.org/10.1016/j.jweia.2015.03.013.

Zhang Enuo, Y.W., ZHEN Wei, NA Xiangqian, “Software Practicalization for Analysis of Wind-Induced Vibrations of Large Span Roof Structures”, Tsinghua Science And Technology (2005), 10(3), 354-358.

Zhang, H., Xin, D., and Ou, J., “Wake control of vortex shedding based on span-wise suction of a bridge model using Delayed Detached Eddy Simulation”, Journal of Wind Engineering and Industrial Aerodynamics (2016), 155, 100-114.

Zhang, X., Xiang, H. and Sun, B., “Nonlinear aerostatic and aerodynamic analysis of long-span suspension bridges considering wind-structure interactions”, Journal of Wind Engineering and Industrial Aerodynamics (2002), 90(9), 1065-1080.

Zhang, W., and Sarkar, P., “Influence of surrounding buildings on the flow around a low-rise building in ABL and tornado-like winds”, Fifth International Symposium on Computational Wind Engineering (CWE2010).

Zhang, Y., Habashi, W., and Khurram, R., “Predicting wind-induced vibrations of high-rise buildings using unsteady CFD and modal analysis”, Journal of Wind Engineering and Industrial Aerodynamics (2015), 136, 165-179.

Zhao, M., Cheng, L. and Zhou, T., “Numerical simulation of vortex-induced vibration of a square cylinder at a low Reynolds number”, Physics of Fluids (2013), 25.

Zheng, Z., and Zhang, N., “Frequency effects on lift and drag for flow past an oscillating cylinder”, Journal of Fluids and Structures (2008), 24, 382-399.

APPENDIX A. CFD SETUP AND PROCEDURES

This is basic guide on how to setup the problems, along with some quick information for assistance of future investigations.

GEOMETRY SETUP

The first step is to bring in the CFX module once the ANSYS workbench is launched.

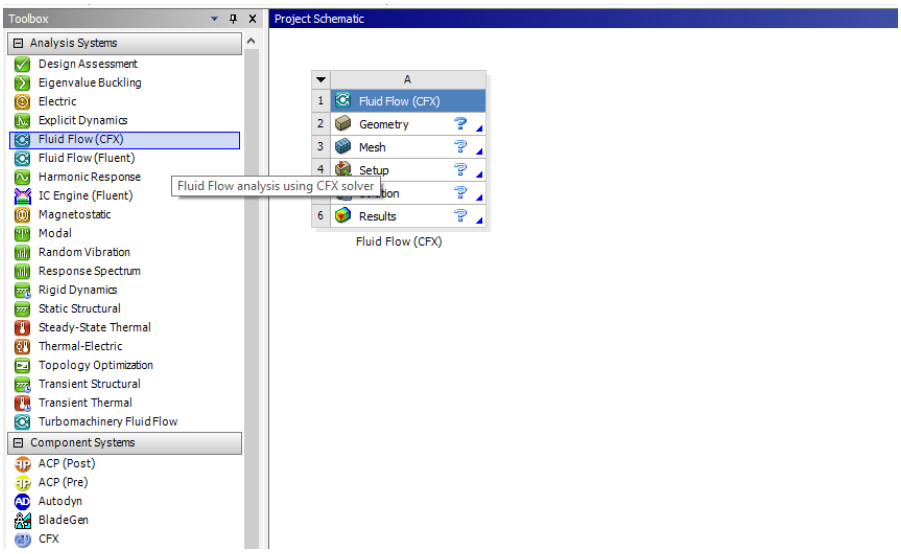

Next, open the DesignModeler (Typically the default option) by right clicking on Geometry or by double clicking for SpaceClaim. DesignModeler will be used from this step forward.

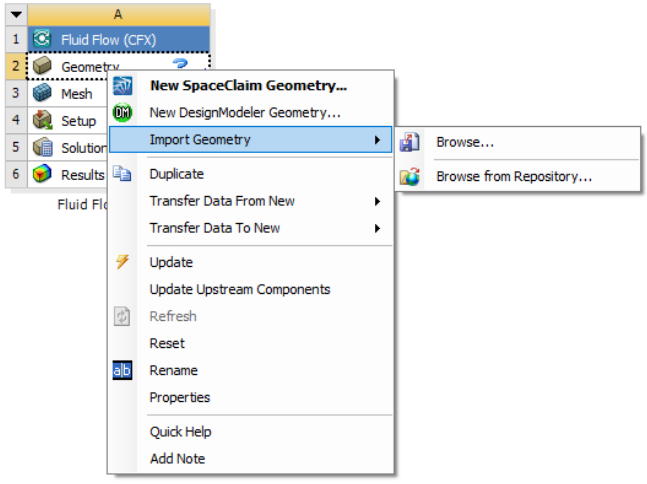

Once DesignModeler is open, the next step is to define the sketch planes for the various components. These various components will be used for the defining of the control volume.

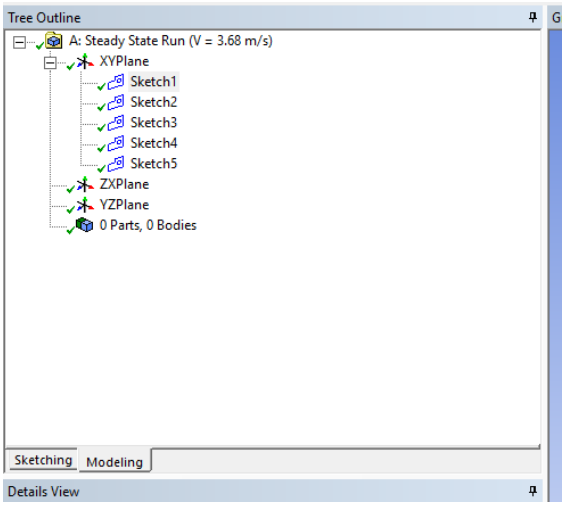

The first sketch plane will be used to draw the object of interest. For the current research, it is a dodecagon (12-sided) polygon that is 4-inches in diameter (face-to-face).

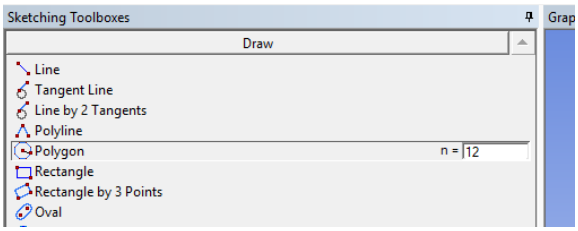

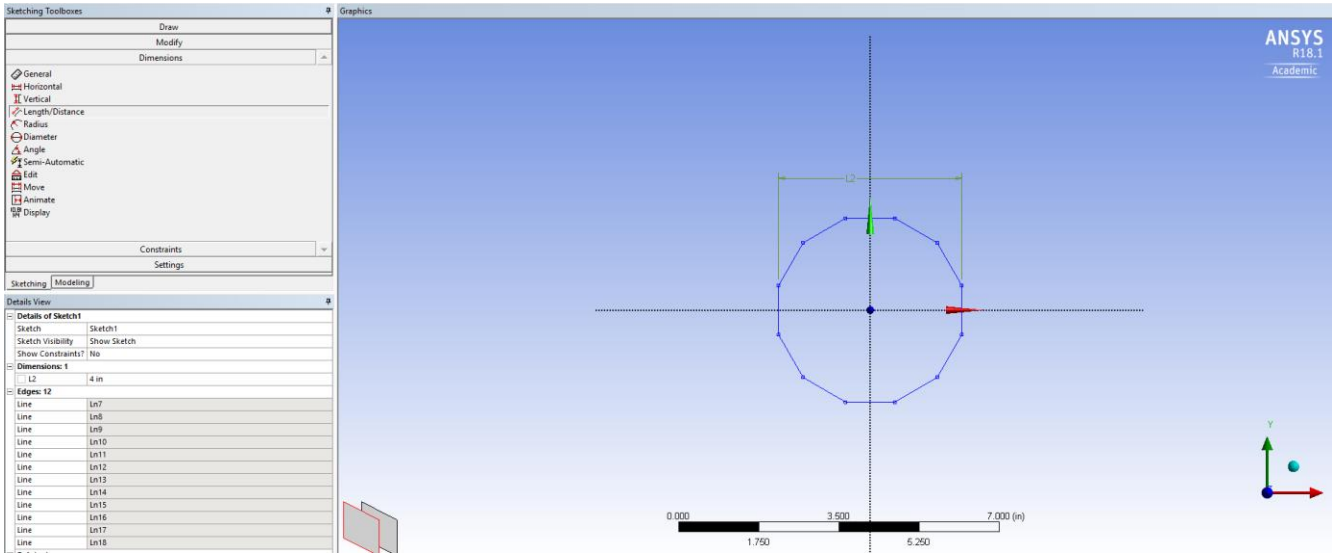

Next the larger control volume will be defined using the rectangular sketch tool on the second sketch plane, with the following dimensions in height and length. The other references control the offset from the origin plane lines for easy reference.

Details View	
Details of Sketch2	
Sketch	Sketch2
Sketch Visibility	Show Sketch
Show Constraints?	No
Dimensions: 4	
H3	200 in
L4	25 in
L5	18 in
V2	36 in
Edges: 4	
Line	Ln8
Line	Ln9
Line	Ln10
Line	Ln11
References: 1	
Ln18	Sketch4

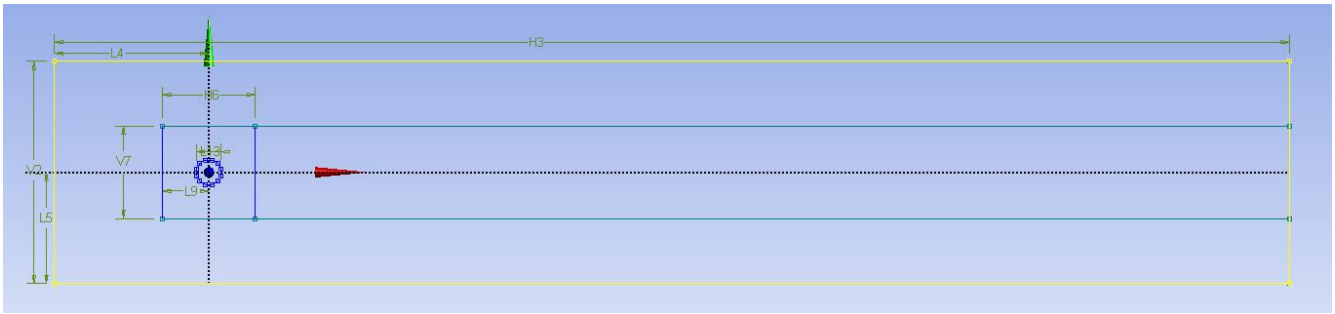

The third sketch plane will be used to define the rectangle around the object of interest. This will be used as a reference tool when defining the mesh parameters.

Details View	
Details of Sketch3	
Sketch	Sketch3
Sketch Visibility	Show Sketch
Show Constraints?	No
Dimensions: 3	
H6	15 in
L9	7.5 in
V7	15 in
Edges: 4	
Line	Ln12
Line	Ln13
Line	Ln14
Line	Ln15
References: 1	
Ln16	Sketch4

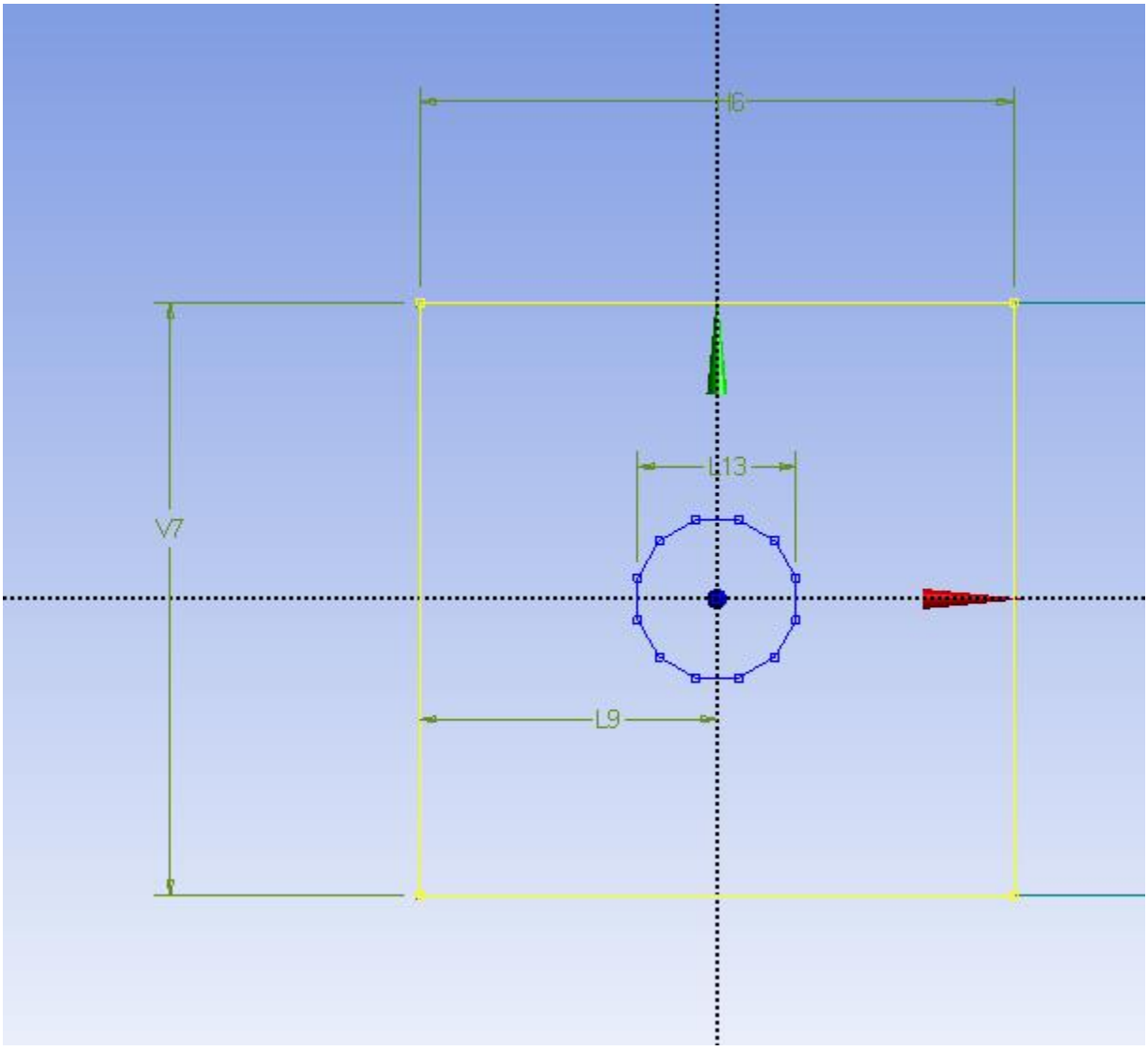

The fourth sketch plane will be used to define the third rectangular area. The third rectangular area will be used to define the mesh for the wake of the cylinder, for the CFD calculations. The references

will be the rectangle defined around the area of interest and the outer rectangle, for the larger control volume.

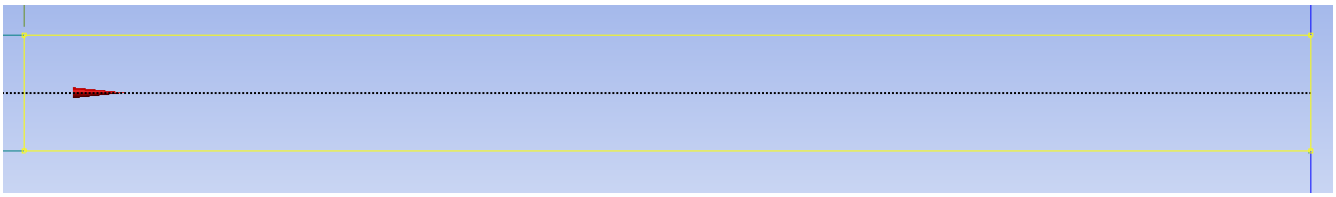

The control volume sketch (Sketch Plane 2) and the object of interest (Sketch Plane 1) will be extruded frozen with 30-inch length to match the full length of the wind tunnel experiments (Chang 2010).

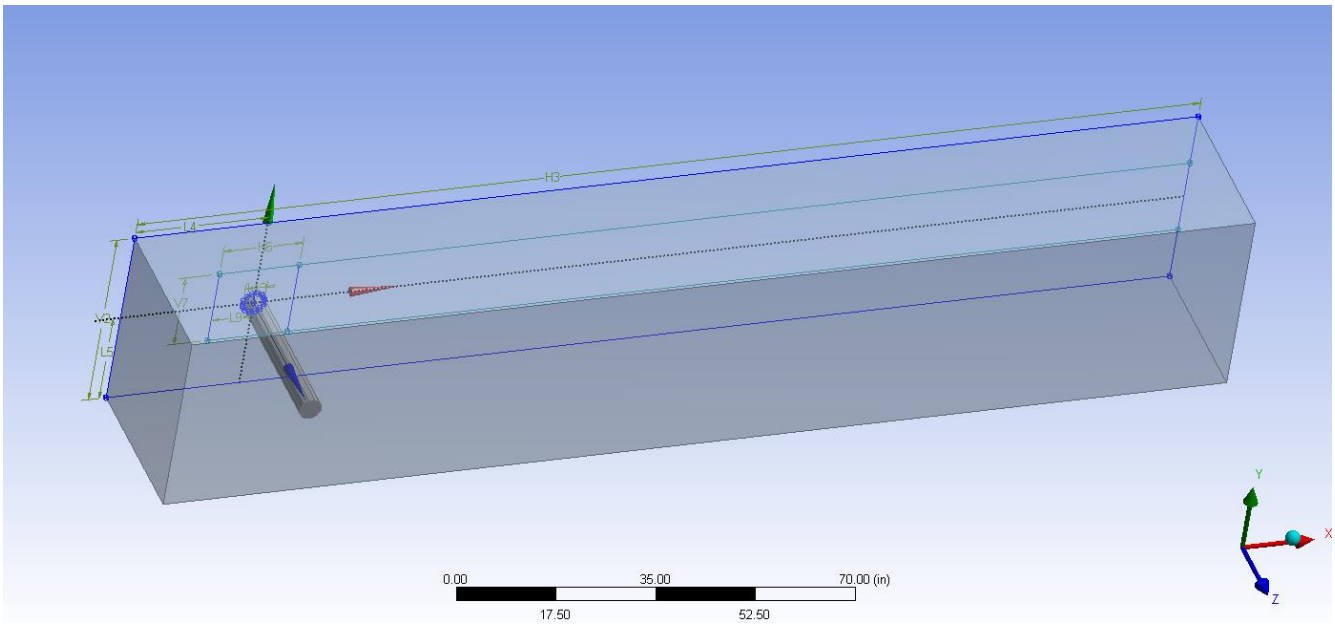

The mesh control sketches (Sketch Plane 3 and Sketch Plane 4) will then be extruded, but will use the extrude cut option to split the control volume into three separate entities.

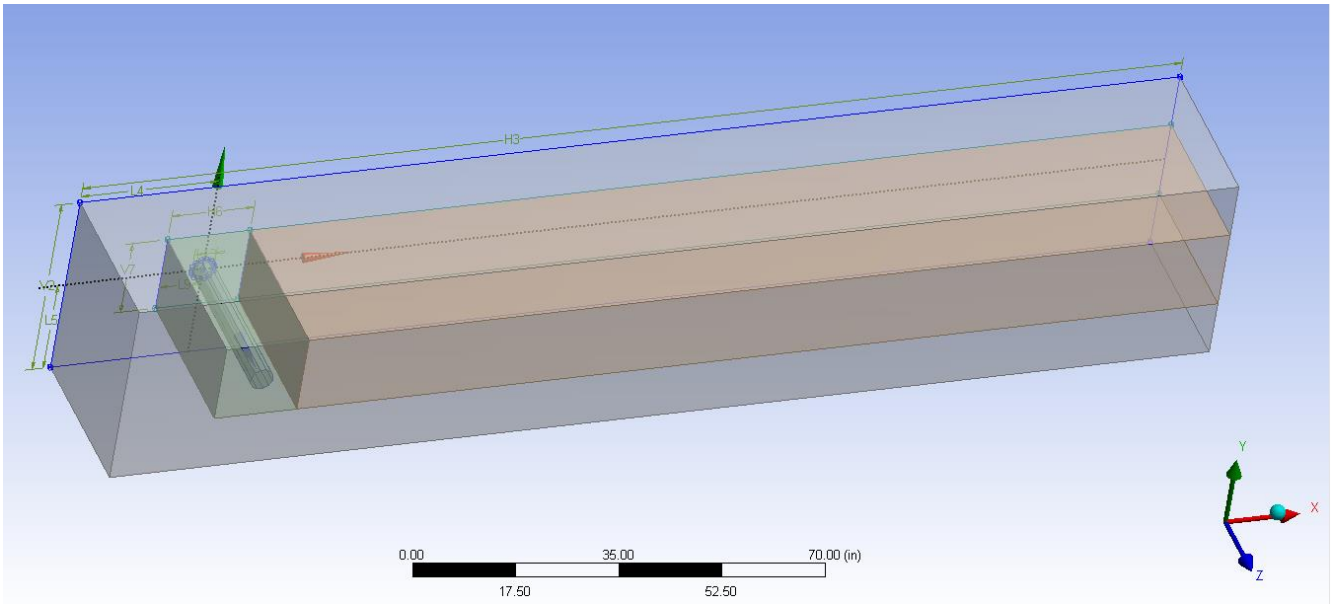

A Boolean body operation will be used. The location of the tool can be found under the “Create” tool bar. The body of interest will be then become separated from the surrounding smaller rectangular control volume, by using the Boolean tool.

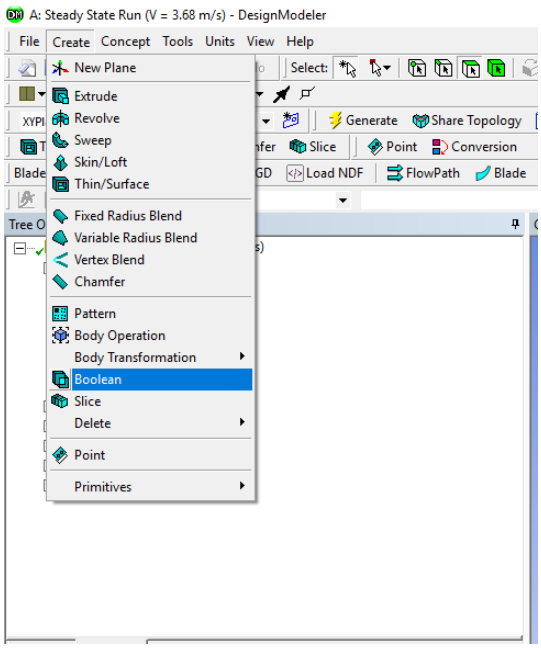

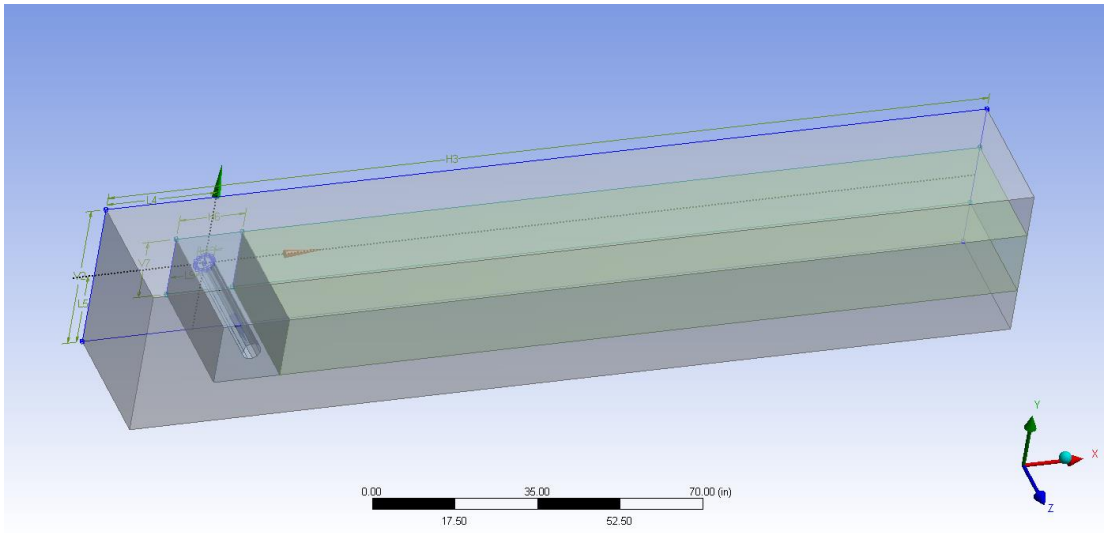

On the DesignModeler tree, the three separate bodies must be defined as a new part. Selecting all the bodies and right-clicking will show an option to form a new part. All the separated control volumes will be used to create a new part.

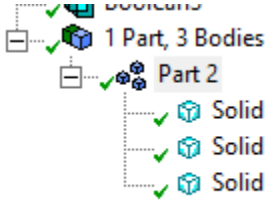

MESHING SETUP

On the meshing tree, the following controls will be described as to what the tool does and how each tool is applied.

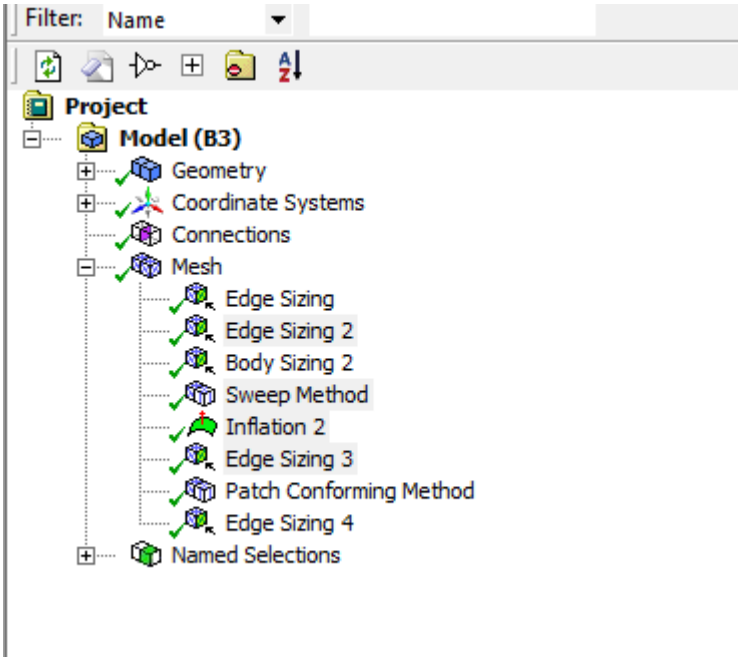

The current highlighted tools are used for the area of interest around the dodecagon cross-section. A swept approach is the preferred mesh control for the near, which describes rectangular volumes. For additional complexity of the geometry the use of triangular volumes will be applied. The edges of the cross-section will start with edge sizing divisions of 15. The inflation layer control will be applied to control the near wall treatment for dealing with the boundary layer with about 30 layers as a starting point. This control for the first layer height is referred to y+, which is necessary with turbulence modeling. Turbulence models which use wall functions will use a y+ of 30. Other turbulence models will require a y+ of 1. For k-ω based turbulence models such as SST or SAS-SST require a y+ of 1. Further reading on calculating y+ can be found in Pope (2000) or Wilcox (1994). Most vendors have tools that can assist with determining first height thickness.

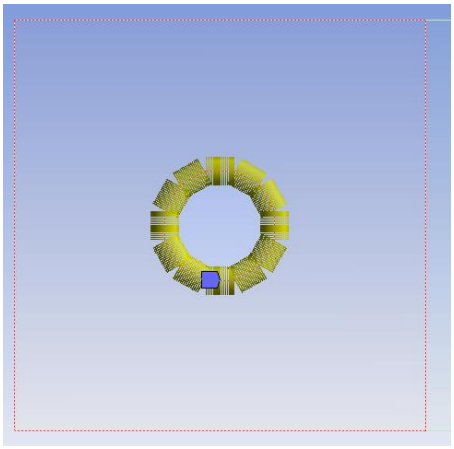

The span-wise direction will have a division sizing of 50 for the default, for the steady-state simulation. The steady-state case will be used to initialize the transient cases. The base case mesh sizing controls are fine for RANS approaches. However, when entering the territory of more encompassing turbulence models such as DES or LES, and to a smaller degree the SAS-SST models, the span-wise sizing must be closer or smaller than the edge sizing. The transient cases will have a span-wise sizing of closer 75 grid sizing. Information for handling meshing for DES hybrid approaches can be found in "Young-Person's Guide to Detached-Eddy Simulation Grids" by Philippe Spalart. For LES, basic information can be found in the ANSYS® CFX user guide.

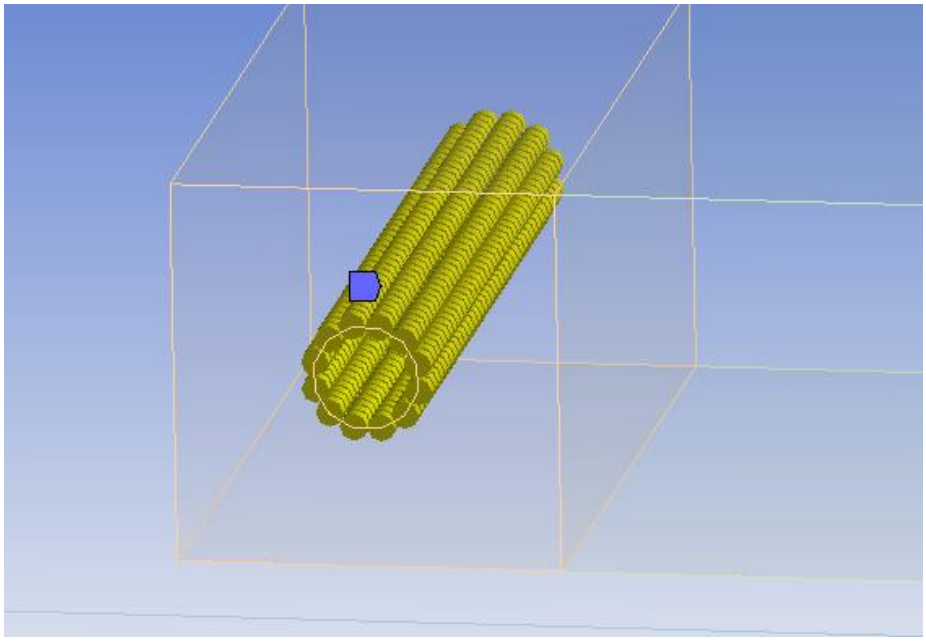

The wake rectangular controls will have spacing edge sizing of about 150 along the horizontal direction, but more will be required once the full the transient cases are started. The vertical grid sizing will be dependent on the mesh controls of the rectangle around the body of interest. Mesh generation will occur in three steps; the rectangle around the body of interest will be meshed first, then the wake control volume, and then the outer area.

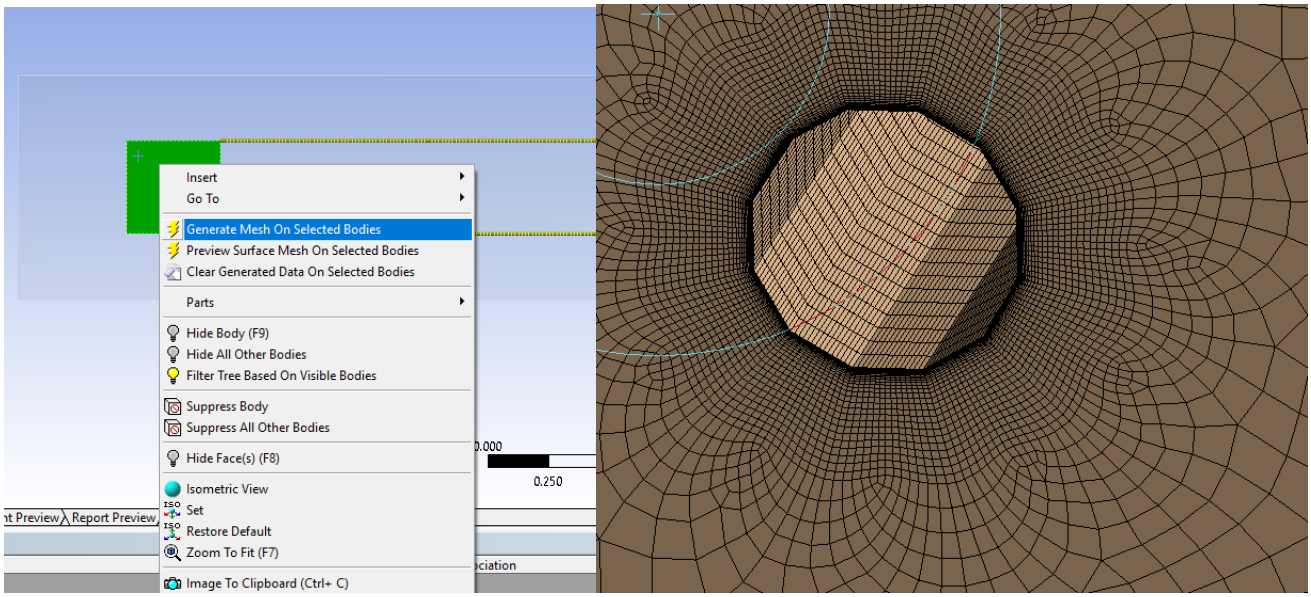

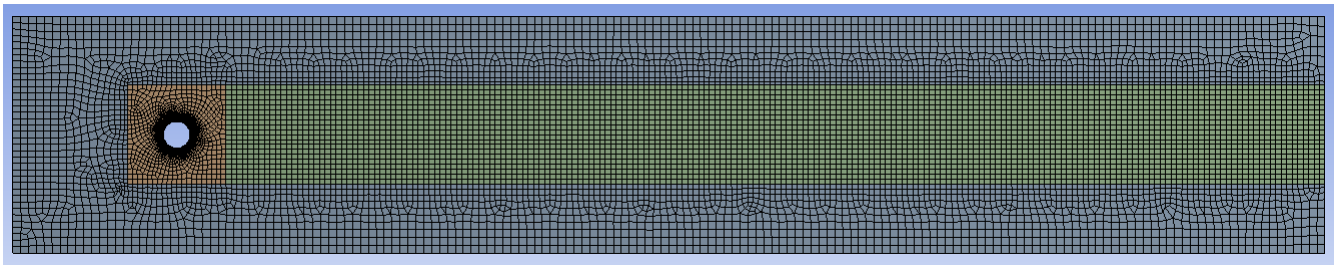

The quality of the mesh is highly important, especially in the area of interest of around the cylinder body. There are both quantitative and qualitatively checks that can be done to ensure the mesh quality in the area of interest is sufficient. Quantitative checks can be done on the orthogonality of the mesh, which closer to 1 means the higher quality the mesh according to the ANSYS® CFX user guide. Other checks can be used to fill the role in the ANSYS® software are aspect ratio and the skewness. Aspect ratio needs to be closer to 1 for areas of interest with. The closer the skewness to 0 the better. The current mesh has most of the elements less than 0.23 in the area of interest. This can be due to the irregular shape transition

for a dodecagonal cylinder to the square body. Another check is to examine the near wall mesh of the cylinder for “sharp elements” that are highly skewed, which can be mitigated with swept mesh and careful consideration of the first wall height and the number of inflation layer. Improper cells that transition from too small to larger quickly can create poor cell quality. Careful examination of the area of interest needs to be considered.

Orthogonal Metrics:

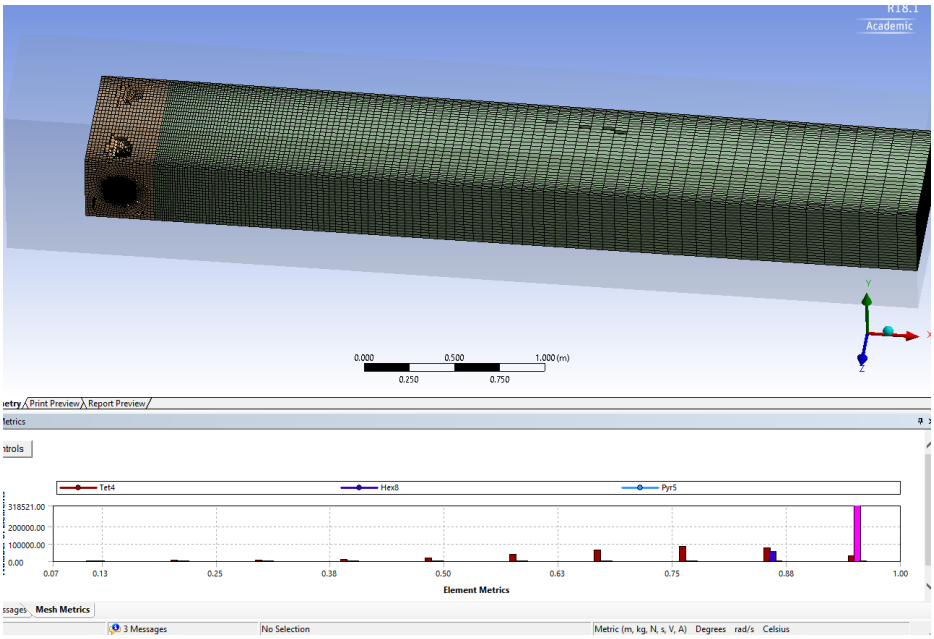

Aspect Ratio Metrics:

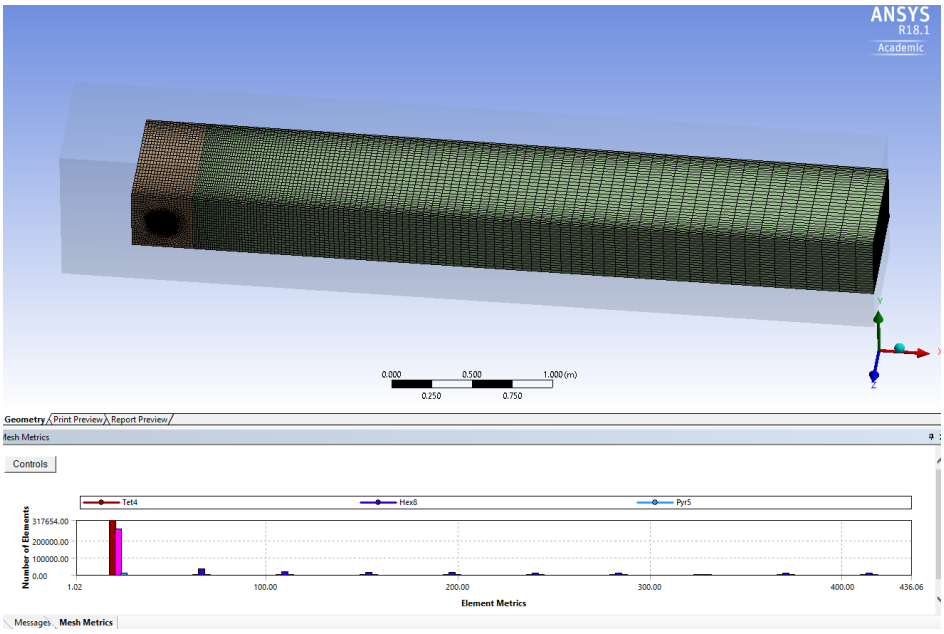

Skewness Metrics:

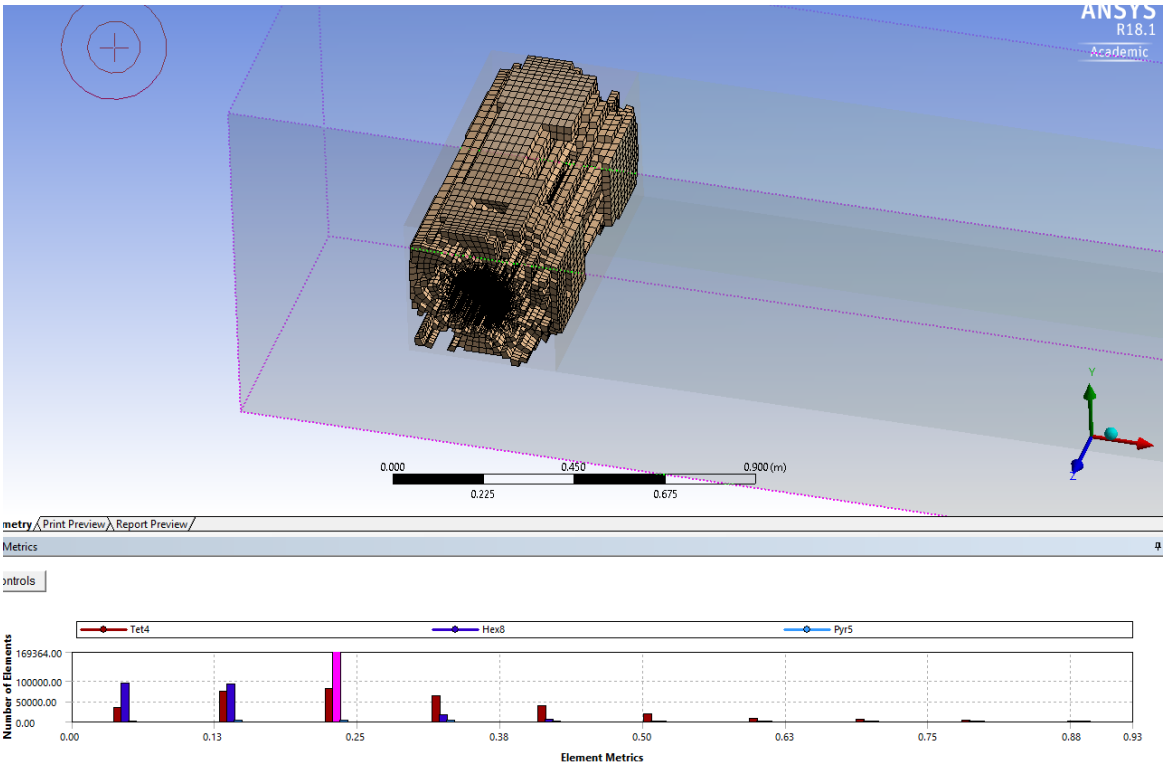

The boundaries conditions will be applied at this step as name selections for the control volume. The leading surface will be referred to as the “inlet”. The back face will be referred to as the “outlet”. The top and bottom will be referred to as “surface walls”, along with the body of interest be referred to as “wall” (Cylinder would allow for clearer assignment). The surfaces in and out of the board will be referred to as “symmetry”.

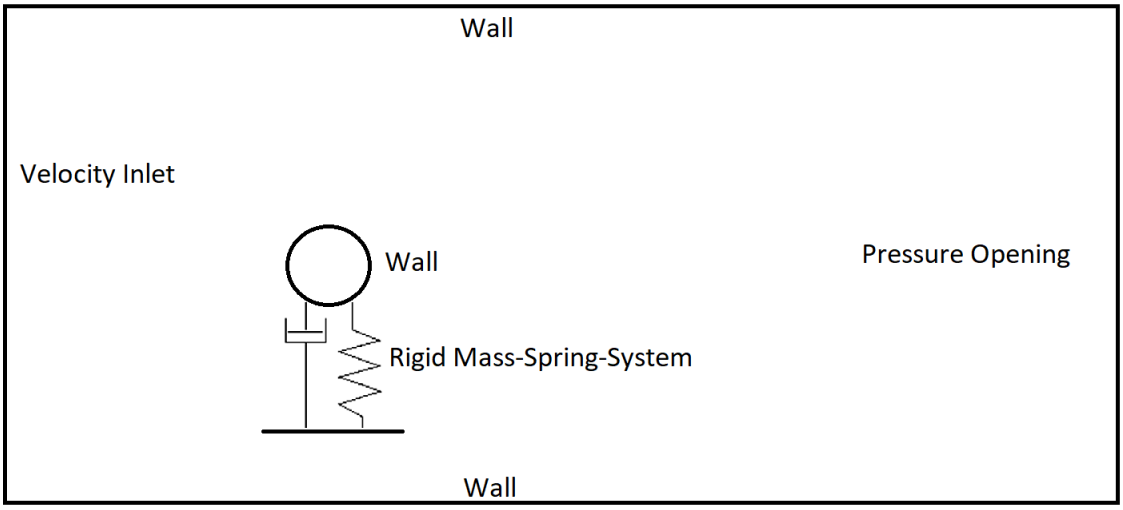

BASE CASE SETUP AND STEADY STATE SIMULATION

The next step is to startup the CFX-Setup Stage, which can be used to define the solver controls for the simulation setup.

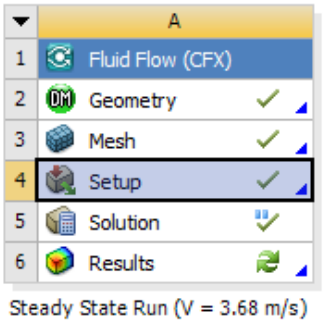

The setup tree will allow for defining the type of simulation required to run, such as boundary conditions, initial conditions, fluid properties, and solver controls.

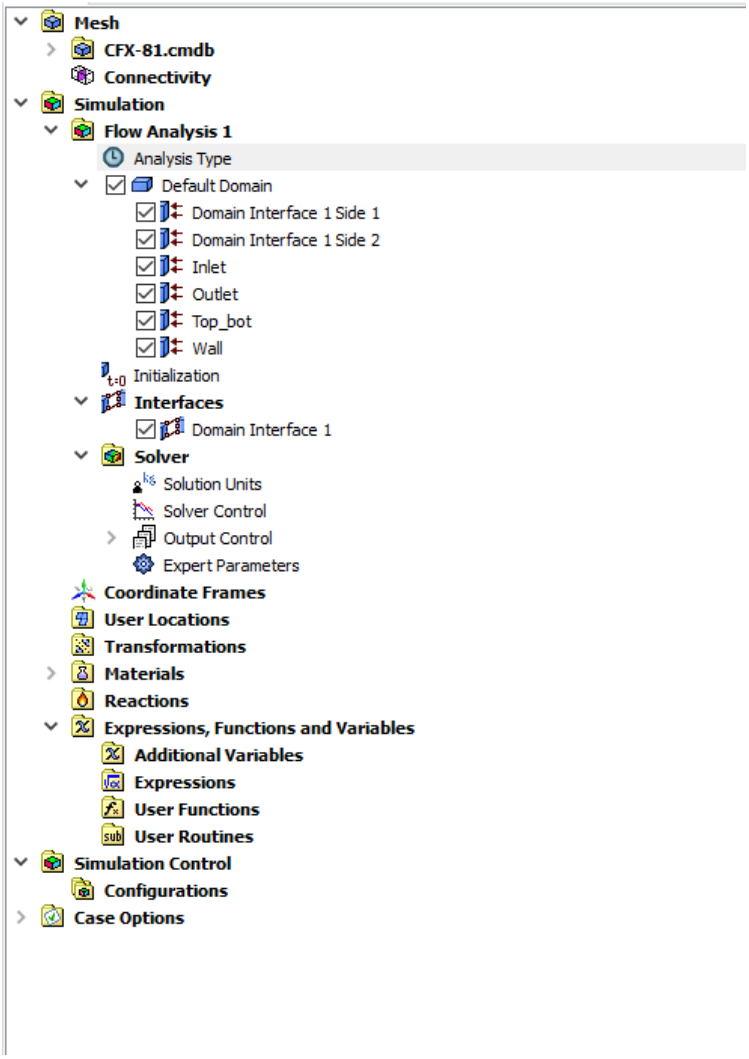

The analyze type for this setup will be “Steady-State”, where only the mean fluid properties will be solved, with no consideration of the temporal terms.

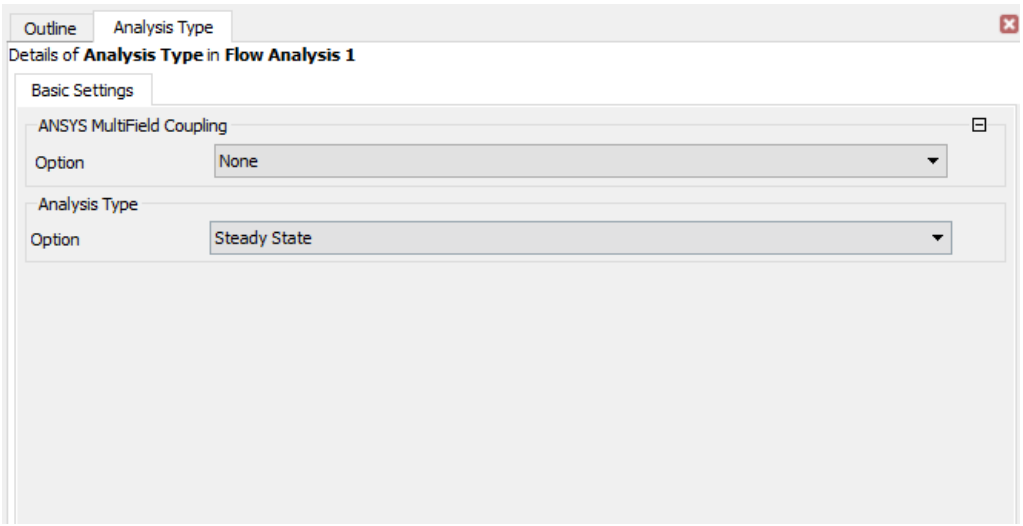

The “Default Domain” will handle the general flow parameters such as fluid properties, where the fluid will be air at seas level or at 25 Celsius. The turbulence model for the steady-state case will be the Shear-Stress Transport (SST) model, where for the current cases the flow regime is considered incompressible and the Energy equation can be neglected (Heat Transfer = None).

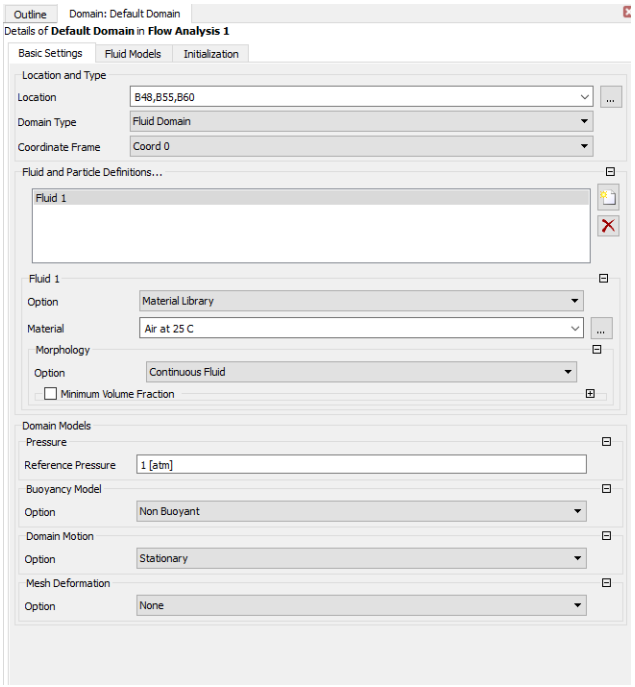

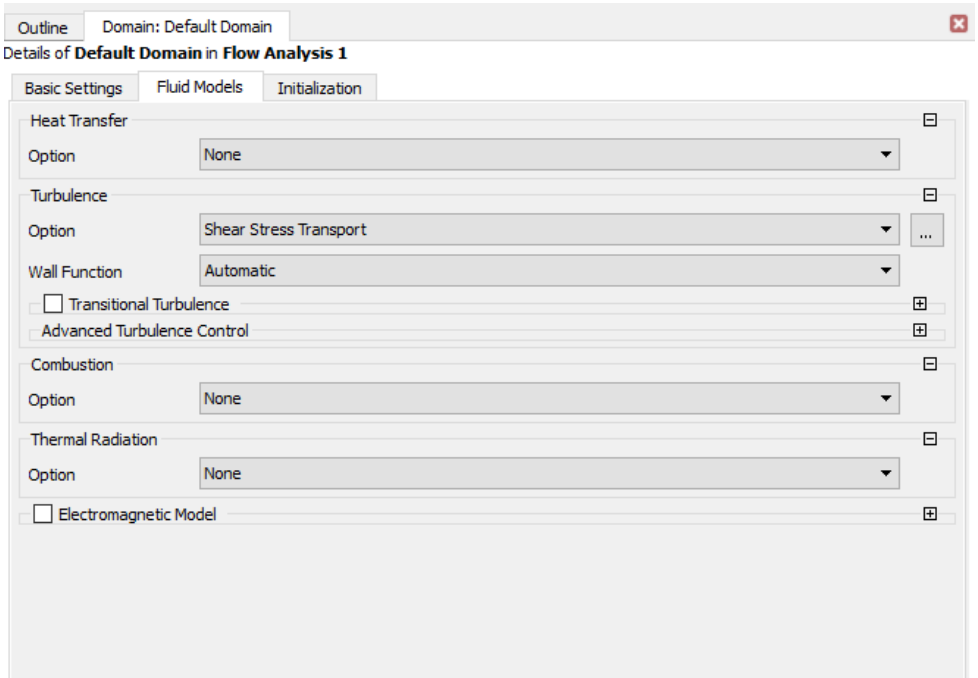

The inlet will be defined as a velocity inlet boundary condition, where the turbulence intensity will be left at default. The example used was a steady-state initialization case for one of the lock-in cases, so the shown velocity is 3.68 m/s. The larger cases, such as for lift and drag, will have velocities higher than 15 m/s. The outlet was defined as the pressure opening with 0 Pa relative pressure. The flow regime was left with a reference pressure of 1 Pa.

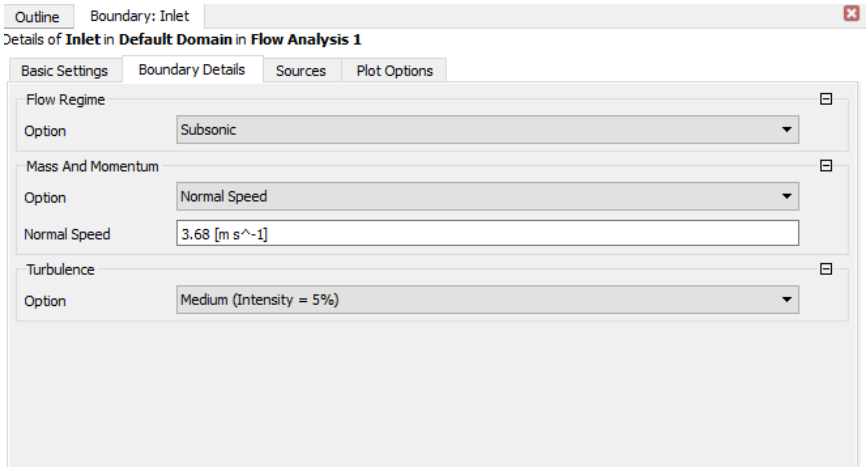

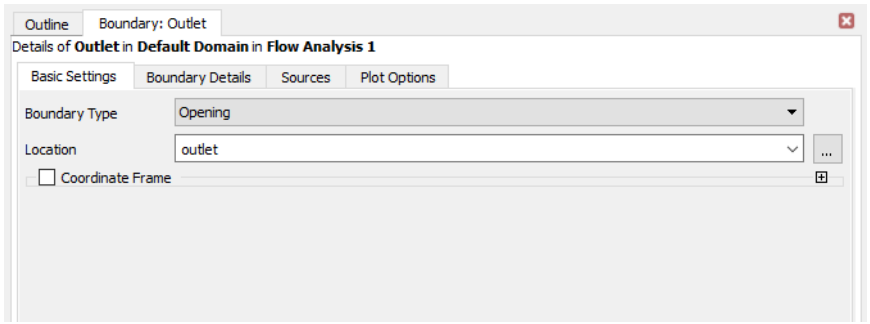

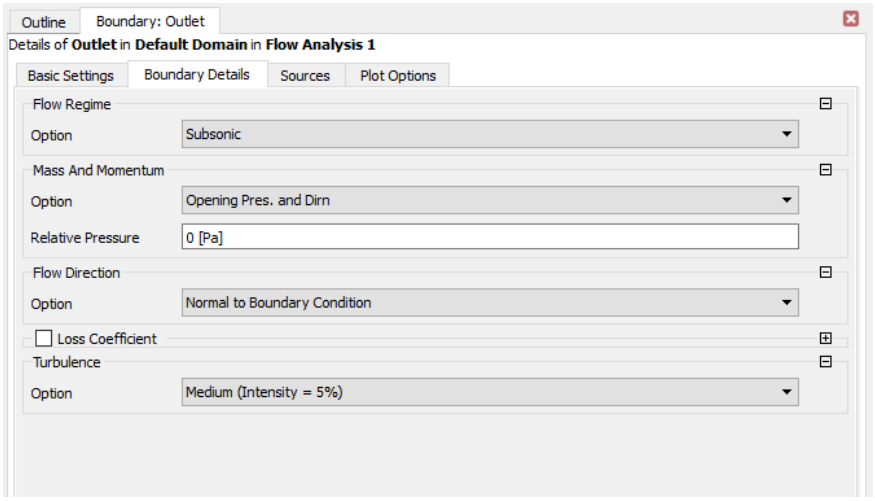

The top and bottom are defined as walls in this simulation with the cylinder wall defined separately.

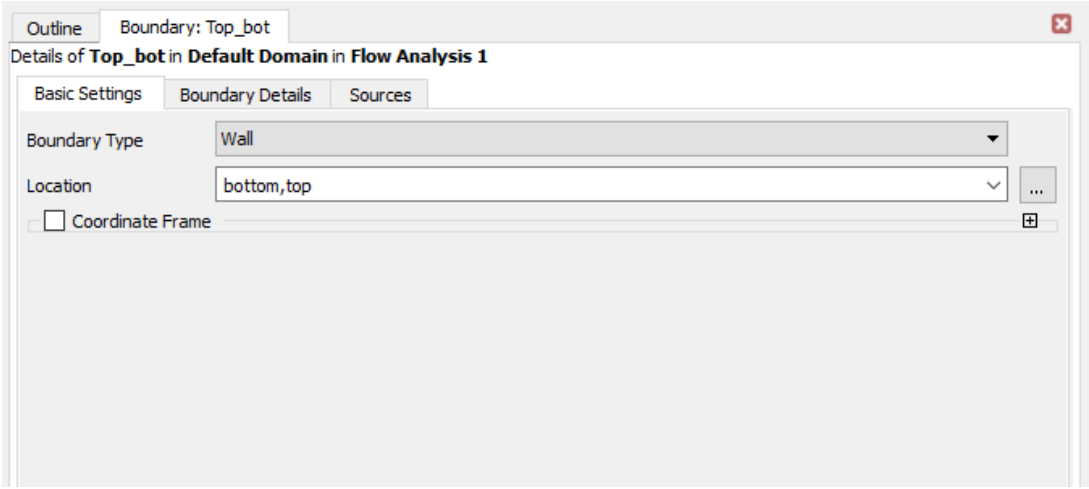

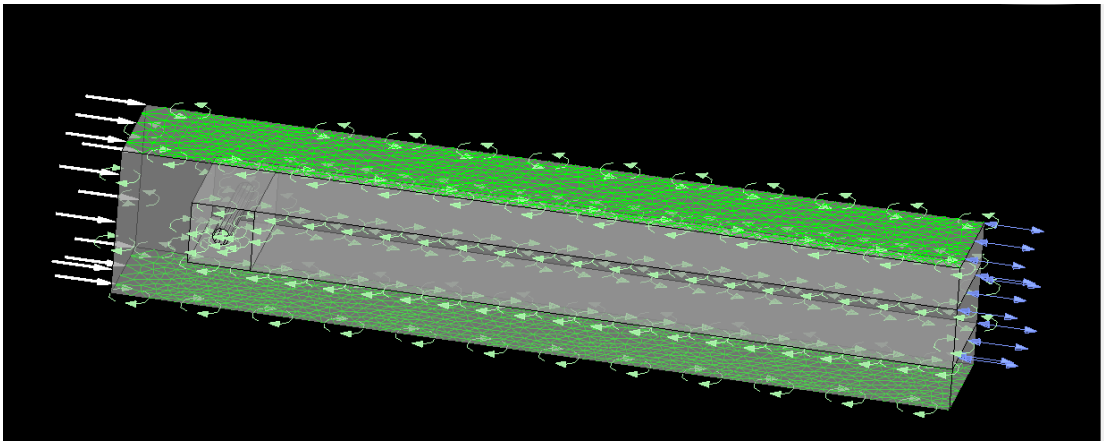

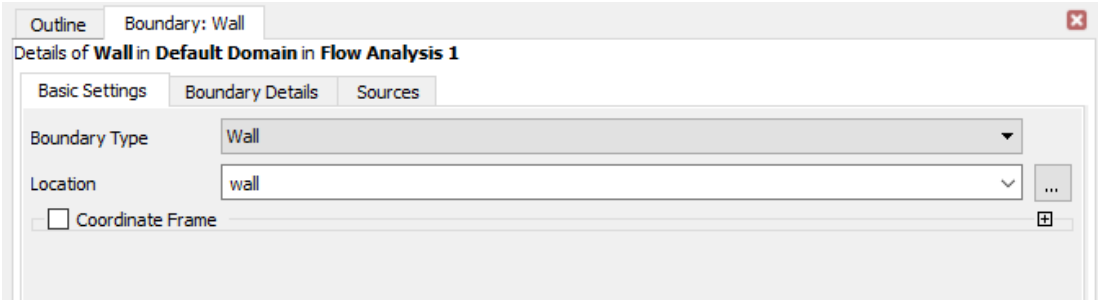

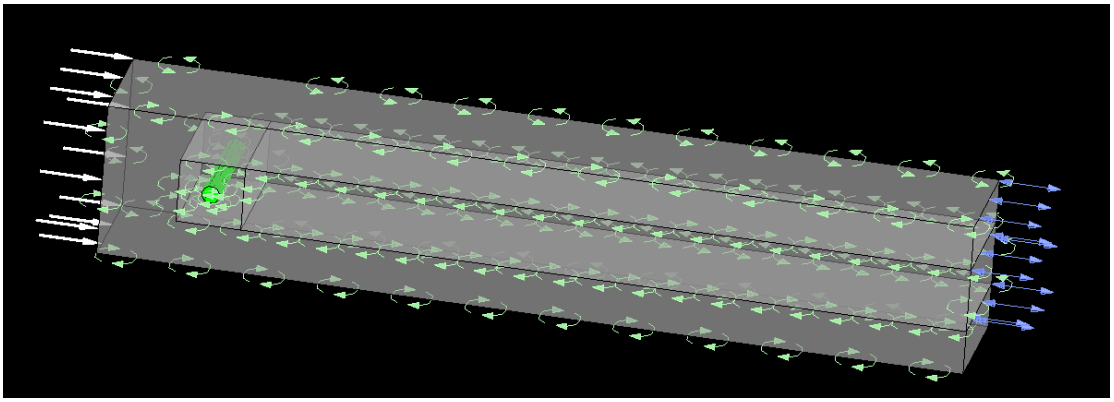

The walls in and out of the board are called symmetry. This is fine for RANS turbulence models. However, for turbulence models such as SAS-SST, DES, or LES, according to the ANSYS® CFX user guide, require periodic boundary conditions. The surfaces are defined as interface that allow for information to pass between them. Next a Domain Interface control connects the information.

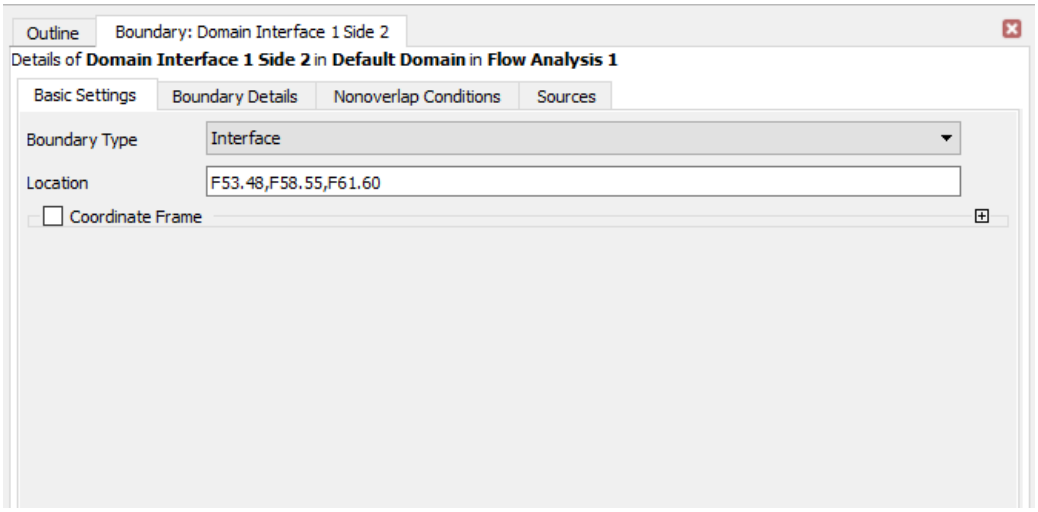

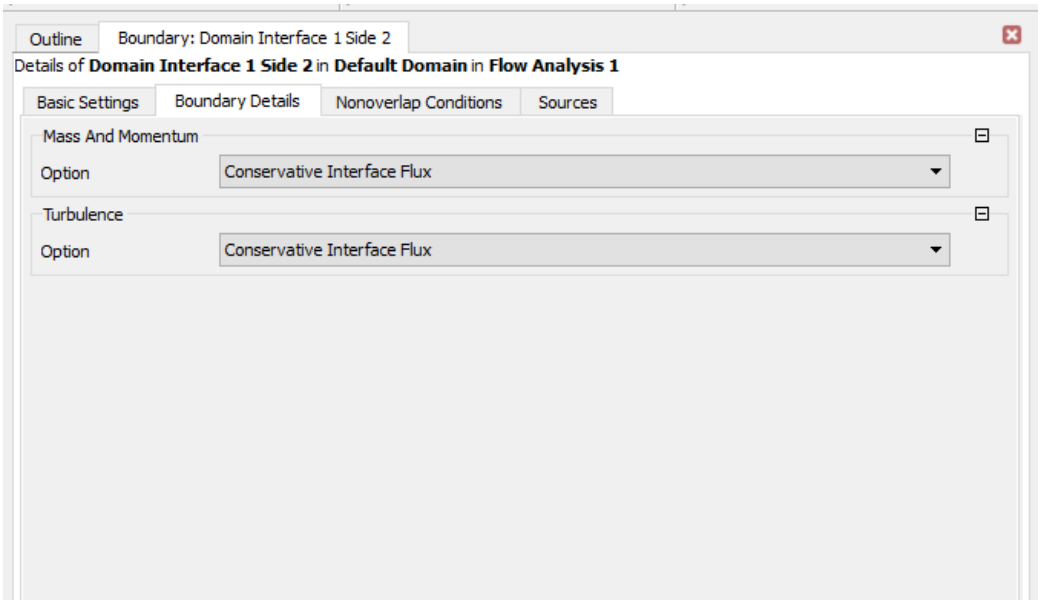

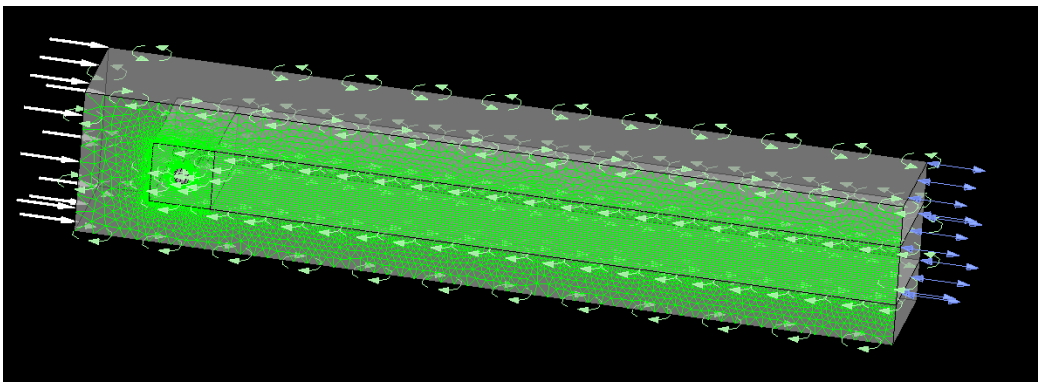

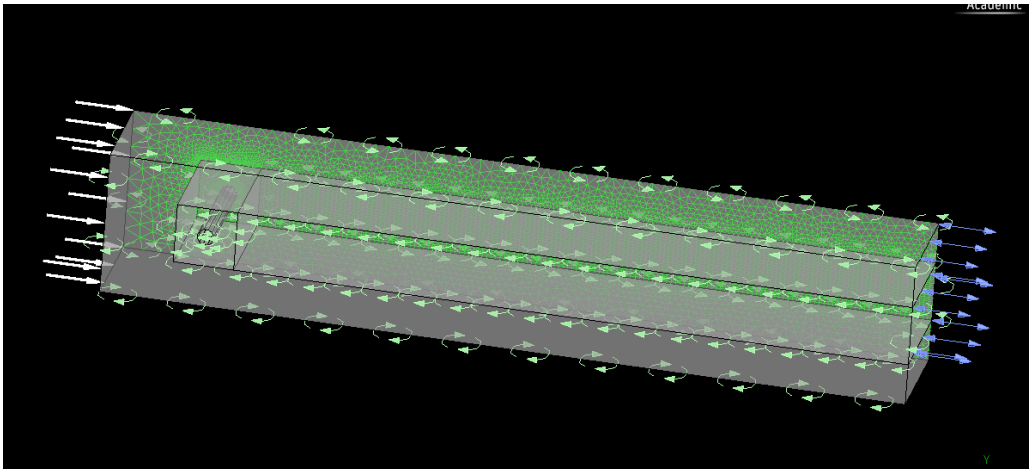

Outline | Domain Interface: Domain Interface 1

Details of **Domain Interface 1** in **Flow Analysis 1**

Basic Settings | Additional Interface Models | Mesh Connection

Interface Type	Fluid Fluid
Interface Side 1	
Domain (Filter)	Default Domain
Region List	F54.48,F59.55,F62.60
Interface Side 2	
Domain (Filter)	Default Domain
Region List	F53.48,F58.55,F61.60
Interface Models	
Option	Translational Periodicity

The global initialization was selected to be arbitrarily close to the inlet velocity for the first step calculations.

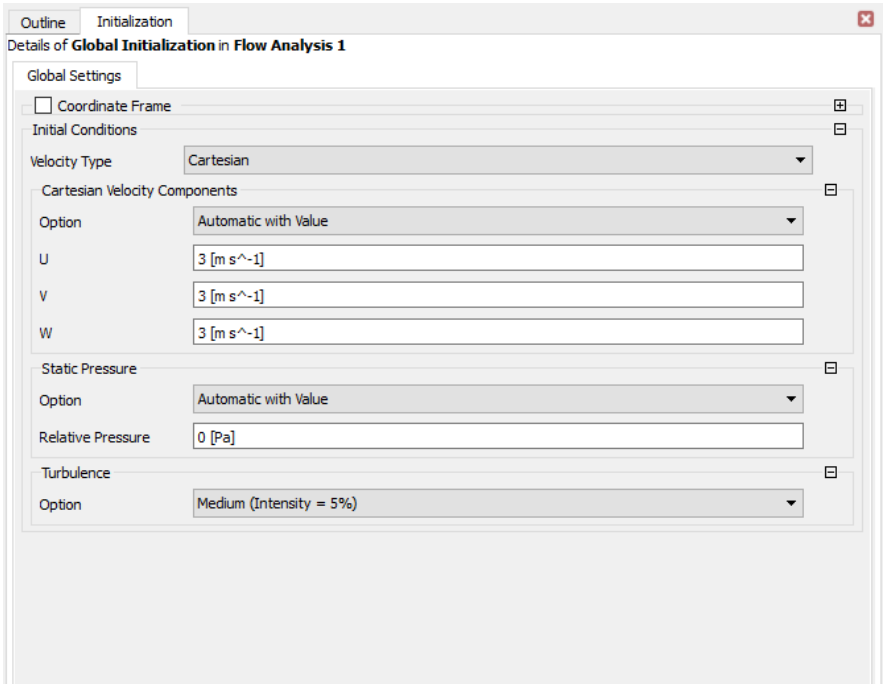

The solver controls will now be defined, where the iterations for low Re flow regimes will convergence below 100. For larger Re flows will require closer to a few hundred iterations. The turbulence numerics and other similar setting are set to High Resolution for increased precision. The convergence criteria were set, for this case, to 10^{-6}.

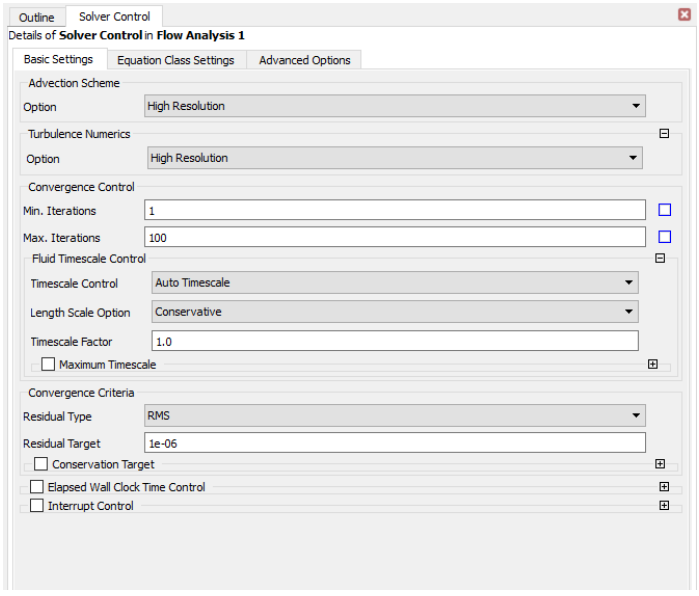

The monitors for a rigid cylinder were set for the drag and lift forces, where the monitors will report the forces in the x and y-directions, respectfully. (NOTE: y-direction is vertical direction or tangential to the flow.)

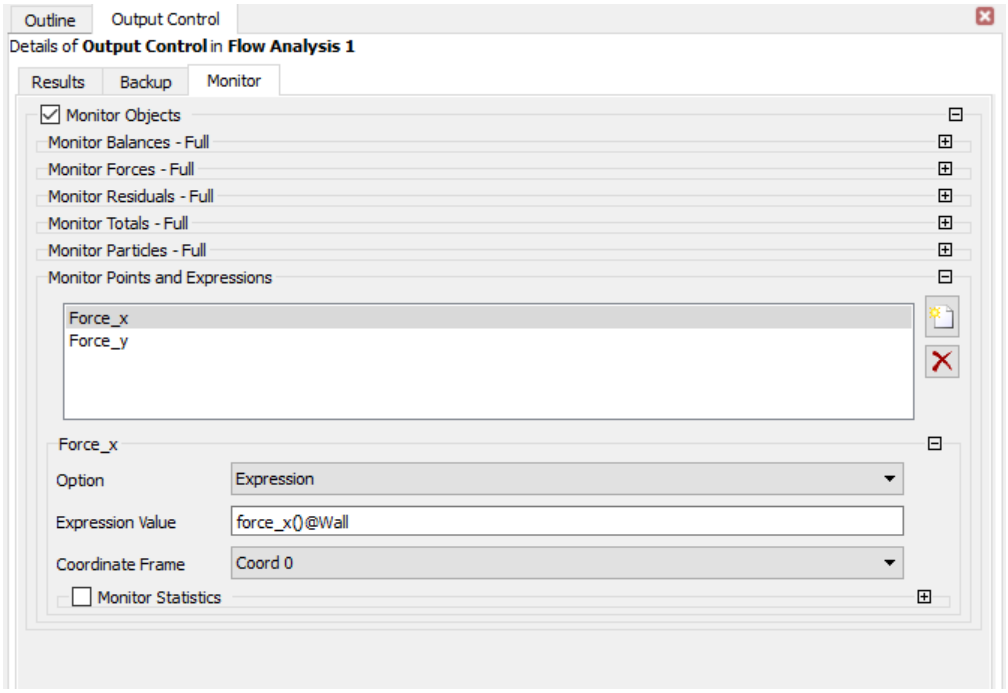

The residual convergence plots for two different steady cases are for 15 m/s and 20 m/s.

15 m/s convergence plot (10^{-6}):

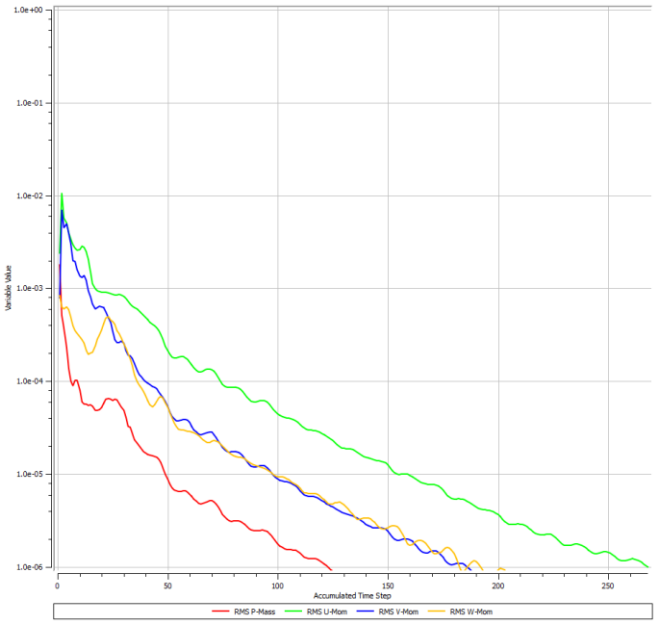

20 m/s convergence plot (10^{-5}):

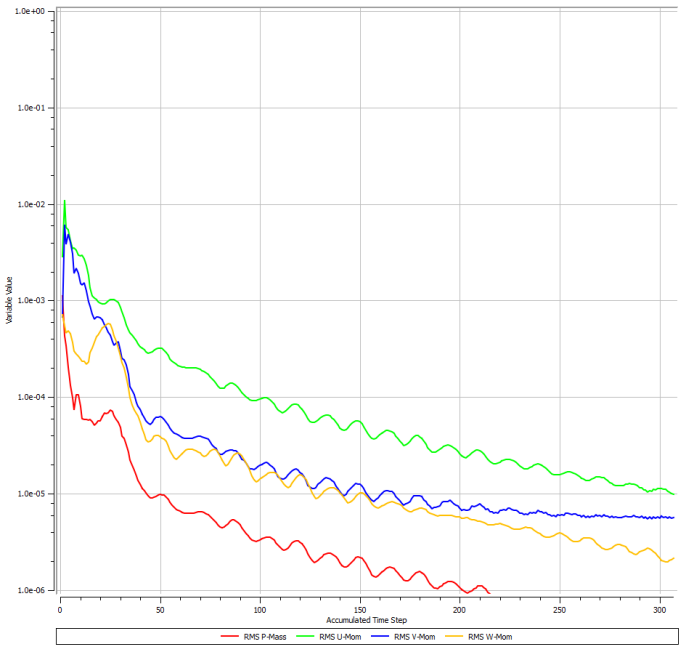

TRANSIENT RIGIDLY SUPPORTED CYLINDER

The steady-state cases were used for the initialization of the transient simulation runs. Due to this, the module will be duplicated using the same geometry conditions and mesh setting for an initial case. Mesh span-wise distance and wake grid sizing will use more divisions, with respect to the turbulence model requirements. The solution from the steady-state was linked to the transient case.

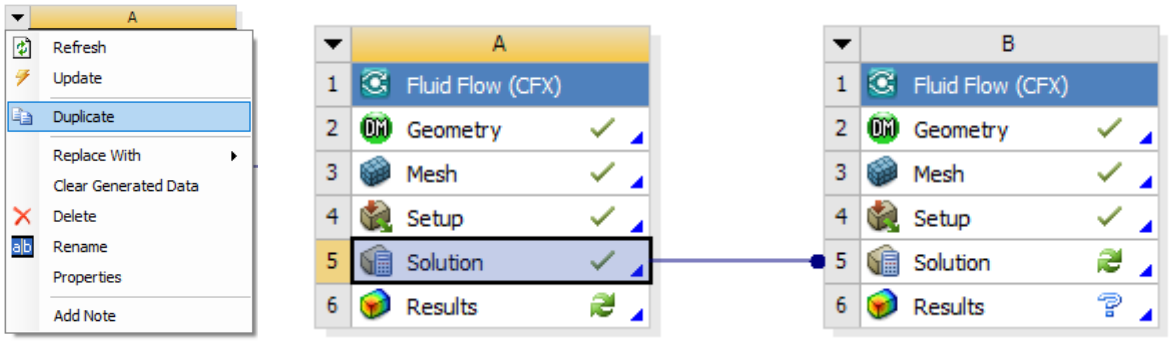

The analyze type will be changed to transient simulation, with a simulation time of several seconds (for this case 12 seconds was selected). A time-step selection was the cylinder diameter divided by the velocity then by 10 to get a sampling rate of 1000. For larger Re, the sampling rate could be larger depending on what is considered required. The temporal effects must be studied as much as the required mesh sizing, for different cases.

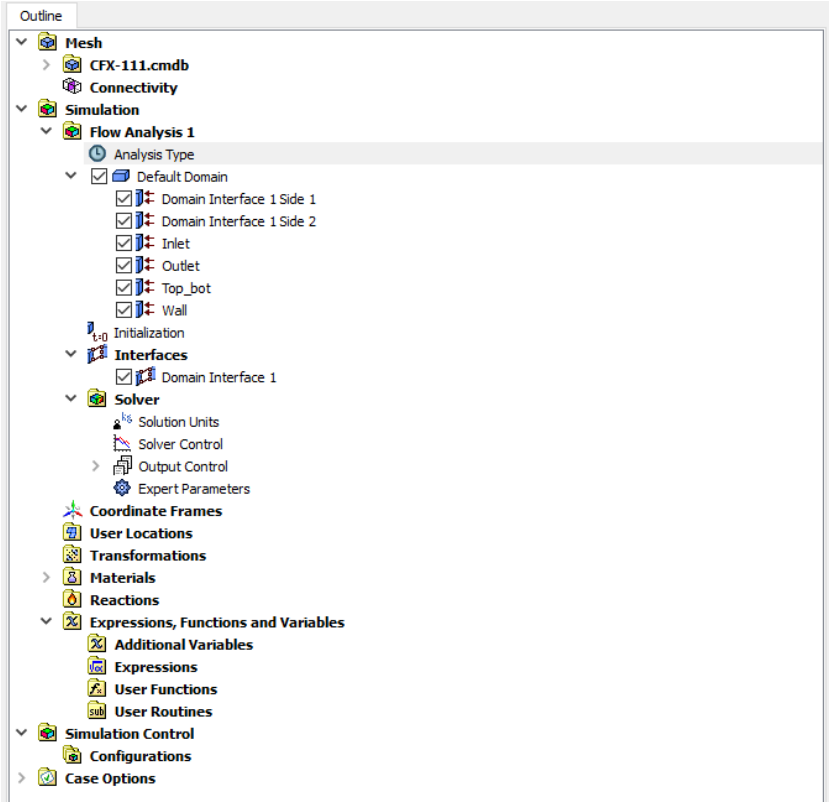

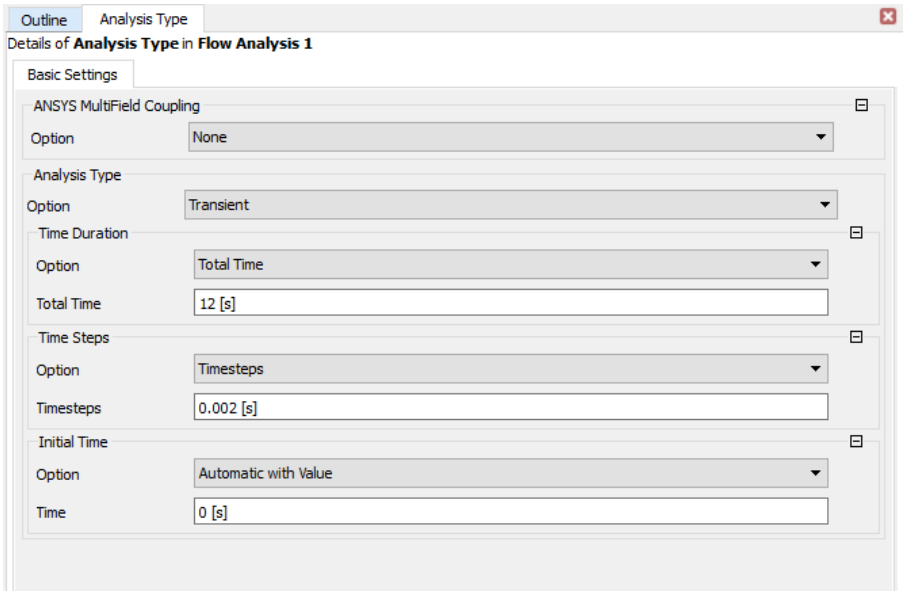

The turbulence model selected as sufficient was the SAS-SST model based on the comparison done in Chapter 6 shown in Table 6.1. The transient controls are left as default, but the numerics as set to High Resolution.

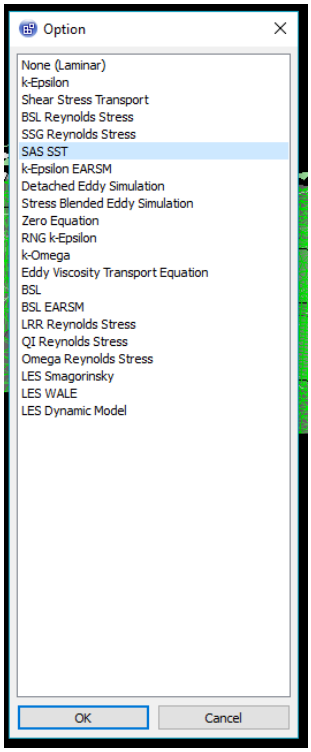

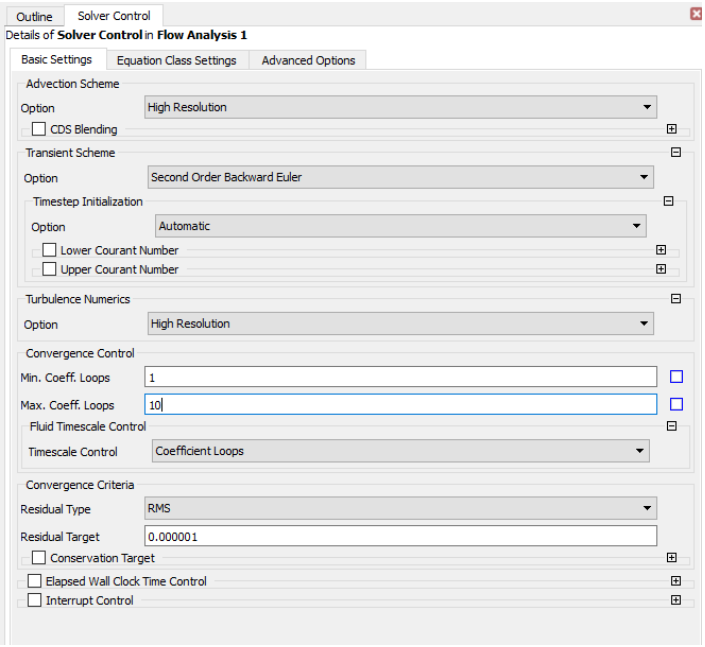

When the simulation reaches a quasi-steady state condition, where the oscillating monitor points maximum and minimum values do not vary from the previous values then results can be post-processed. The monitor point such as the lift force can be truncated where the time-steps can be a few 1000 The time-steps must be compared in terms of seconds for this step. The lift force will be exported to a CSV file, where the information they can be averaged to give the mean lift force in order to calculate lift coefficient (similarly for the drag forces, but lift was selected as the example for the frequency analyze).

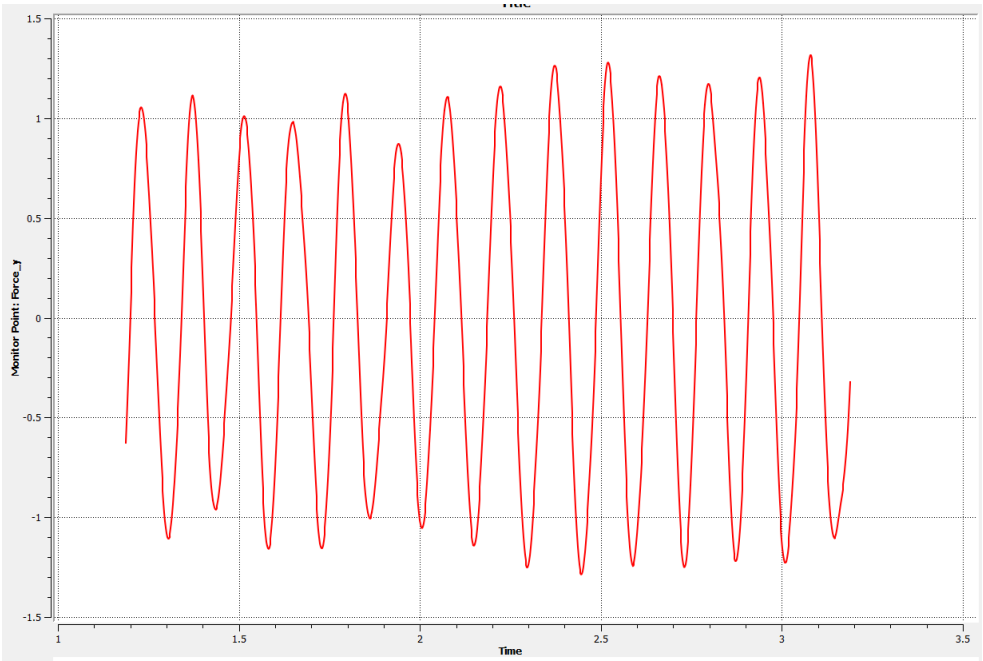

In CFD-Post a user defined line plot will be used to perform a Fast-Fourier Transform (FFT) to determine the frequency of the vortex-shedding. This can be compared to the experimental Strouhal number.

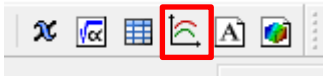

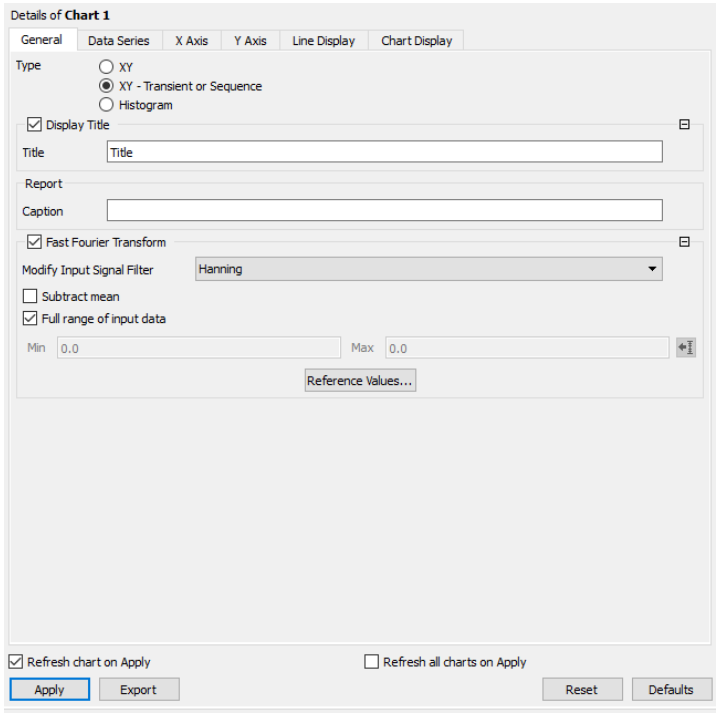

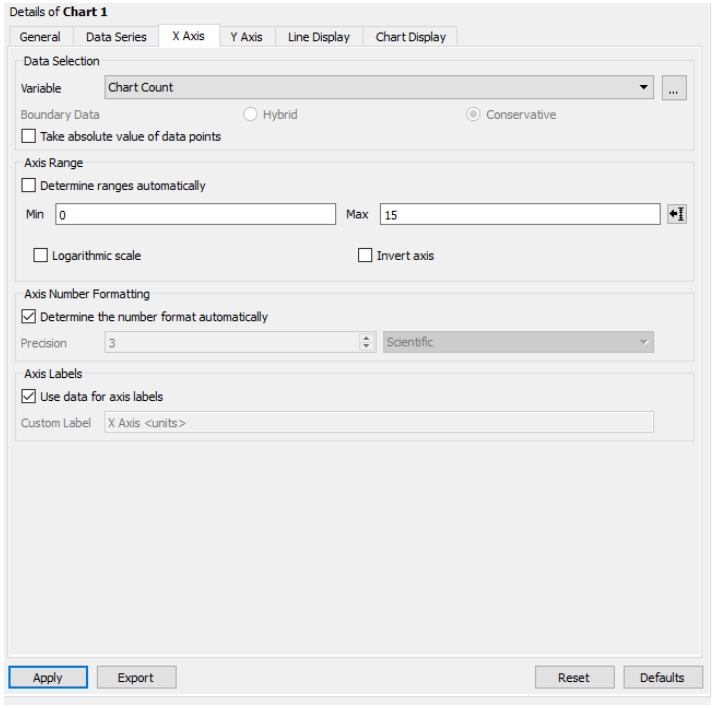

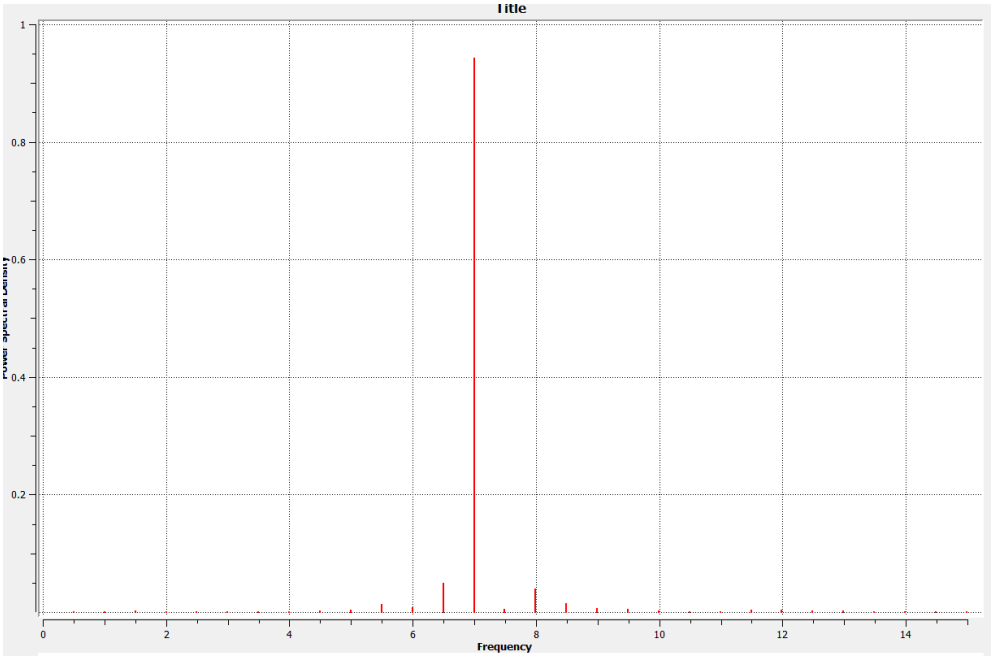

TRANSIENT ELASTICALLY SUPPORTED CYLINDER

Similarly, the moving cylinder (elastically supported) cases can be initialized from a steady-state solution or a similar transient run case. The setup is like the other case transient setup but the rigid body solver be will used to define the cylinder moving mesh approach.

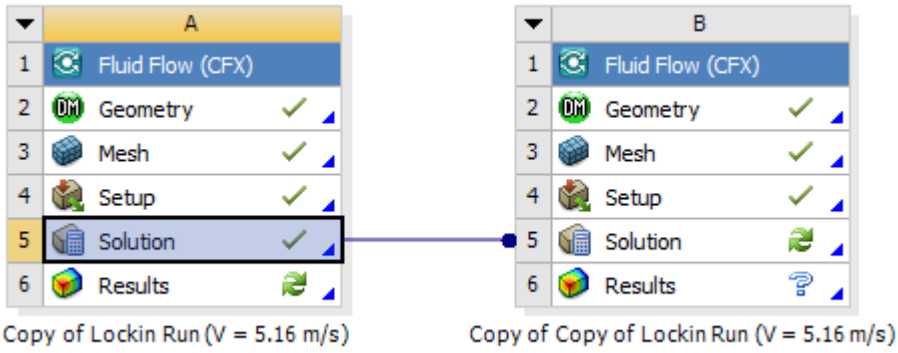

A rigid body (solid body) must be defined in the CFX setup tree. The cylinder will be considered non-rotating. All the moments of inertia will be defined as 0. The mass was calculated using the experimental mass for the first experimental case (Chang 2010) of approximately 2.78 kg. The cylinder wall will be the body where the rigid body will be defined. The forces for the case will be defined as

springs in the y-direction with movement only in y-direction (tangential to the free-stream flow). The spring constant will be defined from experiment as 5786.5 N/m.

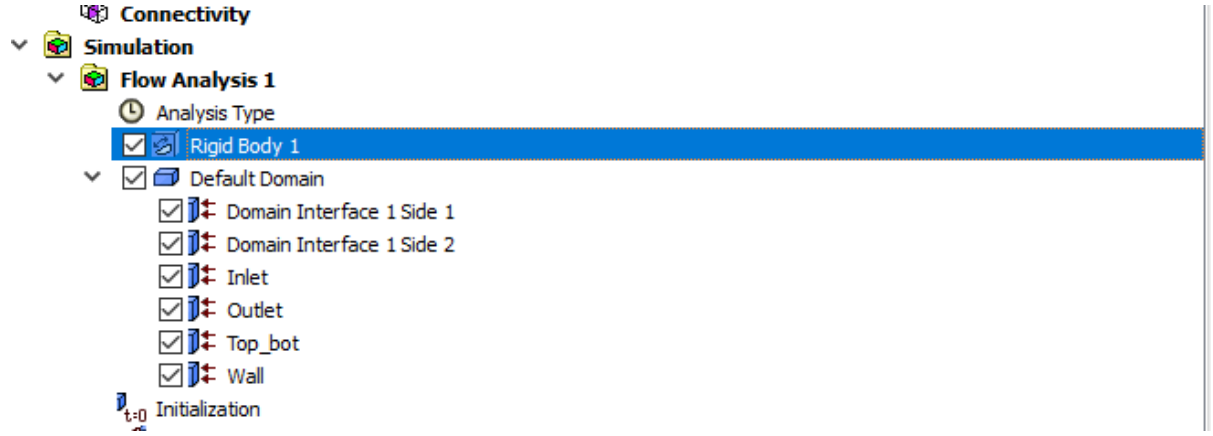

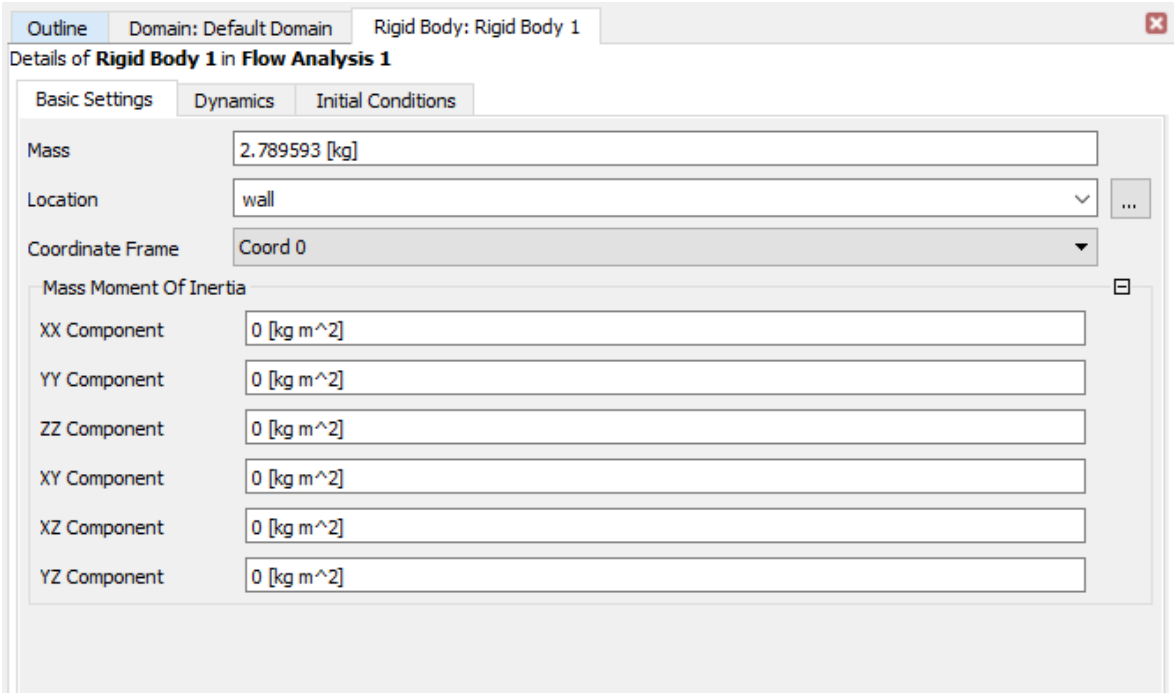

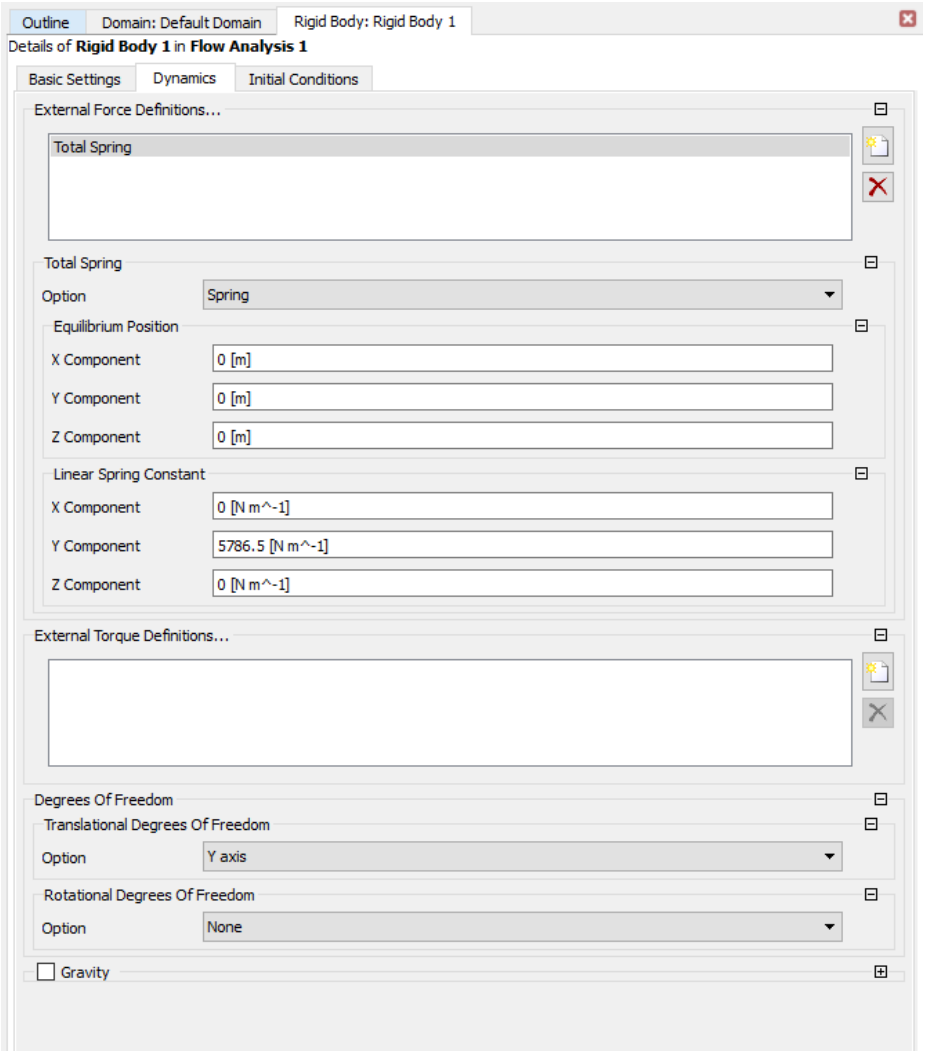

The next step is to define the moving mesh approach in the Default Domain setting, where the only moving mesh area will be at the cylinder wall that will consider the rigid body settings.

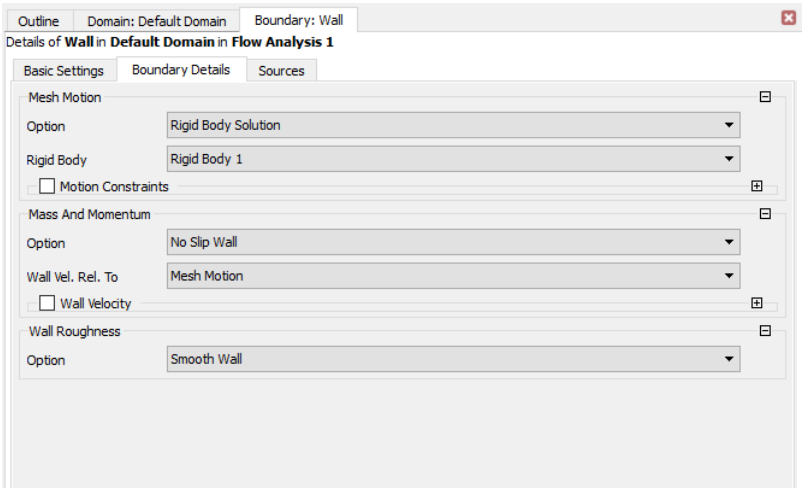

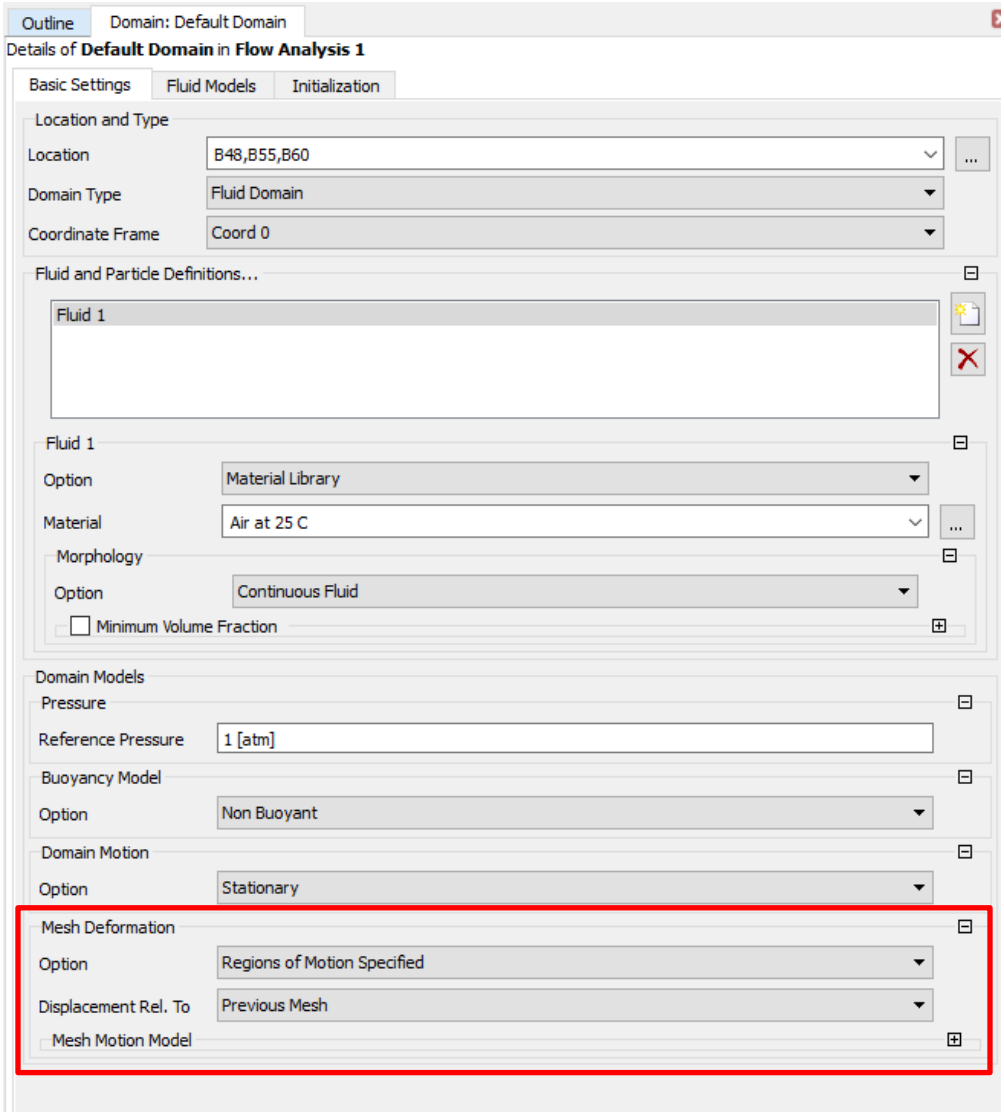

A monitoring point will be used to monitor the mesh motion for the cylinder at the top surface of the cylinder (coordinate point of y of 0.05 meters approximately). A similar monitor to what was used to examine the lift and drag forces. The information taken from any of these monitors can be used to post-processor the frequency in order to check against experimental results. For lock-in, it will be compared to the natural frequency to make sure that the lock-in is being captured.

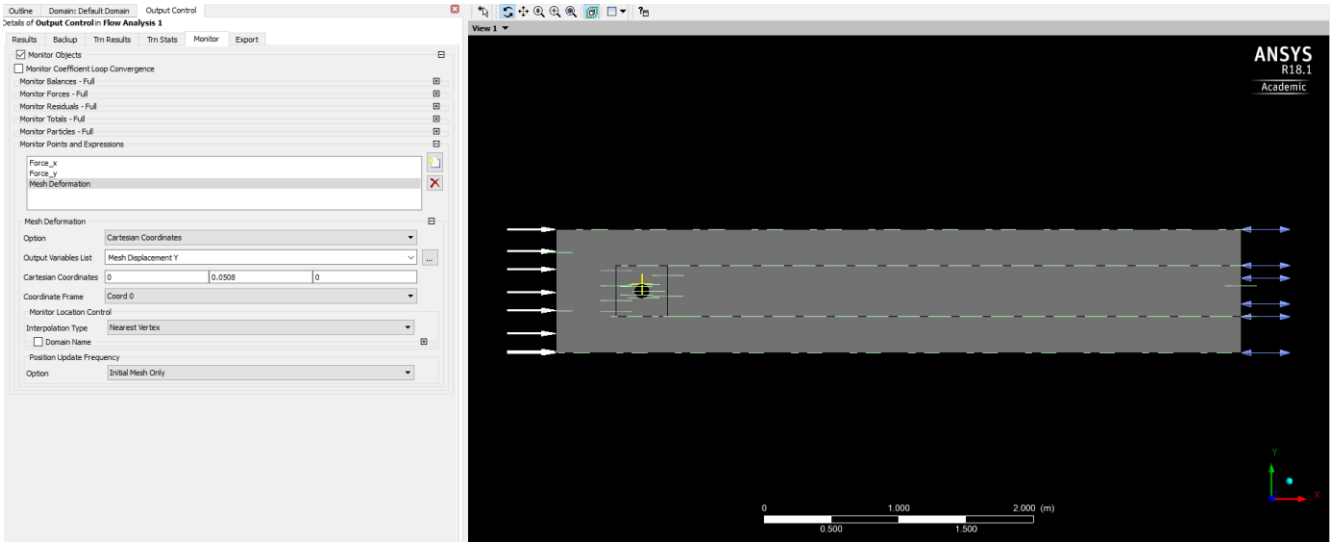
Outline
Domain: Default Domain
Output Control
Details of Output Control in Flow Analysis 1
Results
Backup
Trn Results
Trn Stats
Monitor
Export
Monitor Objects
Monitor Coefficient Loop Convergence
Monitor Balances - Full
Monitor Forces - Full
Monitor Residuals - Full
Monitor Totals - Full
Monitor Particles - Full
Monitor Points and Expressions
Force_x
Force_y
Mesh Deformation
Mesh Deformation
Option
Cartesian Coordinates
Output Variables List
Mesh Displacement Y
Cartesian Coordinates
0
0.0508
0
Coordinate Frame
Coord 0
Monitor Location Control
Interpolation Type
Nearest Vertex
Domain Name
Position Update Frequency
Option
Initial Mesh Only
View 1
ANSYS
R18.1
Academic
0
1.000
2.000 (m)
0.500
1.500